**Integrated Ocean Drilling Program
Expedition 309 Preliminary Report**

Superfast Spreading Rate Crust 2

**A complete in situ section of upper oceanic crust formed
at a superfast spreading rate**

8 July–28 August 2005

Expedition 309 Scientists

PUBLISHER'S NOTES

DISCLAIMER

October 2005

The following scientists and personnel were aboard the *JOIDES Resolution* for Expedition 309 of the Integrated Ocean Drilling Program.

Expedition 309 Scientists

Damon A.H. Teagle
Co-Chief Scientist
School of Ocean and Earth Science
National Oceanography Centre
University of Southampton
European Way
Southampton SO14-3ZH
United Kingdom
dat@noc.soton.ac.uk
Work: (44) 23-8059-2723
Fax: (44) 23-8059-3052

Susumu Umino
Co-Chief Scientist
Department of Biology and Geosciences
Shizuoka University
Ohya 836
Shizuoka 422-8529
Japan
sesumin@ipc.shizuoka.ac.jp
Work: (81) 54-238-4789
Fax: (81) 54-238-0491

Neil R. Banerjee
Expedition Project Manager/Staff Scientist
Integrated Ocean Drilling Program
Texas A&M University
1000 Discovery Drive
College Station TX 77845-9547
banerjee@iodp.tamu.edu
Work: (979) 845-0506
Fax: (979) 845-0876

Florence Einaudi
Logging Staff Scientist
Laboratoire de Géophysique et d'Hydrodynamique en Forage
ISTEEM, cc 056
34095 Montpellier Cedex 5
France
florence.einaudi@dstu.univ-montp2.fr
Work: (33) 4 6714 9309
Fax: (33) 4 6714 9308

Haroldo L. Lledo Vasquez
Inorganic Geochemist
Geological Sciences and Environmental Studies
Binghamton University
4400 Vestal Parkway East
Binghamton NY 13902-6000
USA
hlledov@yahoo.com
Work: (607) 777-4404
Fax: (607) 777-2288

Tetsuya Sakuyama
Inorganic Geochemist
Earth and Planetary Science
University of Tokyo
7-3-1 Hongo
Bunkyo-ku, Tokyo 113-0033
Japan
tetsuya-saku@eps.s.u-tokyo.ac.jp
Work: (81) 3-5841-4670
Fax: (81) 3-5841-8378

Yongjun Gao
Geochemist/Igneous Petrologist
Department of Geosciences
University of Houston
4800 Calhoun Road, SR1 Building
Houston TX 77204
USA
yongjungao@uh.edu
Work: (713) 743-9312
Fax: (713) 748-7906

Douglas S. Wilson
Geophysicist
Department of Geological Sciences
University of California, Santa Barbara
1006 Webb Hall
Santa Barbara CA 93106-9630
USA
dwilson@geol.ucsb.edu
Work: (805) 893-8033
Fax: (805) 893-2314

Emilio Herrero-Bervera
Paleomagnetist
Hawaii Institute of Geophysics and Planetology
University of Hawaii at Manoa
Petrofabrics and Paleomagnetics Laboratory
1680 East West Road
Honolulu HI 96822
USA
herrero@soest.hawaii.edu
Work: (808) 956-6192
Fax: (808) 956-3188

Eugenio A. Veloso Espinosa
Paleomagnetist
Graduate School of Life and Environmental
    Sciences
University of Tsukuba
Tennodai 1-1-1
Tsukuba Science City, Ibaraki 305-8572
Japan
eveloso@arsia.geo.tsukuba.ac.jp
Work: (81) 29-853-9888
Fax: (81) 29-853-6888

Carole Cordier
Igneous Petrologist
Earth Sciences
Universite de Bretagne Occidentale, IVEM
1 Place Copernic
UMR 6538 Domaines Océaniques
29280 Plouzané
France
carole.cordier@sdt.univ-brest.fr
Work: (33) 29 801 7289
Fax: (33) 29 801 6620

Jörg Geldmacher
Igneous Petrologist
IFM-GEOMAR
Leibniz Institute for Marine Sciences Kiel
Wischhofstrasse 1-3
24148 Kiel
Germany
jgeldmacher@ifm-geomar.de
Work: (49) 431-600-2641
Fax: (49) 431-600-2978

Sedelia Rodriguez Durand
Igneous Petrologist
Department of Earth Sciences, PC 344
Florida International University
University Park Campus
11200 Southwest 8th Street
Miami FL 33199
USA
sduran06@fiu.edu
Work: (305) 348-2365
Fax: (305) 348-3877

Takashi Sano
Igneous Petrologist
College of Environment and Disaster Research
Fuji Tokoha University
325 Ohbuchi
Fuji 417-0801
Japan
sano@fuji-tokoha-u.ac.jp
Work: (81) 545-37-2007
Fax: (81) 545-36-2651

Christine Laverne
Metamorphic Petrologist
Université Paul Cézanne Aix-Marseille III
Laboratoire de Pétrologie Magmatique-Case 441
Faculté des Sciences de Marseille Saint Jérome
Avenue Escadrille, Normandie Nieman
13397 Marseille Cedex 20
France
christine.laverne@univ.u-3mrs.fr
Work: (33) 4-91-28-85-18
Fax: (33) 4-91-98-70-32

Christopher E. Smith-Duque
Metamorphic Petrologist
School of Ocean and Earth Science
University of Southampton
European Way
Southampton SO14 3ZH
United Kingdom
csd2@noc.soton.ac.uk
Work: (44) 23-8059-6634
Fax: (44) 23-8059-3052

Lisa A. Gilbert
Physical Properties Specialist
Maritime Studies Program
Williams College and Mystic Seaport
75 Greenmanville Avenue
Mystic CT 06355
USA
lisa.gilbert@williams.edu
Work: (860) 572-5302, ext 5048
Fax: (860) 572-5329

Masako Tominaga
Physical Properties Specialist
Department of Oceanography
Texas A&M University
3F Oceanography Building
3146 TAMU
College Station TX 77843-3146
USA
masako@ocean.tamu.edu
Work: (979) 845-7211
Fax: (979) 845-6331

Laura Crispini
Structural Geologist
Dipartimento per lo Studio del Territorio e delle sue
    Risorse
Università degli Studi di Genova
Corso Europa 26
16132 Genova
Italy
crispini@dipteris.unige.it
Work: (39) 010 353 8204
Fax: (39) 010 352169

Laura Galli
Metamorphic Petrologist
Department of Earth Sciences
Università degli Studi di Milano
Via Mangiagalli, 34
20133 Milano
Italy
lauragalli1@alice.it
Work: (39) 02 5031 5524
Fax: (39) 02 5031 5494

Paola Tartarotti
Structural Geologist
Department of Earth Sciences
Università degli Studi di Milano
Via Mangiagalli, 34
20133 Milano
Italy
paola.tartarotti@unimi.it
Work: (39) 02 5031 5524
Fax: (39) 02 5031 5494

Sara Ann Holter
Student Trainee
Department of Geology
University of St. Thomas
2115 Summit Avenue
St. Paul MN 55105
USA
saholter@stthomas.edu
Work: (763) 350-6258
Fax: (651) 962-5209

Akram Belghoul
Logging Trainee
Laboratoire de Géophysique et d'Hydrodynamique
    en Forage
ISTEEM, cc 056
34092 Montpellier Cedex 5
France
belghoul@dstu.univ-montp2.fr
Work: (33) 4 6714 9336
Fax: (33) 4 6714 9308

Teacher at Sea

Alan C. Gelatt
Romulus Central School
5705 Main Street
Romulus NY 14541
USA
Work: (866) 810-0345
agelatt@rcs.k12.ny.us

Transocean Officials

Alexander Simpson
Master of the Drilling Vessel
Overseas Drilling Ltd.
707 Texas Avenue South, Suite 213D
College Station TX 77840-1917
USA

Wayne Malone
Drilling Superintendent
Overseas Drilling Ltd.
707 Texas Avenue South, Suite 213D
College Station TX 77840-1917
USA

IODP Shipboard Personnel and Technical Representatives

Paula Clark
Marine Computer Specialist

Trevor Cobine
Research Specialist: Physical Properties

Lisa K. Crowder
Assistant Laboratory Officer

Klayton Curtis
Laboratory Specialist: Paleomagnetism

John Eastlund
Applications Developer

Javier Espinosa
Schlumberger Engineer

Kevin Grigar
Operations Superintendent

Ted Gustafson
Marine Laboratory Specialist: Thin Sections

Burnette W. Hamlin
Laboratory Officer

Michael Hodge
Marine Computer Specialist

Leah Shannon Housley
Imaging Specialist

Eric Lynn Jackson
Marine Laboratory Specialist: X-Ray

Jan Jurie Kotze
Marine Instrumentation Specialist

William Mefferd
Laboratory Specialist: Underway Geophysics

Debbie Partain
Yeoperson

Chieh Peng
Assistant Laboratory Officer

Pieter Pretorius
Marine Instrumentation Specialist

Tomoyuki Tanaka
Marine Laboratory Specialist: Core

Paula Weiss
Curatorial Specialist

Bradley Weymer
Marine Laboratory Specialist: Core

Robert M. Wheatley
Laboratory Specialist: Chemistry

ABSTRACT

The Superfast Spreading Rate Crust mission is a multicruise program to drill, for the first time, a complete section of the upper oceanic crust from extrusive lavas, through the dikes, and into the underlying gabbros. Hole 1256D was initiated during Ocean Drilling Program Leg 206 in the eastern equatorial Pacific and is drilled into 15 Ma crust that formed at the East Pacific Rise during a period of superfast spreading (>200 mm/y). This site is chosen to exploit the inverse relationship between spreading rate and the depth to axial low-velocity zones, thought to be magma chambers now frozen as gabbros, observed from seismic experiments. During Integrated Ocean Drilling Program (IODP) Expedition 309 Hole 1256D was successfully deepened to a total depth of 1255 meters below seafloor (mbsf) (1005 m subbasement), having penetrated through >800 m of extrusive normal mid-ocean-ridge basalt, and entered a region dominated by intrusive rocks with numerous subvertical chilled dike margins. The uppermost crust at Site 1256 comprises a >74 m thick ponded lava overlying massive, sheet, and minor pillow flows, some of which exhibit inflation structures requiring eruption onto a subhorizontal surface. This suggests a total thickness of off-axis lavas of 284 m. Sheet and massive lava flows make up the remaining extrusive section (534–1004 mbsf) above subvertical cataclastic zones, intrusive contacts, and spectacular mineralized breccias denoting a lithologic transition zone. The extrusive lavas are less hydrothermally altered than other basement sites (e.g., Sites 417 and 418 and Holes 504B and 896A), and there is no systematic change with depth from oxidizing to reducing seawater alteration. Instead, oxidizing alteration occurs irregularly with depth, most commonly associated with steeply dipping vein networks. Below 1061 mbsf, massive basalts, some with doleritic textures, dominate the sheeted intrusives. Numerous subvertical dikes, commonly with brecciated and mineralized chilled margins, crosscut the sheeted intrusives. These rocks are altered under greenschist facies hydrothermal conditions and have significantly higher thermal conductivity and P-wave velocity. During Expedition 309 Hole 1256D was exited cleanly, and the hole is in excellent condition and ready for deepening. At 1255 mbsf, Hole 1256D is tantalizingly close to the minimum estimated depth for the frozen axial magma chamber predicted to be at 1275–1525 mbsf. IODP Expedition 312 will return to this site in late 2005, and, despite the grueling 15 m/day pace of advance and assuming further benign drilling conditions, is set to deepen Hole 1256D by a further 500 m. The total depth would then be well beyond where geophysical interpretations predict gabbros to occur.

BACKGROUND AND OBJECTIVES

More than 60% of the Earth is covered by oceanic crust formed at the mid-ocean ridges, all of which formed within the last 200 m.y. The formation of new oceanic crust at ridges axes and reincorporation of aged crust into the mantle or its accretion onto continental margins at subduction zones are perhaps the most fundamental components of the plate tectonic cycle. These processes control the physiography of the Earth and the chemical and thermal evolution of the crust and mantle.

Accretion of oceanic crust at mid-ocean ridges from magmas passively upwelled during partial melting of decompressed mantle peridotite is the dominant process of thermal and chemical transfer from the Earth's interior to the crust, overlying oceans, and atmosphere. Conduction and hydrothermal advection of heat at constructive plate boundaries through the oceanic lithosphere and as it matures on the ridge flanks is the major mechanism for heat loss from the interior of the planet. Such hydrothermal interactions influence the chemistry of many elements (e.g., Mg, Sr, U, and K) in the oceans at a similar magnitude to the inputs from rivers draining the continents. Chemical exchange of seawater with the ocean crust leads to major changes in the chemical composition and physical properties of oceanic basement, which, through subduction, influence the composition and heterogeneity of the mantle and the melting and constructional processes occurring in arcs.

Recently, the upper oceanic crust has been shown to be a habitat for microorganisms. Microbes colonize fractures in glassy basaltic rocks, extracting energy and/or nutrients from the glass by dissolving it, leaving behind biomarkers that reveal their former presence. The temperature and depth limits of oceanic basement microbiological activity have yet to be explored, but microbial processes occurring in the submarine deep biosphere may hold the key to the development and survival of life on the Earth and other planets.

Despite the central role that the ocean crust plays in the evolution of our planet, our sampling of in situ oceanic basement is poor, and consequently, our understanding of the fundamental processes involved in the formation and evolution of the oceanic crust remains rudimentary. Samples of basalts, dikes, gabbros, and peridotites have been retrieved by dredging and shallow drill holes from most of the ocean basins, but the geological context of these samples is rarely well established. As such, the nature and variability of the composition and structure of the ocean crust away from transform faults and other tectonic windows remain poorly known. Drilling a complete

crustal section has always been a major goal of scientific ocean drilling (Bascom, 1961; Shor, 1985), but achievement of this goal has been impeded by technical difficulties and the time investments required. The distribution of drill holes in intact oceanic crust of different ages and formed at different spreading rates is extremely sparse (Fig. F1) (see Wilson, Teagle, Acton, et al., 2003, for full documentation of basement drilling). Before Integrated Ocean Drilling Program (IODP) Expedition 309, Hole 504B, drilled during the Deep Sea Drilling Project (DSDP) and Ocean Drilling Program (ODP) on the southern flank of the Costa Rica Rift, was the only hole to penetrate a complete sequence of extrusive lavas and partially through the underlying sheeted dike complex (Alt, Kinoshita, Stokking, et al., 1993). The dike/gabbro boundary has never been drilled, and the nature of the plutonic rocks directly subjacent to the sheeted dike complex is not known, despite this zone being perhaps the most influential in determining the mechanisms of crustal accretion and the geometry of magmatic and hydrothermal interactions. Our poor sampling of ocean crust at different spreading rates and crustal ages and the absence of information on crustal variability compromise our ability to extrapolate observations from specific sites to global descriptions of magmatic accretion processes and hydrothermal exchange in the ocean crust.

Oceanic crust formation and evolution are primary themes for investigation in the *Initial Science Plan for the Integrated Ocean Drilling Program* (International Working Group, 2001) and other major science priority submissions (e.g., Conference on Multiple Platform Exploration of the Ocean [COMPLEX], Pisias and Delaney, 1999; Ocean Drilling Program Geochemistry Futures Workshop, Murray et al., 2002). These documents and others specifically related to the study of the oceanic lithosphere (Second Conference on Scientific Ocean Drilling [COSOD II]; *ODP Long Range Plan,* Ocean Drilling Program, 1996; ODP–International Cooperation in Ridge-Crest Studies–International Association of Volcanology and Chemistry of the Earth's Interior workshop; 4D-Architecture of the Ocean Crust Program Planning Group) reemphasize deep drilling to obtain complete sections of the ocean crust as a priority and note that the deep drilling capabilities of riserless technology have yet to be fully utilized.

Offset drilling strategies, where deeper portions of the ocean crust are sampled by drilling in tectonic windows, have recently been high priorities for ocean drilling (COSOD II, 1987; Ocean Drilling Program, 1996). Drilling at several sites has provided a wealth of new data and understanding of gabbros and peridotites from the lower crust and serpentinized upper mantle (e.g., Hess Deep: Gillis, Mével, Allan, et al., 1993; Kane Fracture Zone area: Cannat, Karson, Miller, et al., 1995; Southwest Indian

Ridge: Dick, Natland, Miller, et al., 1999; 14°–16°N Mid-Atlantic Ridge: Kelemen, Kikawa, Miller, et al., 2004; Atlantis Massif: Expedition 304 Scientists, 2005; Expedition 305 Scientists, 2005). However, serious problems still exist with drilling tectonized rocks with little sediment blanket or without erosional removal of fractured material, and it is also commonly difficult to relate drilled sections to regional geology (e.g., Gillis, Mével, Allan, et al., 1993). Perhaps the most successful deep drilling of the oceanic basement has occurred in crust formed at slow to ultra-slow spreading rates on plutonic massifs exposed near ridge-transform fault intersections (Holes 735B and U1309D). These holes boast deep penetration at high rates of recovery (Dick, Natland, Miller, et al., 1999; Expedition 304 Scientists, 2005; Expedition 305 Scientists, 2005) but are probably not representative of the majority of ocean crust that formed at faster spreading rates and in the middle of ridge segments.

Composite sections are not substitutes for deep in situ penetrations, and drilling deep holes to obtain complete upper crustal sections continues to be a primary challenge for scientific ocean drilling (Dick and Mével, 1996; Murray et al., 2002). Unfortunately, there are no on-land alternatives to drilling in the oceans. Although ophiolites, ancient slices of ocean crust now preserved on land, provided much of the early inspiration for ocean crust studies, the classic outcrops of Semail ophiolite (Oman) and Troodos massif (Cyprus) formed in suprasubduction zone settings and their different magma and volatile chemistries compromise their applicability for understanding processes in the major ocean basins. Macquarie Island (Varne et al., 2000), uplifted along the Australian/Pacific plate boundary ~1000 km south of New Zealand, may be the only outcrop of subaerially exposed ocean crust formed at a mid-ocean ridge, but the island is complexly faulted and is an environmentally sensitive United Nations Educational, Scientific, and Cultural Organization World Heritage site from which drilling, even for scientific purposes, is prohibited.

IODP Expeditions 309 and 312 will build on the success of ODP Leg 206, during which Hole 1256D was established, to drill a complete section of the upper oceanic crust. Hole 1256D in the Guatemala Basin is hosted by 15 m.y. old crust that formed at the equatorial East Pacific Rise (EPR) during a sustained period of superfast seafloor spreading (Fig. F2) (Wilson, Teagle, Acton, et al., 2003). It is the first basement borehole prepared with the infrastructure desirable for drilling a moderately deep hole into the oceanic crust (~1.5–2 km). Following preliminary coring to document the sedimentary overburden at Site 1256, Leg 206 a reentry cone supported by 20 inch casing and large-diameter (16 inch) casing all the way through the sediment cover and cemented 19 m into basement was installed in Hole 1256D during Leg 206. The

cone and casing will facilitate multiple reentries and help maintain hole stability essential for deepening Hole 1256D down through the dikes and into gabbros. The large-diameter casing leaves open the possibility that one or two more casing strings could be installed in Hole 1256D should future expeditions need to isolate unstable portions of the hole. During Leg 206, the upper 502 m of the igneous crust was cored with moderate to high recovery (average = ~48%), and the uppermost crust at this site comprises a sequence of massive flows and thinner sheet flows with subordinate pillow basalt and breccias. The sequence has normal mid-ocean-ridge basalt (N-MORB) composition similar to modern EPR basalts and is slightly to moderately altered. It was extruded over sufficient time to record stable geomagnetic field directions and capture transitional directions in the upper units as the geomagnetic field reversed. Importantly, operations during Leg 206 in Hole 1256D concluded with the hole clean of debris and in excellent condition.

The goal of the IODP Superfast Spreading Rate Crust mission (Expeditions 309 and 312) is to core through the remaining extrusive rocks and the underlying sheeted dike complex and into the upper gabbros. This continuous section of in situ oceanic crust generated at a superfast spreading rate in the eastern Pacific will

- Provide the first sampling of a complete section of ocean crust from extrusive rocks and dikes and into the gabbros. This will confirm whether ocean crust formed at a superfast spreading rate conforms to a "Penrose" ophiolite stratigraphy.
- Confirm the nature of high-level axial magma chambers.
- Define the relationship between magma chambers and their overlying lavas and the interactions between magmatic, hydrothermal, and tectonic processes.
- Provide in situ calibration of seismic velocity and magnetic measurements made from surface ships so that these regional-scale geophysical measurements can be related to geology.

Rationale for Site Selection and Location Criteria for Deep Drilling

The key to proposing the Superfast Spreading Rate Crust campaign (Leg 206 and Expeditions 309 and 312) was to identify a style of crustal accretion where the extrusive lavas and dikes overlying the gabbros were predicted to be relatively thin, thus increasing the likelihood of penetrating through the complete upper crustal section in the fewest drilling days. The recognition that crust formed at a superfast spreading rate is a compelling target for deep drilling follows the observation that there is an

inverse relationship between the depth of axial low-velocity zones imaged by seismic experiments, interpreted to be melt lenses, and spreading rate (Purdy et al., 1992) (Fig. F3). Even allowing for an additional thickness of lavas that flowed from the ridge axis to cover the immediate flanks, the uppermost gabbros should be at relatively shallow depths in superfast-spreading crust. The predicted depth to gabbros at Site 504 on the south flank of the intermediate-spreading Costa Rica Rift is >2.5 km, whereas the depth to the axial low-velocity zones at typical fast spreading rate (~80–150 mm/y) crust on the EPR is ~1–2 km. The estimated depth to an axial melt lens for ocean crust formed at a superfast spreading rate is ~700–1000 m, and the anticipated depth to the gabbros for Site 1256 is ~1000–1300 m, allowing for a reasonable thickness (~300 m) of near-axial lava flows.

Although perhaps only 20% of the global ridge axis is separating at fast spreading rates (>80 mm/y full rate), ~50% of the present-day ocean crust and ~30% of the total Earth's surface was produced by this pace of the ocean spreading. At least in terms of seismic structure (Raitt, 1963; Menard, 1964), crust formed at fast spreading rates is relatively simple and uniform. Deep drilling at Site 1256 will characterize one end-member style of mid-ocean-ridge accretion, and the successful deep sampling of such crust in a single location can reasonably be extrapolated to describe a significant portion of the Earth's surface.

Site Selection

A recent reconsideration of magnetic anomalies at the southern end of the Pacific/Cocos plate boundary has identified crust formed at a full spreading rate of ~220 mm/y from 20 to 11 Ma (Wilson, 1996) (Fig. F2). This is significantly faster than the present fastest spreading rate (~145 mm/y) for crust forming at ~30°S on the EPR. From this region created by superfast spreading, a single drill site in the Guatemala Basin, initially designated GUATB-03C and now known as Site 1256, was selected on young, 15 m.y. old ocean crust. The details of site survey operations and the reasons for the selection of this particular site are outlined in detail in Wilson, Teagle, Acton, et al. (2003).

In addition to the shallow depth to gabbros predicted from formation at a superfast spreading rate, Site 1256 has a number of specific attributes that indicate that this site provides an excellent opportunity to sample a complete section of upper oceanic crust. Site 1256 formed at an equatorial latitude (Fig. F4), and high equatorial productivity resulted in robust sedimentation rates (>30 m/m.y.) and the rapid burial of the

young basement. The thick sediment blanket enabled installation of a reentry cone with 20 inch casing that forms the foundation for deployment of the second 16 inch diameter casing string that was cemented 19 m into the uppermost basement. At 15 Ma, Site 1256 is significantly older than the crust at Hole 504B (6.9 Ma), and lower temperatures are anticipated at midlevels of the crust. As such, high basement temperatures, which can preclude drilling operations, should not be reached until gabbroic rocks have been penetrated. Logistically, Site 1256 has a number of advantages. It is ~3.5 days steaming from the Panama Canal, and the short transit time allows for maximum time on site during drilling expeditions. As transfer between the Pacific and Atlantic Oceans is common due to the scheduling demands of scientific drilling, close proximity to the Panama Canal has allowed the timely rescheduling of return visits to the site.

Geological Setting of Hole 1256D

Site 1256 (6°44.2′ N, 91°56.1′ W) lies in 3635 m of water in the Guatemala Basin on Cocos plate crust formed ~15 m.y. ago on the eastern flank of the EPR (Figs. F2, F4). The depth of the site is close to that predicted from bathymetry models of plate cooling (e.g., Parsons and Sclater, 1977). The site sits astride the magnetic Anomaly 5Bn–5Br magnetic polarity transition (Fig. F5A). This crust accreted at a superfast spreading rate (~220 mm/y full rate; Wilson, 1996) and lies ~1150 km east of the present crest of the EPR and ~530 km north of the Cocos Ridge. The site formed on a ridge segment at least 400 km in length, ~100 km north of the ridge-ridge-ridge triple junction between the Cocos, Pacific, and Nazca plates (Fig. F4). This location was initially at an equatorial latitude within the equatorial high-productivity zone and endured high sedimentation rates (>30 m/m.y.; e.g., Farrell et al., 1995; Wilson, Teagle, Acton, et al., 2003). The sediment thickness in the region is between 200 and 300 m and is 250 m at Site 1256 (Wilson, Teagle, Acton, et al., 2003).

Site 1256 has a seismic structure reminiscent of typical Pacific off-axis seafloor (Fig. F6). Upper Layer 2 velocities are 4.5–5 km/s and the Layer 2–3 transition is between ~1200 and 1500 meters subbasement (msb) (Fig. F7). The total crustal thickness at Site 1256 is estimated at ~5–5.5 km. Further to the northeast of Site 1256 (15–20 km), a trail of ~500 m high circular seamounts rise a few hundred meters above the sediment blanket (Fig. F5B).

Using the site survey multichannel seismic (MCS) data (Wilson et al., 2003), we have constructed a geological sketch map of the uppermost basement in the GUATB-03

survey region (Fig. F8). The bathymetry in the GUATB-03 survey area is generally subdued, and Site 1256 sits atop a region of smooth basement topography (<10 m relief). However, elsewhere in the region, the top of basement shows a number of offsets along northwest-striking normal faults, and an abyssal hill relief of up to 100 m is apparent in the southwest part of the area. Relief to the northeast is lower and less organized. In the northeast sector of the GUAT-3B region, there is evidence for a basement thrust fault with a strike approximately orthogonal to the regional fabric (Wilson et al., 2003; Hallenborg et al., 2003). This feature dips gently to the northwest (~15°) and is clearly discernible to a depth of ~1.3 km on seismic Line EW9903-28 (Wilson et al., 2003), but the feature is less pronounced on seismic Line EW9903-27, indicating that the offset on the thrust decreases to the southwest.

Additional processing (A. Harding, unpubl. data) of ocean borehole seismometer recordings indicates that there is discernible variation in the average seismic velocity (~4.54–4.88 km/s) of the uppermost (~100 m) basement and that there is regional coherence in the velocity variations (Fig. F8A). Two principal features are apparent: a 5–10 km wide zone of relatively high upper basement velocities (>4.82 km/s) that can be traced ~20 km to the edge of data coverage southeast of Site 1256 and a relatively low velocity (4.66–4.54 km/s) bull's-eye centered around the crossing point of seismic Lines EW9903-21 and 25.

The uppermost basement at Site 1256 is capped by a massive lava flow >74 m thick. This flow is relatively unfractured, with shipboard physical properties measurements on discrete samples indicating V_P > 5.5 km/s (Wilson, Teagle, Acton, et al., 2003). As such, it is likely that the area of relatively high uppermost basement seismic velocities delineates the extent of the massive flow penetrated in Holes 1256C and 1256D. Assuming an average thickness of 40 m, this would conservatively suggest an eruption volume >3 km³, plausibly >10 km³. This is extremely large when compared to the size of mid-ocean-ridge axial low-velocity zones that are thought to be high-level melt lenses and which typically have volumes ~0.05–0.15 km³ per km of ridge axis and generally appear to be only partially molten (Singh et al., 1998).

Sheet flows (<3 m thick) and massive flows (>3 m) make up most of the lava stratigraphy cored at Site 1256, and such lava morphologies dominate crust formed at fast spreading rates, away from segment tips (e.g., White et al., 2000, 2002). Subordinate pillow lavas are present in Hole 1256D, and because of the large number of fractures and pillow interstices, seismic velocities are generally lower than more massive lava

flows. We speculate that the bull's eye of relatively low seismic velocities is a thick pile of dominantly pillowed lava flows.

Scientific Objectives of Expeditions 309 and 312

Expeditions 309 and 312 will continue the drilling of a continuous section through volcanic basement and the underlying sheeted dike complex down into the uppermost plutonic rocks in Hole 1256D. The cores recovered from and the wireline measurements made in Hole 1256D will provide unique information to address the following specific scientific objectives:

1. *Test the prediction, from the correlation of spreading rate with decreasing depth to the axial low-velocity zones (e.g., Purdy et al., 1992), that gabbros representing the crystallized melt lens will be encountered at 1000–1300 msb at Site 1256.*

The transition from sheeted dikes to gabbros has never been drilled, and this remains an important objective in achieving a complete or even composite oceanic crustal section. The dike–gabbro transition and the uppermost plutonic rocks are assumed to be the frozen axial melt lens and the fossil thermal boundary layer between magma chambers and vigorous hydrothermal circulation. Detailed knowledge of the dike–gabbro transition zone is critical to discerning the mechanisms of crustal accretion. The textures and chemistries of the uppermost gabbros are presently unknown but are central to understanding crustal construction. At present, we lack samples that link gabbroic rocks to the overlying lavas, leading to the following questions:

- What is the geological nature of the low-velocity zones imaged by MCS reflection studies at the axes of mid-ocean ridges?
- Is the melt lens imaged at mid-ocean ridges made of cumulate rocks from which magmas are expelled to form the dikes and lavas, which then subside to form the lower crust? Or are the uppermost gabbros coarse-grained chemical equivalents of the dikes and extrusive rocks frozen at the base of the sheeted dikes?
- Does most of the crustal accretion occur at deeper levels through the intrusion of multiple thin sills?
- What are the cooling rates of magma chambers?

These questions can be answered through petrological and geochemical studies of gabbros (e.g., Natland and Dick, 1996; Kelemen et al., 1997; Manning et al., 2000; MacLeod and Yaoancq, 2000; Coogan et al., 2002a, 2002b) and the overlying lavas and their mineral constituents.

2. Determine the lithology and structure of the upper oceanic crust from a superfast spreading rate end-member.

Some basic observations regarding the architecture of ocean crust, including the lithology, geochemistry, and thicknesses of the volcanic and sheeted dike sections and how these vary with spreading rate or tectonic setting, are not well known. Karson (2002) provides estimates of the thicknesses of lavas and sheeted dikes from crust generated at fast and intermediate spreading rates (600–900 m lavas and 300–1000 m dikes at Hess Deep; 500–1300 m lavas and 500 to >1000 m dikes in Hole 504B and Blanco Fracture Zone). With the exception of the incomplete section in Hole 504B, these estimates are based on observations of highly disrupted exposures, where structural complexities and the uniqueness of the geological environments indicate that such estimates should be treated with caution. Results of Expeditions 309 and 312 will determine the thicknesses of these upper crustal units at Site 1256 and document the styles of deformation and magmatic accretion. Studies of tectonic exposures of oceanic crust suggest that intense brittle deformation, faulting and distributed zones of fracturing, and large amounts of dike rotation are common within sheeted dike complexes in crust formed at fast and intermediate spreading rates (Karson, 2002; Karson et al., 2002; Stewart et al., 2005). It is difficult, however, to separate primary mid-ocean-ridge geometries from deformation related to the unroofing of these tectonic windows. In contrast, large blocks of the sheeted dike complex in the Semail ophiolite in Oman exhibit little of such faulting or distributed fracturing (Umino et al., 2003). Seismic profiles of the Site 1256 region show well-developed subhorizontal reflectors to ~800–900 msb (Fig. F6), providing little evidence for rotation of the upper crust in this region.

Drilling the sheeted dike complex at Site 1256 will enable evaluation of whether such faulting and fracturing observed in tectonic exposures are representative of oceanic crust or merely related to their complex tectonic settings. Most dikes in sheeted dike complexes in tectonic exposures of crust generated at intermediate and fast spreading rates and in Hole 504B in intermediate-rate crust generally dip away from the spreading axis, suggesting tectonic rotation of crustal blocks (Karson, 2002). Do such rotations also occur in crust generated at superfast spreading rates, and are they similar, or is the crust less tectonically disrupted? A single drill hole may not conclusively answer this question but should provide important constraints.

3. Correlate and calibrate seismic and magnetic imaging of the crustal structure with basic geological observations.

Ground-truthing regional geophysical techniques such as seismic and magnetic imaging is a key goal of the IODP *Initial Science Plan* and related documents (e.g., COMPLEX). A fundamental question we will address in this experiment is how velocity changes within seismic Layer 2 and whether the Layer 2–Layer 3 transition relates to physical, lithological, structural, and/or alteration variations in the volcanic rocks, dikes, and gabbros. At Site 504, in crust generated at an intermediate spreading rate ridge, the Layer 2–Layer 3 transition lies within the 1 km thick sheeted dike complex and coincides with a metamorphic change (Detrick et al., 1994; Alt et al., 1996), but it is unknown whether the results from Hole 504B are representative of ocean crust in general or of crust generated at different spreading rates. Is the depth to gabbros shallower in crust generated at a superfast spreading rate, as predicted, and what are the relative thicknesses of volcanic and dike sections compared with crust constructed at slow or intermediate spreading rates?

Marine magnetic anomalies are one of the key observations that led to the development of plate tectonic theory, through recognition that the ocean crust records the changing polarity of the Earth's magnetic field through time (Vine and Matthews, 1963). It is generally assumed that micrometer-sized grains of titanomagnetite within the erupted basalts are the principal recorders of marine magnetic anomalies. However, recent studies of tectonically exhumed lower crustal rocks and serpentinized upper mantle indicate that these deeper rocks may also be a significant source of the magnetic stripes (Hosford et al., 2003). Coring a complete section through the sheeted dike complex will allow evaluation of the contribution of these rocks to marine magnetic anomalies. Whether these deeper rocks have a significant influence on the magnetic field in undisrupted crust is unknown, as is the extent of secondary magnetite growth in gabbros and mantle assemblages away from transform faults. Sampling the plutonic layers of the crust will test the Vine-Matthews hypothesis by characterizing the magnetic properties of gabbros through drilling normal ocean crust on a well-defined magnetic stripe, away from transform faults.

4. Investigate the interactions between magmatic and alteration processes, including the relationships between extrusive volcanic rocks, sheeted dikes, and underlying gabbroic rocks.

Little information presently exists on the heterogeneity of hydrothermal alteration in the upper crust or the variability of associated thermal, fluid, and chemical fluxes. How these phenomena vary at similar and different spreading rates is unknown.

Metamorphic assemblages and analyses of secondary minerals in material recovered by deep drilling can provide limits on the amount of heat removed by hydrothermal systems and place important constraints on the geometry of magmatic accretion and the thermal history of both the upper and lower crust (e.g., Manning et al., 2000; MacLeod and Yaoancq, 2000; Coogan et al., 2002a, 2000b). Fluid flow paths, the extent of alteration, and the nature of deep subsurface reaction and shallower mixing zones are all critical components of our understanding of hydrothermal processes that can only be tackled by drilling. These problems can be addressed by examining the "stratigraphy" and relative chronology of alteration within the extrusive lavas and dikes, by determining whether disseminated sulfide mineralization resulting from fluid mixing and a large step in thermal conditions is present at the volcanic–dike transition (as in Hole 504B and many ophiolites), and by evaluating the grade and intensity of alteration in the lower dikes and upper gabbros. The lowermost dikes and upper gabbros have been identified as the conductive boundary layer between the magma chambers and the axial high-temperature hydrothermal systems, as well as the subsurface reaction zone where downwelling fluids acquire black-smoker chemistry (Alt, 1995; Alt et al., 1996; Vanko and Laverne, 1998; Gillis et al., 2001). However, extensive regions of this style of alteration or zones of focused discharge are poorly known, and information from ophiolites may not be applicable to in situ ocean crust (Richardson et al., 1987; Schiffman and Smith, 1988; Bickle and Teagle, 1992; Gillis and Roberts, 1999). Drilling beyond the boundary between the lower dikes and upper gabbros will help trace recharge fluid compositions, estimate hydrothermal fluid fluxes (e.g., Teagle et al., 1998, 2003; Laverne et al., 2001; Gillis et al., 2005), and integrate the thermal requirements of hydrothermal alteration in sheeted dikes and underlying gabbros with the magmatic processes in the melt lens. Detailed logging of cores combined with geochemical analyses will enable determination of geochemical budgets for hydrothermal alteration (e.g., Alt et al., 1996; Alt and Teagle, 1999, 2000; Bach et al., 2003). Is there a balance between the effects of low-temperature alteration of lavas versus high-temperature hydrothermal alteration of dikes and gabbros? This is a critical check on global budgets for many elements (Mg, K, ^{87}Sr, U, and ^{18}O) presently estimated from vent fluid chemistries, riverine inputs, and thermal models (e.g., review of Elderfield and Schultz, 1996).

The discovery of microorganisms that colonize and extract energy from volcanic glass in the upper oceanic crust has added new dimensions to seafloor alteration studies. Microbial alteration of volcanic glass has been shown to decrease with basement depth at other sites (Furnes and Staudigel, 1999). The temperature and depth limits to subbasement microbiological activity remain unknown but can be investigated by

deep sampling and study of microbial alteration textures, chemical and isotopic indicators, and molecular microbiology (e.g., Blake et al., 2001; Alt et al., 2003; Banerjee and Muehlenbachs, 2003).

Principal Results of ODP Leg 206

The major objectives of Leg 206 were to establish a cased reentry hole that is open for future drilling and to achieve a target penetration in excess of 500 msb. Before basement drilling was initiated, a series of holes was drilled to thoroughly characterize the sediments and magneto- and biostratigraphy of the sedimentary overburden and to determine the casing depth into basement for the main hole. Four holes were drilled during Leg 206 with Holes 1256A, 1256B, and 1256C recovering a near-complete record of the 250 m thick sedimentary overburden. Pilot Hole 1256C penetrated 88.5 m into basement, with Hole 1256D being the cased reentry hole with a large reentry cone supported by 95 m of 20 inch casing and 269.5 m of 16 inch casing cemented into the uppermost basement. The total depth of penetration of Hole 1256D during Leg 206 was 752 mbsf, including 502 m drilled into basement. Recovery of igneous rocks was good, and excellent in places, with average recovery rates of 61.3% and 47.8% in Holes 1256C and 1256D, respectively (Wilson, Teagle, Acton, et al., 2003).

The sedimentary overburden is divided into two units: Unit I (0–40.6 mbsf) is clay rich, with a few carbonate-rich layers; Unit II (40.6–250.7 mbsf) is predominantly biogenic carbonate. The interval from 111 to 115 mbsf is rich in biogenic silica, which forms a distinct diatom mat, deposited at ~10.8 Ma. Chert nodules are a common feature below 111 mbsf, and red-brown iron oxide–rich silicified sediments that may be recrystallized metalliferous sediments are present directly over the basement (within ~1 m). The primary control on the interstitial water chemistry at Site 1256 is diffusion between seawater and basement fluids, with a continuous chert bed at 158 mbsf providing a low-diffusivity barrier. Calcareous microfossil biostratigraphy is in good agreement with magnetostratigraphy. Calculated sedimentation rates vary from ~6 to 36 m/m.y. and decrease with time as the site moved away from the high-productivity zone near the paleoequator and the cooling lithospheric plate subsided (Wilson, Teagle, Acton, et al., 2003).

Approximately 60% of the igneous basement in Holes 1256C and 1256D consists of thin (tens of centimeters to <3 m) basaltic sheet flows separated by chilled margins (Fig. F9). Massive flows (>3 m thick) are the second most common rock type, including the thick ponded flow near the top of the holes. Minor intervals of pillow lavas

(~20 m) and hyaloclastite (a few meters) and a single dike were recovered in Hole 1256D. The low proportion of pillow lavas (<10%) indicates rapid lava emplacement on low topographic relief, consistent with thermal model predictions of <1 km vertical thickness of the dike zone.

The uppermost lavas, sampled only in Hole 1256C because of setting casing in Hole 1256D, are composed of thin basaltic sheet flows a few tens of centimeters to ~3 m thick, separated by chilled margins and containing rare intervals of recrystallized sediment. Basement Units 1256C-18 and 1256D-1 each consist of a single cooling unit of cryptocrystalline to fine-grained basalt, interpreted to be a ponded lava flow and serving as a clear marker unit for correlation of the igneous stratigraphy between holes. A total of 32 m of this unit was cored in Hole 1256C, of which 29 m was recovered. This ponded flow is much thicker 30 m away in Hole 1256D, where it has a minimum thickness of 74.2 m, indicating steep paleotopography. The groundmass of the interior of the flow is fine grained but is deformed and thermally metamorphosed ~1.5 m from its base. The transition from axial eruptions to lavas that flowed out onto the ridge flanks was not determined during Leg 206. However, it was recognized that the thickness of the massive ponded flow requires significant basement relief in order to pool the lava, and this would only be developed significantly off axis (5–10 km).

The remainder of the section in Hole 1256D (with the exception of Units 1256D-3, 4a, 4c, 8c, 16d, and 21) consists of sheet flows tens of centimeters to ~3 m thick with uncommon massive flows 3.5–16 m thick. These sheet and massive flows are aphyric to sparsely phyric, cryptocrystalline to microcrystalline basalt and are distinguished by common chilled margins with fresh or altered glass.

One ~20 m thick interval of aphyric to sparsely phyric cryptocrystalline pillow basalt with glassy chilled margins was recovered from near the top of the section (Unit 1256D-3), as well as two 1.0–1.7 m thick hyaloclastite intervals (Units 1256D-4c and 1256D-21). Also recovered was a 0.3 m thick interval of volcanic breccia composed of angular fragments of cryptocrystalline basalt embedded in a matrix of altered glass (Unit 1256D-4a).

The basalts show large variations in grain size and textures from holohyaline in the outermost chilled margins of lava flows to the coarser intergranular textures in the lava pond. The basaltic lavas are dominantly aphyric to sparsely phyric, but where phenocrysts are present, olivine is the dominant phase, with subordinate plagioclase, minor clinopyroxene, and rare spinel. Measurements of petrographically fresh sam-

ples revealed general downhole variations with Mg# (= Mg/[Mg + Fe]), Cr, Ni, and Ca/Al ratios broadly increasing with depth, whereas TiO_2, Fe_2O_3, Zr, Y, Nb, V, and Sr broadly decrease with depth, although smaller-scale variations are superimposed on these trends (Fig. F9). All the Leg 206 lavas from Site 1256 plot in the N-MORB field on a Zr-Y-Nb ternary diagram.

In the lavas directly below the large massive flow, there is a sharp increase in Mg# accompanied by an increase in incompatible element concentrations (Fig. F9). The combination of high Mg# and high incompatible element concentrations argues against differentiation as the cause of the enrichments and suggests that there is variation in the primitive magma composition.

Rocks throughout Holes 1256C and 1256D exhibit a dark gray background alteration, where the rocks are slightly to moderately altered and olivine is replaced and pore spaces are filled by saponite and minor pyrite as the result of low-temperature seawater interaction at low cumulative seawater/rock ratios. Vein-related alteration manifests as different-colored alteration halos along veins. Black halos contain celadonite and result from the reaction of young ocean crust (<1–2 Ma) with distal upwelling low-temperature hydrothermal fluids enriched in iron, silica, and alkalis (Edmond et al., 1979; see summary in Alt, 1999). The iron oxyhydroxide–rich brown mixed halos are later features, which formed by circulation of oxidizing seawater. The brown halos have a similar origin and formed along fractures that were not bordered by previously formed black halos. This vein-related alteration occurs irregularly throughout Hole 1256D below the massive Unit 1 but is concentrated in two zones of greater permeability and, consequently, increased fluid flow, at 350–450 and 635–750 mbsf. The appearance of albite and saponite partially replacing plagioclase below 625 mbsf indicates a change in alteration conditions. This change may result in part because of slightly higher temperatures at depth as the lava/dike boundary is approached or from interaction with more evolved fluid compositions (e.g., decreased K/Na and elevated silica).

When compared with other basement sites, Hole 1256D (Fig. F10) contains far fewer brown, mixed, and black alteration halos. The abundance of carbonate veins in Hole 1256D is also lower than at many other sites. Site 1256 is, however, quite similar to Site 801, also in crust generated at a fast-spreading ridge, albeit 170 m.y. ago. One important feature is the lack of any oxidation gradient with depth in Hole 1256D, in contrast to the stepwise disappearance of iron oxyhydroxide and celadonite in Hole 504B and the general downward decrease in seawater effects at Sites 417 and 418. In

contrast, alteration appears to have been concentrated into different zones that may be related to the architecture of the basement, such as lava morphology, distribution of breccia and fracturing, and the influence of these on porosity and permeability. Clearly, there is greater variation in the processes of alteration occurring in the oceanic crust than is recorded at Sites 504, 417, and 418, which have served as "reference" sections to date. This illustrates the point that models for the formation and alteration of oceanic basement based on crust formed at slow and intermediate spreading rates cannot automatically be applied to crust generated at fast spreading rates.

Structures in the basement at Site 1256 include both igneous features and postmagmatic deformation. Igneous structures such as flow layering, preferred phenocryst orientation, or fine layering delineated by coalesced spherulites or vesicles are observed near the chilled margins of sheet flows but are best developed near the upper and basal margin of the massive ponded flow (Units 1256C-18 and 1256D-1). The massive ponded flow exhibits other features not observed in the rest of the hole, such as the folding of flow layering and shear-related structures, highlighting the complex internal dynamics occurring during the emplacement and cooling of this large igneous body. Folds at the top of ponded lava have gently dipping axial planes, whereas such features become steeper toward the bottom. Shear indicators, such as pull-aparts and tension gashes, now filled with late-stage magma, are more common toward the base of the ponded lava.

Brittle deformation is common throughout the upper crust sampled by Holes 1256C and 1256D and includes veins with various morphologies, shear veins, joints, and breccias. There is no systematic variation in the structural attitude (true dip) with depth, and this probably reflects the influence of other factors, such as grain size or lava morphology, rather than regional tectonics or the local stress field. Aphyric basalt in sheet flows exhibits a more irregular fracture pattern than coarser grained lavas. Shear veins indicate both normal and reversed senses of shear, suggesting the occurrence of some, although probably local, compressional components. Shear veins are most common in the massive ponded lava (Units 1256C-18 and 1256D-1) and in sheet flows from Cores 206-1256D-27R through 43R, where the geometries of the infilling fibers indicate reversed senses of shear. Brecciated rocks of different styles occur throughout the cores but are most common in the sheet flows. Textural features indicate that most breccias formed either by reworking of lava tops (both chilled and cryptocrystalline basalt) or by the fracturing of rock assisted by relatively high fluid pressures.

Basalt samples from Site 1256 show a strong tendency to have been partially or fully remagnetized during drilling, much more so than for most other DSDP and ODP sites. However, in many cases, a preoverprint component can be discerned, if not always measured accurately, with the shipboard equipment. For Hole 1256D, most samples from igneous Units 1256D-3 through 8a and 14 through 26 demagnetize to a shallow inclination, as expected for the equatorial paleolatitude. For Hole 1256C, all samples have steep inclinations and most are dominated by overprint, but a few samples from Units 1256C-3, 7, 18c, 18h, and 22 show evidence for a stable, steep component distinct from the overprint. The steep inclination may reflect eruption during the magnetic polarity transition between Chrons 5Br and 5Bn, which would imply transport of these uppermost lavas >5 km from the ridge axis.

The basement rocks cored during Leg 206 at Site 1256 show little variation in physical properties with depth. The rocks in and above the massive ponded flow (Units 1256C-1 through 18 and 1256D-1; ~276–350 mbsf) have an average bulk density of 2.89 ± 0.03 g/cm^3, which is not significantly different from the basalts below when considered together (2.8 ± 0.1 g/cm^3). However, there is a significant decrease in average density (2.7 ± 0.1 g/cm^3) for the lava flows immediately below Unit 1256D-1 from 350 to 451 mbsf (Units 1256D-2 through 8a). The average porosity of the basement rocks drilled during Leg 206 is 5% ± 3% within a total range from 2% to 19%. The average thermal conductivity (TC) of basalts from Hole 1256D is 1.8 ± 0.1 W/(m·K). V_P of discrete basalt samples from Leg 206 varies from 4.2 to 6.2 km/s (average = 5.4 ± 0.1 km/s). A notable exception to the uniform velocity structure of the upper 500 m of basement is a distinct decrease and increase in variability in V_P to 4.8 ± 0.3 km/s in the lavas immediately below the massive ponded lava (Units 1256D-2 through 4c; 350–400 mbsf). The ponded lavas have a slightly higher discrete sample V_P (5.5 ± 0.1 km/s) than most of the rocks below, which have an average V_P of 5.4 ± 0.1 km/s. Magnetic susceptibility (MS) varies from ~0 to 10,000 × 10^{-5} SI in the upper 500 m of Hole 1256D basement. The ponded lavas have an average MS of 5100 × 10^{-5} ± 900 × 10^{-5} SI, and below 350.3–752 mbsf, MS values increase systematically with depth, from ~1000 × 10^{-5} to 5000 × 10^{-5} SI, with an average MS of 3000 × 10^{-5} ± 1800 × 10^{-5} SI. Natural gamma ray measurements were rarely above background in the basement rocks of Leg 206, with the exception of a potassium-rich zone (Unit 1256C-18; 294–308 mbsf) in the massive ponded lava.

A full suite of logging tools was run in Hole 1256D following the completion of coring operations. The tools utilized, in order of deployment, were the triple combination (triple combo) tool string, the Formation MicroScanner (FMS)-sonic tool string, the

Ultrasonic Borehole Imager (UBI), and the Well Seismic Tool (WST). The logging showed that Hole 1256D was in excellent condition with no constrictions or ledges. Caliper readings from both the triple combo and the FMS-sonic tool strings show the borehole diameter to be mostly between 11 and 14 inches, with only four short intervals >16 inches. The downhole measurements and images recorded show a large amount of variation, reflecting the massive units, lava flows, pillow lavas, and hyaloclastites recovered in Hole 1256D (Fig. F9).

Predictions of Depth to Gabbros

The recognition that there is a relationship between spreading rate and the depth to axial low-velocity zones imaged by MCS experiments across the axes of mid-ocean ridges and through to the axial melt lenses is fundamental to the pursuit of the Superfast Spreading Rate Crust mission. Extrapolation of the depth to the axial low-velocity zones versus spreading rate relationship (Fig. F3) (Purdy et al., 1992) to a superfast spreading rate akin to that occurring during the accretion of crust at Site 1256 ~15 m.y. ago on the EPR (200–220 mm/y; Wilson, 1996) indicates that the melt lens would have been located at depths between ~725 and 1000 m beneath the axis. As the new plate cools and moves away from the ridge axis, it will become buried by lavas that flow short distances down the ridge slope (~1–2 km), as well as by larger lava bodies that flow significant distances (~5–10 km) off axis, such as the >74 m thick massive lava pond (Units 1256C-18 and 1256-D1) that formed the upper crust at Site 1256 or similar features recognized on the modern EPR (e.g., Macdonald et al., 1989).

In planning Expeditions 309 and 312, the depth to gabbros was estimated by assuming that the total thickness of near-axis and off-axis lavas was between 100 and 300 m, giving a total estimated depth to gabbros of between 825 and 1300 msb (Fig. F11; Table T1). Our selection of 100–300 m of lava flows comes from a number of lines of evidence. MCS experiments on the EPR estimate Layer 2A thicknesses of ~300 m in the near-axis region (Hooft et al., 1996; Carbotte et al., 1997a), although the geological nature of this seismic layer remains poorly understood. Stronger evidence comes from petrologic descriptions of the rocks from the uppermost basement at Site 1256 drilled during Leg 206. The very uppermost basement, designated during Expedition 309 as the "lava pond" (Units 1256C-1 through 18 and 1256D-1; 250–350.3 mbsf), comprises thin basaltic sheet flows a few tens of centimeters to ~3 m thick (Units 1256C-1 through 1256C-17) overlying a massive ponded flow (Units 1256C-18 and 1256D-1) of ~30 to ~74 m of fine-grained basalt in Holes 1256C and 1256D, respectively (Wilson, Teagle, Acton, et al., 2003). Although the massive flow is much thicker

in Hole 1256D than in 1256C, it is interpreted as a single lava body whose interior was liquid at the same time in both locations. The dramatic increase in thickness over 30 m of lateral distance and a total thickness in excess of 74 m required at least this much paleotopography to pool the lava. On fast-spreading ridges, such topography does not normally develop until ~5–10 km from the axis (e.g., Macdonald et al., 1989), and we suspect that these magmas flowed a significant distance off axis before ponding in a faulted depression.

Immediately underlying the lava pond is a sequence of massive flows, pillow lavas, and sheet flows (Units 1256D-2 through 15; 350.3–533.9 mbsf) grouped together as the "inflated flows." Although rocks exhibiting a number of eruptive styles are included here, the critical criteria for this subdivision is the occurrence of subvertical elongate fractures filled with quenched glass and hyaloclastite (e.g., Sections 206-1256D-21R-1 and 40R-1) at the top of the lava flows. These features indicate flow-lobe inflation, which requires eruption onto a subhorizontal surface with less than a few degrees slope (Umino et al., 2000, 2002); therefore, it is unlikely that such lavas formed directly at the ridge axis. Such inflation features are not observed in cores deeper in Hole 1256D. Taken together, the cumulative thickness of the lava pond and the inflated flows is ~280 m, close to our preferred estimate of ~300 m for the thickness of off-axis lava flows.

Seismic data from the site survey Cruise EW9903 offer significant clues about the expected downhole lithologic variations. The velocity-depth function inferred from seismic refraction (Fig. F7) (A. Harding, unpubl. data) shows a uniform gradient from ~4.8 km/s at the sediment/basement interface to 5.3 km/s at ~600 msb, with the gradient then sharply increasing and velocity reaching 5.9 km/s at ~800 msb. The gradient abruptly returns to a moderate value, with velocity of 6.5 km/s at ~1250 msb. The gradient decreases gradually, with nearly uniform velocity of ~6.8 km/s between 2000 and 3000 msb. MCS reflection data (Fig. F6) (Hallenborg et al., 2003) show several nearly horizontal reflections with kilometers of horizontal extent to nearly 5.5 s travel time, or ~800–900 msb. For the upper ~800 m, the relatively lower velocities and horizontal reflection character suggest that flows constitute a substantial fraction of the uppermost crust at Site 1256. At greater depth, the decrease in velocity gradient below ~1250 msb marks the seismic Layer 2/3 boundary. Unfortunately, the gradual nature of the change in gradient means that the depth of this transition cannot be assigned a depth more precisely than 1250–1500 msb. Whether this boundary corresponds the presence of gabbro remains to be tested.

OPERATIONS

Port Call

The *JOIDES Resolution* arrived at Puerto Cristobal, Panama, and dropped anchor at 0752 h on 8 July 2005. The ship was advised that the berth at PIMPSA terminal in Balboa was not available, and the port call activities were moved to San Cristobal. The vessel was moved to Pier 7A, and Expedition 309 began with first line ashore at 1420 h on 8 July. Port call was concluded with last line released at 1620 h on 12 July.

Transit to Site 1256

The last line away from Berth 7A, Cristobal, Panama, was cast at 1620 h on 12 July 2005, and the vessel was under way through the Panama Canal, exiting the Miraflores Locks (**iodp.tamu.edu/scienceops/gallery/exp309/Panama_canal**). The ship passed under the Bridge of the Americas on 13 July and began the transit to Site 1256. The transit was relatively benign, with the ship rolling/pitching moderately while averaging 10.1 kt over the 822 nmi distance. The vessel arrived at Site 1256 and thrusters were lowered at 1030 h on 16 July. The vessel was placed in dynamic positioning mode by 1100 h (Table **T2**).

Hole 1256D

Predrilling Logging Operations

A bottom-hole assembly (BHA) consisting of a logging bit and 10 drill collars was assembled, marking the beginning of operations for Expedition 309. The drill string was assembled to a depth of 2467 meters below rig floor (mbrf), and the vibration isolated television (VIT) camera was launched to monitor reentry. Hole 1256D was located, the ship was offset 50 m northwest, and the positioning beacon was dropped at 1930 h on 17 July 2005. Hole 1256D was reentered at 1945 h (Movie **M1**), and the drill string was lowered to a depth of 4370 mbrf, at which point it began taking weight, indicating ~27 m of fill.

The drill string was raised to a depth of ~4368 mbrf, and the top drive was picked up. The Water Sampling Temperature Probe (WSTP) was lowered into the drill string to obtain a water sample and temperature measurement at 724.6 mbsf (4369.6 mbrf). The water sample was found to be murky, and low salinity (26‰) indicated the filters had become clogged with silt before the sampler was completely purged of nanopure

water. The WSTP temperature measurement gave a flat-line temperature of 60°C because of a software failure in the tool. It was decided to run the WSTP again to get a better water sample. While the WSTP was cleaned for its second run, the APCT tool was deployed to obtain accurate temperature readings above 60°C. Temperature at 712.6 mbsf was 64.5°C and at 724.6 mbsf was 65.8°C. The second run of the WSTP, taken at 4357.6 mbrf, returned a good water sample.

The bit was raised to 3907 mbrf, and preparations were made for logging. Hole 1256D was logged using the triple combo and the FMS-sonic tool strings to determine hole condition and gauge prior to beginning coring operations. The Schlumberger logging tools were lowered into the drill string at 0030 h on 18 July. The hole was logged from 724.4 mbsf to casing depth. The tools were removed from the drill string at 0530 h on 19 July. The logging BHA was then retrieved, and an RCB coring assembly was prepared.

Basement Coring in Hole 1256D

At 2325 h, Hole 1256D was reentered with an RCB assembly. The drill string was lowered to a depth of 4370 mbrf, and a center bit was dropped. The hole was then washed and reamed to a depth of 4395 mbrf, when the bit began taking weight. The center bit was pulled, and the first core barrel was dropped. A 50 bbl mud sweep was circulated, and coring operations began (Table T2). The hole was cored without incident to a depth of 4466.5 mbrf (821.1 mbsf). The bit accumulated a total of 51.7 rotating hours and was in relatively good condition. To minimize the risk of downhole bit failure and to ensure that the hole diameter was in gauge, it was decided that subsequent bits would be changed approximately every 50 h (Table T3).

The drill string was redeployed and reentered Hole 1256D at 1911 h on 22 July 2005 with a new CC-9 bit. The bit was lowered to bottom, and coring was resumed at 2330 h that day. Core 309-1256D-86R was recovered with 3.65 m recovery, but all the core catcher dogs were missing and it appeared that some of the core had fallen out of the core barrel. The next core barrel was dropped, and high pump pressures were noted. The barrel was pulled, and a deplugger was deployed twice to clear any obstructions. A core barrel was dropped again, and pressures had returned to a normal range. Coring was resumed at 1045 h on 23 July. The bit was pulled after Core 309-1256D-96R with 52.1 rotating hours.

After the drill string was recovered, a new bit was deployed and the drill string reentered Hole 1256D at 1610 h on 26 July. The drill string began taking weight at 4525

mbrf. The top drive was picked up, and the hole was washed and reamed to bottom. The hole was cored without incident from 4543.2 to 4604.2 mbrf (897.8–958.8 mbsf). Penetration rates and recovery dropped through this cored interval. The bit was pulled after 52.8 rotating hours.

The drill string was recovered and a new bit deployed. The bit was lowered to a depth of 3640 mbrf, and the WSTP was deployed to obtain a bottom seafloor water sample and temperature measurement. The WSTP was then recovered, and Hole 1256D was reentered at 1015 h on 30 July. The bit was lowered to a depth of 4514 mbrf. The top drive was picked up, and the hole was reamed to bottom. Coring resumed at 4604.2 mbrf (964.8 mbsf). Coring continued without incident to a depth of 4619.8 mbrf (Core 309-1256D-110R). After retrieving this core and dropping the next core barrel, the driller noticed a pressure drop of 200–250 psi. The core barrel was pulled and depluggers were dropped twice in attempts to clear the bit throat. Pressures were still lower than normal.

While retrieving Core 309-1256D-111R, the driller again noticed pressure drops of 200–250 psi when lifting the BHA off bottom. The pressure increased when weight was applied to the bit, indicating that there was a crack in the BHA, and the drill string was retrieved. Major damage was clear to the 8.5 inch bit sub assembly ~15 inches from the bit (Fig. F12). A straight horizontal gash had opened for ~150° (11 inches) of the circumference of the ¾ inch thick bit sub wall, with more ragged fracture tips propagating a further ~75° around the pipe from each end of the clean fracture. When in tension with the drill bit hanging from the sub, the fracture opened up to 1 cm and the bit was held on by only ~4.25 inches of the bit sub wall. Such a failure of the bit sub assembly had not been witnessed before in the shipboard memory of scientific ocean drilling, and the rapid diagnosis and response of the Transocean operations team certainly averted a time-consuming major equipment loss in Hole 1256D. Bit number 4 was pulled after only 17.8 rotating hours and had cored 20.4 m.

The drill string was recovered and a new bit deployed. Hole 1256D was reentered on 1 August. The bit was lowered to a depth of 4514 mbrf. The top drive was picked up, and the hole was reamed to bottom. Coring resumed at 4624.6 mbrf (979.2 mbsf). Mud sweeps were increased to 50 bbl to ensure cutting removal. Bit number 5 was pulled on 4 August with 50.1 rotating hours.

Hole 1256D was reentered for the seventh time on 5 August. The bit was lowered to a depth of 4657 mbrf. The top drive was picked up, and the hole was reamed to bot-

tom. Coring resumed at 1430 h on 5 August at 4696.7 mbrf (1051.3 mbsf). Bit number 6 was pulled on 8 August with 50.8 rotating hours.

The drill string was recovered and a new bit deployed. Hole 1256D was reentered at 0148 h on 9 August. The bit was lowered to a depth of 4715 mbrf (1069.6 mbsf). The top drive was picked up, and the hole was reamed to bottom. Coring resumed at 0800 h on 8 August at 4754.3 mbrf (1108.9 mbsf). While cutting Core 309-1256D-146R, the driller noticed a 100 psi pressure drop. The drill string was pulled off bottom, and a 350 psi drop in pressure was noted. Core 309-1256D-146R was recovered at 1330 h on 11 August after a 3.0 m advance and a recovery of 3.5 m. After dropping another core barrel, the pressures remained 350 psi lower than normal. It was suspected that there was another crack in the BHA. The decision was made to pull the drill string and inspect the BHA for cracks. When the bit cleared the reentry cone, the vessel was repositioned ~50 m from the cone.

The BHA was on deck at 2300 h on 11 August. All drill collars and subs were inspected for cracks. Bit number 7 was pulled after 42.5 rotating hours. With no cracks in the BHA found, a new bit was made up to the drill string and the drill string was again lowered. One stand of 5½ inch transition pipe was laid out, as well as the tapered drill collar and crossover sub because of excessive wear at the connections.

A core barrel was dropped into the BHA while running in with bit number 8. The drill string was filled with seawater every 25 stands, and the pressure was checked. Pump pressure increases were noted at 25 and 50 stands, but there was no further pressure increases with 75 and 100 stands deployed, indicating there might be a crack in the drill string above the BHA. The VIT camera was lowered when 100 stands were below the rotary table. A pill of high-viscosity mud was pumped as a tracer as the camera was lowered. The camera passed through very cloudy water just above the BHA, indicating that mud had exited the drill pipe somewhere and drifted down. The camera was pulled up above the BHA, and another mud pill was circulated. As the VIT camera was again lowered toward the BHA, a vigorous jet of drilling mud was observed streaming from the 5 inch pipe (Movie M2) about two stands above the 5½ inch transition pipe. The drill string was pulled back up to the rig floor, the crack was found in the 5 inch pipe, and the bottom two stands of 5 inch drill pipe were replaced (Fig. F13).

The drill string was again lowered below the rotary table. Hole 1256D was reentered for the ninth time at 0230 h on 13 August (Movie M3). A core barrel was dropped,

and coring resumed at 0730 on 13 August. Bit number 8 was pulled on 16 August after 57.8 h of coring.

The drill string was recovered and a new bit deployed. Hole 1256D was reentered at 0304 h on 17 August, a core barrel was dropped, and coring resumed. The ninth and final RCB coring bit of Expedition 309 was pulled on 20 August. A mud sweep was pumped before the final core barrel was retrieved at 1100 h on 20 August. The bit was pulled to the casing shoe and lowered back to bottom. No fill was encountered. A mud sweep was pumped around, and the drill string was pulled out of the hole. Bit number 9 was pulled after 53.1 rotating hours.

Postdrilling Logging Operations

A logging BHA was made up, and the hole was reentered at ~0800 h on 21 August. The bit was set at 3905.5 mbrf (260.1 mbsf), ~9 m above the casing shoe, and preparations were made for logging Hole 1256D.

The first logging run with the triple combo tool string started taking weight ~29 m above bottom, at 4871 mbrf (1225.6 mbsf). The logging run started at this depth and continued to 4200 mbrf (554.6 mbsf). This allowed for full coverage of the section drilled during Expedition 309 and approximately the bottom 200 m of the original hole from Leg 206. The FMS-sonic tool string was rigged up and lowered into the hole. The FMS was unable to pass 4868 mbrf (1222.6 mbsf). The tool logged up to 4300 mbrf (654.6 mbsf). Attempts to close the arms and lower the tool to log the entire length of the hole failed. The FMS was pulled out of the hole, encountering ~700 lb overpull while entering the drill pipe. When the tool exited the drill pipe, the arms were in the open position. The arms were manually closed, and the tool was laid out.

The third logging run utilized the UBI. The UBI was deployed with a sinker bar to enhance deployment speed. The UBI encountered fill at 4865 mbrf (1219.6 mbsf) and logged up to 4745 mbrf. The fourth logging run was to be a vertical seismic profile utilizing the three-component WST and the generator-injector air gun. The tool was lowered into the drill pipe at 0400 h on 23 August. The tool began taking weight at 3920 mbrf (274.6 mbsf) and was worked down to 4020 mbrf (374.6 mbsf) but could not be lowered any further. The tool was pulled out of the hole, taking 800 lb of overpull to enter the drill pipe. When the tool reached the surface, several kinks were noted in the Schlumberger wireline cable. A total of 60 m of wireline cable was cut, and the cable was reheaded. The back-up FMS tool was rigged up, function tested, and lowered into the hole for a log of the complete hole. The tool was unable to pass 4861

mbrf (1215.6 mbsf). The tool logged up to 3950 mbrf (304.6 mbsf). Following the completion of the FMS-sonic log, the wireline heave compensator was tested to evaluate the performance of the new drum-compensator and compare it to the performance of the older Lamont-Doherty Earth Observatory wireline compensator. The tools were pulled out of the drill string and were laid out.

Transit to Balboa

The ship was secured for transit and was under way at 1300 h on 24 August 2005. The transit was relatively benign with the ship rolling/pitching moderately while averaging 10.1 kt over the 822 nmi distance. The *JOIDES Resolution* arrived at Balboa, Panama, at 0000 h on 28 August. The ship was at anchorage by 0029 h.

SCIENTIFIC RESULTS

Expedition 309, Superfast Spreading Rate Crust 2, successfully deepened Hole 1256D by 503 m to a total depth of 1255.1 mbsf, or 1005.1 msb. At the end of Expedition 309, Hole 1256D penetrates a total of >750 m of extrusive lavas and proceeds a further 250 m into a region dominated by intrusive rocks. At 1255 mbsf, Hole 1256D is tantalizingly close to the predicted minimum estimated depth for the frozen axial magma chambers (1275 mbsf; Fig. F14). Following the completion of a comprehensive wireline logging program, Hole 1256D was successfully exited and left clear of equipment with only minor unconsolidated fill at the bottom of the hole. Hole 1256D is in excellent condition and ready for deepening.

Expedition 309 (July–August 2005) will be followed closely by Expedition 312 (November–December 2005), which will continue to deepen Hole 1256D. Despite our grueling pace of advance (~15 m/day), progress with deepening Hole 1256D was steady (Fig. F14). Optimistically anticipating the same benign drilling conditions and good fortune, assured of highly astute rig floor operations, Expedition 312, with 37 days of drilling operations, is set to deepen Hole 1256D by a further 500 m. This is well beyond the depths where geophysical interpretations predict gabbros to occur (~1275–1525 mbsf; Fig. F14; see "Predictions of Depth to Gabbros" and "Background and Objectives").

Predrilling Experiments

The first scientific operation of Expedition 309 was to deploy the wireline WSTP to collect a sample of the fluid at the bottom of Hole 1256D and measure the ambient thermal conditions in the hole using the Advanced Piston Corer Temperature (APCT) and Temperature/Acceleration/Pressure (TAP) tools. The WSTP was followed by wireline logging runs using the triple combo and FMS-sonic tool strings to assess the condition and caliper of the hole and check for borehole wall breakouts and unstable regions. There was ~27 m of loose fill in the bottom of Hole 1256D that precluded running the wireline tools to the full depth of the hole (752 mbsf).

The temperature profile made with the TAP tool on the triple combo shows a steady increase in temperature from the base of the casing (269 mbsf) to a maximum temperature of 67.5°C recorded at the deepest logging depth (~725 mbsf). Heat flow measured in the sedimentary section of Hole 1256B to a depth of 158 mbsf was 113 mW/m² (Wilson, Teagle, Acton, et al., 2003). In the basement section in Hole 1256D, TC averaged 2.0 W/(m·K) in the ponded lava flow above 350 mbsf and 1.7 W/(m·K) below 350 mbsf. For uniform heat flow of 113 mW/m² downhole, these conductivities predict a thermal gradient of 0.056 K/m above 350 mbsf and 0.067 K/m below 350 mbsf. These predictions are reasonably close to the observed gradients of 0.067 and 0.071 K/m, probably within uncertainties of the TC measurements and the inevitable slight disturbance of the ambient hole temperature due to the passage of the drill string and wireline tools. This suggests that there is little advection of heat by fluid in the Site 1256 basement or major vertical fluid movements in Hole 1256D.

The 67.5°C deep borehole fluid collected from the bottom of Hole 1256D (~725 mbsf) is chemically very distinct from seawater. Relative to Site 1256 bottom seawater, the borehole fluid is hotter, slightly more neutral (pH = ~7.4), and has significantly lower alkalinity (0.85 mM). Salinity is unchanged (35‰). The largest changes are in the concentrations of dissolved ions with major reductions in the concentrations of boron (–18%), sulfate (–19%), potassium (–41%), lithium (–47%), and magnesium (–55%). In contrast, the strontium concentration is slightly increased (18%), and the calcium content is very strongly elevated (415%). The deep borehole fluid is also significantly different from the composition of the ~35°C uppermost (~250 mbsf) basement fluid estimated from pore water chemical gradients measured at Site 1256 during Leg 206 (Wilson, Teagle, Acton, et al., 2003). The deep borehole fluid has lower Li (–15%), Mg (–25%), and K (–30%) concentrations but higher dissolved silica (14%), sulfate (84%), and calcium (122%) concentrations relative to the uppermost basement fluid.

When the deep borehole fluid is compared to the well-characterized basement fluids from the eastern flank of the Juan de Fuca Ridge (Elderfield et al., 1999), most ions are present in concentrations similar to those predicted for a 67.5°C fluid. The exception is the Mg concentration of the deep borehole fluid, which at ~24 mM is higher than would be expected for a fluid reacted with basement at >60°C. The disagreement between the concentration of Mg in hot deep borehole fluids and that predicted from uppermost basement fluids or laboratory experiments has previously been noted for wireline fluid samples recovered from Hole 504B (e.g., Becker, Foss, et al., 1992). However, the chemistry of the deep borehole fluid from Hole 1256D is closer to equilibrium than the most pristine borehole fluids, which were taken from the deepest available points in Hole 504B during the different drilling expeditions there. Those fluids have Mg concentrations similar to those of the uppermost basement fluid at Site 504. In contrast, the fluid from the bottom of Hole 1256D has Ca (and Li and K) concentrations close to those expected for a fluid in chemical equilibrium with 67.5°C basement and, unlike Hole 504B, the Mg concentration is at least partially decreased toward the predicted composition.

The primary purpose of the initial logging operations was to check Hole 1256D for borehole wall breakouts and variations in hole diameter though comparison with measurements made at the end of Leg 206. The initial phase of wireline logging indicated that, before the commencement of drilling, the borehole conditions in Hole 1256D are excellent, and no ledges or obstructions were encountered. Caliper readings from both the triple combo and FMS-sonic tool strings show good borehole conditions, with a diameter typically between 10 and 12 inches. The FMS-sonic tool string followed a different pathway during the Expedition 309 pass compared with the Leg 206 passes, and consequently, in many intervals the FMS image coverage of the borehole wall has increased. Sonic velocities measured by the Dipole Sonic Imager appear to be of high quality. Several narrow zones (at 517, 597, 602, and 685 mbsf) with strong differences in the orthogonally arranged calipers on the FMS-sonic tool were identified during both Leg 206 and Expedition 309. These intervals may correspond to borehole breakouts, and the north–south orientation of the borehole enlargements suggests a west–east maximum stress direction. A tight spot recognized on Leg 206 at 486 mbsf was also recorded during the Expedition 309 predrilling passes, and a new zone was identified at 472 mbsf (9.3 inches).

Ocean Crust formed at Superfast Spreading Rate: Deep Drilling the Ocean Basement in Hole 1256D

Hole 1256D was reentered with a rotary core barrel (RCB) assembly and CC-9 coring bit at 2325 h on 18 July 2005, and ~27 m of loose fill was cleared from the bottom of the hole so that it was open to the full depth achieved during Leg 206 (752 mbsf; 502 msb). Rotary coring of the basement continued until 20 August (~33 days), when the hole was conditioned for wireline logging operations. A total of nine CC-9 RCB hard-formation coring bits were used, and Hole 1256D was deepened by ~503 m to 1255.1 mbsf (~1005.1 msb; Cores 309-1256D-75R through 170R). Drilling proceeded without core liners from Core 309-1256D-91R to stop the jamming of fractured basalt in the core liner sleeve and core liner, which sometimes prevented the capture of additional core. Because of the slow penetration rates, often less than 1 m/h, we recovered the core barrel after every 4–5 m advance from Core 309-1256D-103R. Including wireline time, reaming, hole-cleaning, and other drilling activities, a rough approximation of daily progress at ~15 m/day may be useful for planning future deep drilling of the oceanic basement and a target for progress during Expedition 312 (Fig. F14).

At 1005 msb, Hole 1256D is the fourth deepest hole drilled into oceanic basement since the launch of scientific ocean drilling in 1968 and the second deepest penetration into in situ ocean crust (Fig. F15). Hole 504B, deepened during seven DSDP and ODP legs into 6.9 Ma crust on the southern flank of the intermediate-spreading Costa Rica Rift, remains the deepest penetration of in situ ocean crust. Prior to Expedition 309, Hole 504B was the only hole to sample a complete sequence of extrusive rocks as well as the transition from extrusive rocks to sheeted dikes (Alt, Kinoshita, Stokking, et al., 1993).

Preliminary Subdivision of the Upper Oceanic Crust at Site 1256

To facilitate description and discussion of the crustal stratigraphy at Site 1256 and assist in the interpretation of cores recovered during Expedition 309, we present a preliminary subdivision of the upper crust sampled so far in Hole 1256D (Table T4; Fig. F16). Detailed descriptions are presented in the following sections. These subdivisions were suggested principally from igneous stratigraphy and were made before the wireline logging was undertaken. As such, they should be considered with the proviso that the boundaries suggested are preliminary and that they may change as further information becomes available.

The upper crust at Site 1256 can be portioned into five basement subdivisions, which, in descending order down the hole, are the lava pond, inflated flows, sheet and massive flows, transition zone, and sheeted intrusives (Table T4). The uppermost two zones were cored during Leg 206, as was the upper ~220 m of the sheet and massive flows.

Lava Pond

The lava pond caps the uppermost crust at Site 1256. This domain includes Units 1256C-1 through 18 and 1256D-1 (~250–350.3 mbsf). The uppermost lavas were not recovered in Hole 1256D because 16 inch casing was set 19.5 m into basement and the interval was not cored. In Hole 1256C, the rocks immediately below the sediments comprise thin basaltic sheet flows a few tens of centimeters to ~3 m thick separated by chilled margins and rare intervals of recrystallized sediment (Units 1256C-1 through 1256C-17). The massive ponded flow, sensu stricto (Units 1256C-18 and 1256D-1), is defined at its top by a ~75 cm rind of glassy to cryptocrystalline aphyric basalt that overlies ~30 to ~74 m of fine-grained basalt in Holes 1256C and 1256D, respectively. The massive ponded flow becomes abruptly cryptocrystalline ~1.5 m from the base of the flow. Although the massive flow is much thicker in Hole 1256D than in 1256C, it is interpreted as a single lava body whose interior was liquid at the same time in both locations. The dramatic increase in thickness over 30 m of lateral distance and a total thickness in excess of 74 m indicates that there was at least this much paleotopography in order to pool the lava. On fast-spreading ridges, such topography does not normally develop until ~5–10 km from the axis (e.g., Macdonald et al., 1989), and we suspect that these lavas flowed a significant distance off axis before ponding in a faulted depression.

Inflated Flows

Immediately underlying the lava pond is a sequence of massive flows, pillow lavas, and sheet flows (Units 1256D-2 through 15; 350.3–533.9 mbsf) grouped together as the inflated flows. Although rocks exhibiting a number of eruptive styles are included here, the critical criterion for subdivision is the occurrence of subvertical elongate fractures filled with quenched glass and hyaloclastite (e.g., Sections 206-1256D-21R-1 and 40R-1) at the top of the lava flows. These features indicate flow-lobe inflation that requires eruption onto a subhorizontal surface at less than a few degrees (Umino et al., 2000, 2002).

35

Sheet and Massive Flows

The bulk of the extrusive lavas at Site 1256 are included in the sheet and massive flows (Units 1256D-16 through 39b; 533.9–1004.2 mbsf). A total of 218 m of this subdivision was drilled during Leg 206, with a further 252 m of penetration during Expedition 309. This sequence consists of sheet flows tens of centimeters to ~3 m thick with subordinate massive flows >3 to 16 m thick and uncommon breccias. The flows are aphyric to sparsely phyric, cryptocrystalline to microcrystalline basalts. Units are distinguished by the presence of chilled margins or by grain-size variations. Throughout this interval, glassy chilled margins are common.

Transition Zone

It is the very essence of a transitional sequence that boundaries are loosely defined and subjective. In Hole 1256D, the transition zone from Units 1256D-40 through 44a (1004.1–1060.9 mbsf) is identified by the occurrence of a number of criteria and different rock types as opposed to the appearance of one specific feature. Shore-based analysis of wireline logs and further petrographic and geochemical investigations will help refine the boundaries of this zone. Most of the rocks within the transition zone are aphyric, cryptocrystalline sheet flows. The top of the transition zone is marked by a cataclastic massive unit (Section 309-1256D-117R-1, 85 cm). This comprises subvertically oriented cryptocrystalline basalt clasts hosted within a very highly altered fine-grained basalt that has been incipiently brecciated and deformed along numerous fine veins and cataclastic stringers. Core 309-1256D-120R (~1018 mbsf) includes the first sign of a subvertical intrusive contact other than the single occurrence further upcore in Section 206-1256D-32R-2 at ~475 mbsf. Dike chilled margins become more common downhole, although extrusive textures and vesicles are still encountered. It should be noted that subvertical fracture sets possibly indicative of diking into the host rocks near Hole 1256D are common from ~900 mbsf. Breccias of various styles are common in the transition zone, including a spectacular mineralized volcanic breccia that comprises Unit 1256D-42a (interval 309-1256D-122R-1, 20 cm, to 122R-2, 30 cm; ~1028 mbsf). In the transition zone, secondary mineral assemblages (chlorite-smectite, albite, chlorite, actinolite, anhydrite ± minor prehnite, epidote, and laumonite) indicative of hydrothermal alteration at subgreenschist to greenschist facies temperatures start to become more common.

Sheeted Intrusives

The upper boundary to the sheeted intrusives is defined by a change from sheet flows to massive basalts at 1060.9 mbsf (Unit 1256D-44a; Core 309-1256D-129R). From that level, subvertical intrusive contacts are common, and these can be sharp or irregular and lobate, the latter style indicating the intrusion of magma into hypersolidus rocks (e.g., interval 309-1256D-149R-1, 30–97 cm; 1156 mbsf). Extrusive rocks could be present in this domain, although there are no unambiguous indicators of eruption. Groundmass grain sizes vary from glassy to microcrystalline, although a few samples deeper in this subdivision are fine grained with holocrystalline doleritic textures. No fresh glass was found in the sheeted intrusives, but altered glass is present along some dike chilled margins and associated breccias. There is a step change in physical properties with significant increases in average TC (from 1.8 ± 0.2 to 2.1 ± 0.1 W/[m·K]) and seismic velocity (5.4 ± 0.3 to 5.8 ± 0.1 km/s). The average porosity of massive basalts decreases from 4% ± 1% to 2% ± 1% across the 1060.9 mbsf boundary. Whether the massive basalts that are the dominant host rock of the sheeted intrusives are dikes or sills remains uncertain. Unfortunately, an unambiguous subvertical contact that grades continuously from a glassy chilled margin to a microcrystalline to fine-grained massive basalt has so far not been recovered.

Igneous Petrology

Basement rocks recovered during Expedition 309 in Hole 1256D from 752 to 1255 mbsf were divided into 39 igneous units (Units 1256D-27 through 65), labeled continuously from the last rocks recovered during Leg 206 (Table **T5;** Fig. **F17**) (Wilson, Teagle, Acton, et al., 2003). The basement cored during Expedition 309 has been divided into three crustal sections: the sheet and massive flows, which continue from Leg 206, a lithologic transition zone, and the sheeted intrusives (Fig. **F16**).

The sheet and massive flows (Units 1256D-16 through 39; 533.9–1004.1 mbsf) are mainly composed of sheet flows and massive flows. Sheet flows (with individual cooling units ranging from tens of centimeters to <3 m thick) make up 80% of the total sheet and massive flows cored during Leg 206 and Expedition 309. However, in the portion of this subdivision drilled during Expedition 309, sheet flows account for only 65% of the rock recovered, indicating a greater prevalence of massive flows deeper in the section. Individual flows are commonly separated by chilled margins containing altered or fresh glass. Where contacts were not recovered, individual flows could be distinguished by systematic changes in grain size. Using these criteria, minimum thicknesses of individual flows or cooling units range between 0.11 and 1.68

m with an average thickness of 0.55 m ± 0.35 m. The flows are predominantly aphyric (<1% phenocrysts), and grain size ranges from glassy at the chilled margins to cryptocrystalline or microcrystalline (Fig. F18). Rare sheet flow interiors are fine grained. The groundmass of sheet flows generally consists of plagioclase and clinopyroxene microlites, with interstitial titanomagnetite and altered glass, similar to those described during Leg 206. Where phenocrysts occur (for example in Units 1256D-28, 35b, and 37), these rocks have plagioclase, clinopyroxene, and olivine phenocrysts, in order of decreasing abundance, commonly clustered in a glomeroporphyritic texture (Fig. F19). Unit 1256D-35c contains three small (0.5–2.2 cm) holocrystalline gabbroic xenoliths (intervals 309-1256D-107R-1, 44–52 cm, 108R-1, 20–36 cm, and 108R-1, 132–138 cm) consisting of fine-grained olivine, plagioclase, and clinopyroxene (Fig. F20).

In contrast to the thinner sheet flows, minimum thicknesses of the massive flow units vary from 3.2 to 11.3 m with an average of 6.3 m (cumulative thickness calculated using only the pieces recovered). The thickest, Unit 1256D-31, consists of a single cooling unit of fine-grained basalt below a 12 cm cryptocrystalline to microcrystalline upper contact (Fig. F21). A total of 26 m of this unit was cored, of which 11.3 m was recovered. In contrast to the sheet flows, fine-grained rocks are more common in the massive lavas (Fig. F17). The massive flows are aphyric and nonvesicular, with the exception of Subunit 1256D-39a. This basalt is sparsely clinopyroxene-olivine-plagioclase-phyric and is moderately vesicular (8%) (Fig. F22). Thin section observations show that the most finely grained rocks collected from the massive flows have intergranular to intersertal groundmass textures (Fig. F23).

The transition zone (Units 1256D-40 through 43; 1004.1–1060.9 mbsf) is characterized by increasing abundance of volcanic breccias interbedded within sheet flows. The top of this zone is defined by the cataclastic massive unit (Unit 1256D-40; interval 309-1256D-117R-1, 85 cm, through 118R-1, 66 cm). The upper part of this unit (interval 309-1256D-117R-1 [Pieces 9–14, 97–142 cm]) has a complex structure with fine- to medium-grained basalt in contact with brecciated clasts of cryptocrystalline basalt (Fig. F24). The fine- to medium-grained basalt contains highly altered glass clasts and is disrupted by an intensive network of thin chlorite-smectite veins imparting an incipient cataclastic texture. Thin section examination of these rocks (Sample 309-1256D-117R-1, 122–125 cm) shows that fractured crystals have a seriate texture, deformed and cemented by a banded matrix that shows flow structures. With increasing distance below the top of the unit, the igneous texture is better preserved and more homogeneous, mesostasis is less abundant, and crystals are less fractured (inter-

vals 309-1256D-117R-2, 9–72 cm, through 118R-1, 0–66 cm). In this lower part of Unit 1256D-40, the cataclastic massive unit consists of fine-grained dolerite with a partially developed subophitic texture (interval 309-1256D-117R-2, 23–26 cm). A few pieces, similar to the disrupted rocks of the upper part of this cataclastic unit, occur in intensively veined sheet flows in Units 1256D-37 and 41. This may support the interpretation that these disrupted rocks indicate the nearby presence of a dike or fault zone. Interval 309-1256D-120R-1, 9–26 cm, of the transition zone, however, captures the first unambiguous subvertical intrusive contact.

A second type of breccia is present in interval 309-1256D-122R-1, 25 cm, through 123R-1, 109 cm, where 2.8 m of mineralized volcanic breccia and breccia intercalated with basalt was recovered and defines Unit 1256D-42 (Fig. F25). This unit can be further subdivided based on abundance of basaltic rocks. The upper part, Subunit 1256D-42a, consists solely of volcanic breccia (interval 309-1256D-122R-1, 25–149 cm, through 122R-2, 0–30 cm), but in Subunit 1256D-42b, the breccias are intercalated with aphyric, cryptocrystalline to microcrystalline basaltic sheet flows. These breccias comprise angular to subangular aphyric cryptocrystalline basaltic clasts (0.5–4.5 cm) and subangular to elongate clasts of altered glass with rare flame-shape clasts (0.1–1.5 cm), cemented by chalcedony, saponite, calcium carbonate, albite, anhydrite, and sulfides (Fig. F25).

The transition zone also hosts the last occurrence of a glassy margin not associated with either a dike contact or clastic brecciation. This margin was recovered in the lower half of sheet flow Unit 1256D-43 (~1060 mbsf).

The upper boundary to the sheeted intrusives (Units 1256D-44 through 65; 1060.9–1255.1 mbsf) is defined by a distinct change from sheet flows to massive basalts at 1060.9 mbsf. Extrusive rocks could be present in this section, but evidence for eruption remains ambiguous. The massive basalts are most commonly aphyric and nonvesicular. Most rocks are microcrystalline (Units 1256D-44 through 46, 49 through 50, 52A, 54 through 55, and 59 through 65) and fine-grained (Units 1256D-47, 48, 51, and 53a) basalts, but rare units are cryptocrystalline to microcrystalline (Units 1256D through 56a, 57a, and 58) basalt. Thin sections of the massive basalts show holocrystalline and commonly doleritic groundmass textures (Fig. F26).

In contrast to shallower in Hole 1256D, subvertical intrusive contacts, thought to be dikes, are common, suggesting that the massive basalts of the sheeted intrusives represent the beginning of the sheeted dike complex. In general, two types of contacts

can be distinguished: sharp or irregular direct contacts and brecciated contacts. Most contacts belong to the latter category, with brecciated zones one to several centimeters wide along the contact. All contacts have developed chilled margins. The chilled margins of the dikes are composed of glassy to cryptocrystalline aphyric basalts that have quenched against cryptocrystalline to fine-grained, massive basaltic hosts. Breccias at the contacts comprise fragments of altered glass initially quenched at the chilled margin with subordinate, angular to subangular clasts of the host rock and cemented by anhydrite, chlorite, and sulfide (Fig. F27). One spectacular example is a >50 cm long vertical contact in interval 309-1256D-140R-1, 26–80 cm (Unit 1256D-47), with a sulfide-impregnated dike margin breccia with complex intrusive relationships and intricate multiple margin-parallel sulfide veins crosscut by anhydrite veins.

In interval 309-1256D-155R-1 (Piece 20, 84–90 cm), the chilled margin forms a convex lobe, indicating that the host rock was not rigid during the intrusion (Fig. F28A). Further evidence for multiple intrusions are seen in Sections 309-1256D-161R-1 to 161R-2 (Unit 1256D-56b), where at least two intrusions are present. An inner sparsely clinopyroxene-olivine-plagioclase phyric dike has intruded a sparsely clinopyroxene-olivine-plagioclase-phyric spherulitic cryptocrystalline rock, itself chilled against an aphyric microcrystalline host rock (Fig. F28B). Another example of dike intrusion into a ductile host rock is observed in interval 309-1256D-163R-1, 113–122 cm. This contact is lobate and highly complex with fractured pieces of the chilled margin dispersed in the host rock (Fig. F28C).

The overall mineralogical characteristics of basement drilled during Expedition 309 are similar to Leg 206 basalts, although there are some important differences. More than 60% of the basalts drilled during Leg 206 are sparsely phyric with olivine, plagioclase, and clinopyroxene phenocrysts (Wilson, Teagle, Acton, et al., 2003), and the proportion of aphyric basalts is <40% for Leg 206. In contrast, the vast majority of basalts recovered during Expedition 309 are aphyric (>80%) (Fig. F29). This difference is demonstrated by the downhole variation of phenocryst contents and by a decrease with depth of the total phenocryst content (Fig. F17). More than half of Leg 206 basalts have three major phenocryst phases (clinopyroxene, olivine, and plagioclase), whereas only rare samples (eight) of the Expedition 309 basalts have more than two phenocryst phases (Fig. F29). Phenocryst-bearing basalts collected during Leg 206 are dominantly olivine-phyric (>80%), whereas in Expedition 309 basalts, plagioclase is the most common phenocryst phase and olivine is the least abundant among the three phenocryst phases (Fig. F29). The different observation teams during Leg 206 and Expedition 309 may account for some of this difference, but such bias should be

relatively minor. The general change from sparsely phyric to aphyric and from dom-
inantly olivine to plagioclase phenocrysts appears to be a real downhole trend.

Geochemistry

The freshest rocks from each igneous unit were selected for elemental analysis by
shipboard inductively coupled plasma–atomic emission spectroscopy (ICP-AES) to
obtain a downhole record of primary magmatic compositions (Fig. F30). All samples
have chemistries within the range of MORB with SiO_2 = 48–55 wt%, FeO = 9.4–14.0
wt%, MgO = 6.2–8.9 wt%, CaO = 7.1–12.8 wt%, Na_2O = 1.8–5.0 wt%, Cr = 21–367
ppm, Sr = 71–129 ppm, Zr = 56–133 ppm, and Ba = 1–37 ppm. The range of the Mg#
is 45–62, with an average value of 53. These values broadly overlap the results from
Leg 206 (Fig. F31) and correspond to typical values for MORB (Su and Langmuir,
2003). Although there is considerable scatter in the data, linear magmatic fraction-
ation trends are present for TiO_2, FeO, CaO, Na_2O, and Zr versus MgO (Fig. F31).

There are subtle variations in the basalt chemistry downhole, with a number of step
changes or reversals of fractionation trends possibly indicating cycles of fraction-
ation, replenishment, and, perhaps, assimilation (e.g., at ~600, 750, 908, and 1125
mbsf). Analyses of cryptocrystalline basalts that are unambiguously dikes are chemi-
cally indistinguishable from massive basalts into which these dikes were intruded.
There do not appear to be any systematic geochemical differences between sheet
flows, massive flows, and dikes (Fig. F30).

Similar to analyses of basalts from Leg 206, TiO_2 and Y show a good positive linear
correlations with Zr, due to their similar geochemical behavior (Fig. F32). Leg 206 ba-
salts above 750 mbsf were classified into three groups based on a distinct gap in the
TiO_2-Zr concentration: high Zr-TiO_2, low Zr-TiO_2, and high Zr groups. With addi-
tional data analyzed during Expedition 309, this data gap disappears and the three-
fold subdivision is probably not valid. Rare samples from the inflated flows in Hole
1256D fall off the Y versus Zr and TiO_2 versus Zr trends, suggesting some minor vari-
ation in source composition.

Basalts from different igneous subdivisions in Holes 1256D and 1256C all have MgO
in the range 6–9 wt%, and when trace element compositions of Site 1256 basalts are
compared to compilations of EPR MORB, they are within one standard deviation of
the average, albeit on the relatively trace element–depleted side of average EPR MORB
(Fig. F33). Note that Site 1256 basalts have higher Zr/Y and Zr/TiO_2 ratios than the
strongly trace element–depleted MORB from Hole 504B (Fig. F34). From all the basalts

from Site 1256, the lava pond is the only unit that is relatively enriched in V and depleted in Cr compared to the EPR MORB. The lava pond includes the rocks with the highest incompatible element (Zr, TiO_2, Y, and V) concentrations and the most depleted in compatible elements (Cr and Ni), suggesting that it is more evolved than the rest of the basalts from Hole 1256D (Fig. F33).

Compared with other first-order mid-ocean-ridge segments along the EPR, the basalts from Site 1256 have very low Zr/TiO_2 and Zr/Y ratios (Fig. F35). Although there is overlap among segments and large scatter in the data for each segment, Zr/TiO_2 and Zr/Y ratios appear to decrease with increasing spreading rate. The origin of this relationship is unclear, but spreading rate may affect magma fractionation or partial melting of the mantle, or else reflect regional-scale mantle heterogeneity.

Alteration

One of the principal objectives of the combined missions (Leg 206 and Expeditions 309 and 312) is to investigate the alteration processes that occur in a section of upper crust that formed at superfast spreading rates (200–220 mm/y) to test whether these differ from those documented in crust formed at slow and intermediate spreading rates. Of particular interest during Expedition 309 is the opportunity to observe the transition between low-temperature alteration and high-temperature hydrothermal alteration in a continuous section of oceanic crust. To date, this transition has only been described in Hole 504B. All rocks in the ocean crust intersected by Hole 1256D are partially altered to secondary minerals, and the products of fluid-rock exchange are manifest by background alteration, alteration halos related to veins, isolated alteration patches, and veins and breccias (Figs. F36, F37, F38).

Two main alteration types were encountered in the section of Hole 1256D drilled during Expedition 309. From 752 to 965 mbsf, rocks that had reacted with seawater at low temperatures, similar to the range of conditions encountered in Leg 206 cores, are present. The background alteration is uniform, from 85% to 100% dark gray, because of the presence of saponite filling vesicles and replacing olivine and plagioclase; clinopyroxene phenocrysts and chalcedony and calcium carbonate filling vesicles; and miarolitic voids (Fig. F36). The predominant vein mineral phases related to low-temperature alteration in Hole 1256D include saponite, celadonite, iron oxyhydroxides, chalcedony, and minor pyrite (Figs. F37, F38). Celadonite is commonly intergrown with iron oxyhydroxides with later overgrowths of saponite. Specific vein-related alteration types identified in Hole 1256D include black halos, brown halos, mixed halos, simple light green, light gray, dark green, and light gray halos, and discontinuous

pyrite halos (Fig. F36). Black, brown, and mixed halos and dark patches are common throughout the rocks from 752 to 918 mbsf and are related to veins filled by saponite, celadonite, and iron oxyhydroxides. These halos result from the more pervasive replacement of the host rock groundmass, as well as olivine and plagioclase phenocrysts. The formation of black halos derives from an early low-temperature seawater–basalt interaction under anoxic conditions, which initiated during cooling of the lava within 1–2 m.y. of basalt emplacement (Böhlke et al., 1980; Honnorez, 1981; Laverne, 1993; summary in Alt, 2004). Subsequent interaction of the basalts with cold oxidizing seawater produces brown halos characterized by replacement of primary phases by saponite and iron oxyhydroxides. From 918 to 964 mbsf, black, brown, and mixed halos are absent (Fig. F36) and dark gray background alteration with abundant saponite and pyrite is ubiquitous. These rocks, as well as saponite- and pyrite-bearing intervals cored during Leg 206 (e.g., 554–562 mbsf), result from the interaction of basalt with low-temperature basement fluids that have chemically evolved from seawater through water–rock reactions.

The interval from 964 to 1028 mbsf is an alteration transition zone and is characterized by the presence of pyrite-rich alteration halos and mixed-layer chlorite/smectite instead of pure saponite (Fig. F39). We also observe an increase in the occurrence of anhydrite in this zone. This alteration mineral assemblage suggests slightly more elevated temperatures (100°–200°C) than are found higher in the crust. The alteration transition zone ends at ~1028 mbsf with the occurrence of the mineralized volcanic breccia. From ~1028 mbsf, green and dark green background alteration, particularly in the coarser grained rocks, occurs as a consequence of the moderate to complete replacement (up to 100%) of basaltic clasts and glass in the mineralized volcanic breccia to saponite/chlorite and minor talc. The first occurrences of actinolite, prehnite, titanite, and epidote are recorded at 1027, 1032, 1051, and 1095 mbsf, respectively (Fig. F39). These minerals are indicative of hydrothermal alteration under subgreenschist to greenschist facies conditions. In this part of the crust, alteration halos occur both as simple dark gray, dark green, light gray, and light green halos and composite halos in which every combination of these colors is possible. These halos comprise 10%–100% secondary minerals with chlorite, actinolite, titanite, albite, and pyrite as the main secondary minerals replacing plagioclase and clinopyroxene and filling interstitial spaces along with minor quartz, chalcopyrite, epidote, and prehnite.

Although there are a few spectacular examples of highly altered and partially mineralized rocks (e.g., the mineralized volcanic breccia at ~1029 mbsf), the rocks from Hole 1256D are less altered compared to most other basement sites (e.g., Sites 417 and

418, Holes 504B and 896A). Within the extrusive lavas, Hole 1256D contains a much smaller amount of black, brown, and mixed alteration halos compared to Holes 504B and 896A, and this alteration style is not systematically present within the uppermost region of the crust. Instead, these alterations by relatively oxidizing fluids occur irregularly with depth and are most commonly associated with well-developed steeply dipping vein networks. As observed during Leg 206, the amount of calcite within Hole 1256D is very low compared to other basement penetrations.

Although pyrite is abundant in the Expedition 309 cores, intense quartz-epidote-Fe, Cu, Zn, Pb sulfide stockworklike mineralization as was intersected in Hole 504B was not intersected in the alteration transition zone. However, anhydrite, which is sparse in Hole 504B (Teagle et al., 1998), is abundant at Site 1256.

Structure

The basalts recovered during Expedition 309 exhibit brittle structures and minor brittle-ductile structures. The main structural features are represented by veins, vein networks, cataclastic zones, shear veins, microfaults, and breccia (Fig. **F40**). Primary igneous structures include syn- to late-magmatic structures, partially linked to flow and solidification of lava. Three main types of breccia were recovered during Expedition 309: incipient breccia, hyaloclastite, and hydrothermal breccia.

In the sheet and massive flows (752–1004.2 mbsf), structures and fracturing are heterogeneously partitioned and are most intensely developed at the top of the massive flows. Vertical sets of veins, cataclastic zones, and shear veins are present in massive units, whereas breccias (incipient breccia) are more common in sheet flows. On the whole, the vertical vein sets become more common from ~900 mbsf. Most structures are related to the cooling of lava and are represented by curved, radial, Y-shaped, and irregular veins filled with secondary minerals.

The transition zone (1004.2–1060.9 mbsf) is characterized by the appearance of steeply dipping chilled dike margins and the concurrent presence of cataclastic zones, breccias (mostly hyaloclastite), and vertical veins. The cataclastic massive unit in Section 309-1256D-117R-1 consists of rounded to angular clasts of dolerite and glassy spherulitic to variolitic basalt. Three to four centimeters of cataclasite separates doleritic basalt fragments from chilled fragments (Fig. **F41**). The damaged zone is characterized by a complex network of tiny veins, mostly dark green, dark brown, and light green, on the cut surface of the core. The light green veins have an aphanitic vitreous luster and disturb and cut across dark brown cataclastic saponite-bearing bands. These

bands are composed of cataclasite and protocataclasite cut by veins of ultracataclasite and gouge. The crosscutting relationships between the different type of "fault-rocks" are visible in thin section (Fig. F41). Vein networks and cataclastic banding have caused incipient brecciation of the host rock, and larger fragments show only minor relative rotation. Flow-related microstructures and laminations are observed in very narrow (0.2–0.5 mm wide) veins. In thin section, fragments of plagioclase show intergranular and intragranular deformation. Clasts are surrounded by a banded matrix that displays flow textures and is made up of subangular and rounded fragments of minerals and altered glass of variable grain size.

The intensity of fracturing downhole is mostly slight with the exception of the mineralized volcanic breccia (Unit 1256D-42; Sections 309-1256D-122R-1 and 122R-2), a hyaloclastite with abundant sulfide minerals. This volcanic breccia consists of aphyric basalt clasts with subangular to subrounded shapes (ranging in size from 2 mm to 7 cm), volcanic glass clasts, glassy shards, and subrounded to rounded altered glassy shards (Fig. F42). Basalt clasts exhibit the textural features of sheet flows, such as spherulitic to variolitic textures (see Fig. F42) and lava flow-related folding. Clasts are embedded in a scarce fine-grained clay matrix cemented by sulfides, carbonate, and silica. In interval 309-1256D-122R-1, 52–125 cm, the mineralized volcanic breccia grades from an almost pure hyaloclastite with rare sulfides to mineralized hyaloclastite. There is a concomitant increase in basalt clasts and matrix volume with respect to glassy clasts (Fig. F43).

Numerous chilled margins were recovered in cores from the transition zone and the sheeted intrusives, and these contacts are increasingly common with depth. From ~1004 mbsf, where such contacts are subvertical, they are interpreted as dike contacts. Chilled margins range from lobate and interfingered to sharp. In the sheeted intrusives, the occurrence of dike chilled margins becomes very common. Many of these dike chilled margins are associated with, or highly disrupted by, diffuse veining and brecciation (Fig. F44). Multiple dikes and banded dikes also occur. The true dip of the chilled margins ranges from 50° to 90° with a mode at ~70°–75° (Fig. F45). Preliminary interpretation of FMS and UBI images indicates that these features dip steeply to the northeast. The sheeted intrusives are also characterized by the first notable occurrence of systematic conjugate veins. From 1090.7 mbsf (Unit 1256D-45) downhole, all the structural features, except shear veins, are common and more abundant. Shear veins are present only in the uppermost portion of the massive basalt (Unit 1256D-44).

Paleomagnetism

The primary goal of paleomagnetic studies is to assess the roles of different rock types that make up the upper oceanic crust in generating marine magnetic anomalies. Magnetic remanence data were collected before and after progressive alternating-field or thermal demagnetization.

Because of the strong drilling overprint and uncertainty about how completely the overprint has been removed by demagnetization, we cannot yet make strong statements based on the paleomagnetic results from Expedition 309. Rocks from the lower parts of Expedition 309 recovery have higher coercivities and a pronounced increase in the apparent quality of data that occurs over the interval 970–1030 mbsf. Because of the equatorial paleolatitude of the site, polarity remains ambiguous until absolute declinations can be obtained based on orienting pieces relative to the downhole logging images of the borehole wall. The component of the drilling overprint that may remain would affect inclination more than declination, so for samples for which data analysis suggests that much of the drilling overprint has been removed (e.g., Fig. **F46**), generally from >1000 mbsf, declination values will be reliable enough to determine polarity in oriented pieces. If the number of oriented pieces is small but the polarity pattern is clear from those pieces or from measurements of the downhole magnetic field, the declinations from the more stable unoriented samples should be adequate for orienting pieces for structural purposes once the polarity has been determined separately.

The generally positive inclinations are not what is expected for the low paleolatitude. The most obvious possibility is that a significant portion of the drilling overprint remains on nearly all of the samples. A potential alternative is that there is a pervasive present-field overprint. Another alternative, tectonic tilting, cannot be entirely discounted. However, any tilting must predate deposition of the ponded lava flows at the top of the section, and the nearly north–south original strike of the ridge axis does not provide a favorable orientation for changing inclination as a response to slip on ridge-parallel faults.

Plots of the magnetic intensity against depth show a recurrent concave pattern (Fig. **F47**), which shows reasonable agreement with the cryptocrystalline boundaries of igneous units and subunits. Higher intensities are related to upper and lower boundaries of "cooling units," whereas lower intensity peaks occur within units. Although further shore-based analyses are required, these trends probably result from changes in the size and distribution of primary minerals (e.g., Petersen et al., 1979), in partic-

ular titanomagnetite. About 70% of the igneous units and subunits show repeated concave patterns (Fig. F47), suggesting the presence of multiple cooling units (with the observed magnetic intensity pattern) within each lithologic unit. Our calculations suggest that the average thickness of these cooling units is ~1.0 ± 0.5 m (Fig. F47).

Physical Properties

P-wave velocities of Expedition 309 basalts range from 4.8 to 6.1 km/s (average = 5.5 ± 0.3 km/s) (Fig. F48). This average value is similar to those estimated at a regional scale based on seismic reflection data and is consistent with shipboard values from Leg 206. From 752 to 1106 mbsf, average V_P increases ~0.05 km/s for each 50 m down Hole 1256D to nearly 6.0 km/s at 1130.6 mbsf. V_P is slightly higher below 1060 mbsf (5.8 ± 0.1 km/s) than above (5.4 ± 0.3 km/s), but everywhere it may be reduced locally by alteration and fracturing.

The average grain density of Expedition 309 basalts is 2.94 ± 0.04 g/cm^3, and the average bulk density is 2.86 ± 0.07 g/cm^3, similar to basalts recovered during Leg 206 (2.92 ± 0.07 and 2.82 ± 0.10 g/cm^3, respectively) (Fig. F48). The densities of discrete samples do not show a strong downhole increase with depth, even considering differences in rock type. Massive and sheet flow units have the same density within error (2.88 ± 0.04 and 2.86 ± 0.07 g/cm^3). Porosity values range from 2% to 14% (average = 4%). There is a decrease in porosity from the massive units above 1060 mbsf to those below this level: 4% ± 1% to 2% ± 1%, respectively (Fig. F49).

TC measurements yielded values of 1.7–3.1 W/(m·K) (average = 2.0 ± 0.3 W/[m·K]), over the depth range of ~752–1255 mbsf (Fig. F50). The average TC from the top of the sheet and massive flows (533 mbsf) to 1060 mbsf is 1.8 ± 0.2 W/(m·K). There is a significant increase in TC starting in the transition zone and a distinct steplike increase to 2.1 ± 0.1 W/(m·K) at 1060 mbsf, at the top of the sheeted intrusives (Fig. F50). Of the major rock types recovered during Expedition 309 and Leg 206, massive basalts and dikes of the sheeted intrusives have significantly higher average thermal conductivities than massive flows, sheet flows, pillows, and hyaloclastites (Fig. F50). The mineralized volcanic breccia has the highest TC of all rocks measured at Site 1256: 2–3.1 W/(m·K).

Whole-round cores were run through the multisensor track prior to splitting. Rather than considering all multisensor track data, only measurements from the middle of pieces >8 cm were used for analysis. MS ranged from ~0 to 10,000 × 10^{-5} SI, with the

highest values corresponding to massive lava flows, massive basalts, and dikes. In the transition zone and into the sheeted intrusives (1004.2–1255.1 mbsf), the variability in MS does not correspond to rock type and appears to be more influenced by the intensity and style of alteration.

Downhole Measurements

Following the completion of drilling in Hole 1256D, a wiper trip was run over the complete basement interval and the hole was prepared for wireline logging operations. In all, five tool strings were used in the following order: the triple combo, the FMS-sonic, the UBI, the WST, and a second run of the FMS-sonic. All deployments were successful except the WST, which suffered from wireline difficulties caused by running this light tool into the open hole. The vertical deviation measured at 1200 mbsf reaches 4.3°, and the hole azimuth varies between 250° and 290°. Caliper readings from both the triple combo and FMS-sonic tool strings show generally good borehole conditions (Fig. F51). The average hole diameter measurements from the FMS-sonic calipers are 11.25 inches for C1 and 10.90 inches for C2; this slight difference is the result of an elliptical borehole between 807 and 966 mbsf. Wide sections (>13 inches) are particularly common in this interval, as well as between 1048 and 1060 mbsf. Comparison of the caliper data from the pre- and postdrilling operations of the upper 500 m shows that the borehole is being progressively enlarged with continued drilling.

Overall, combined results of standard geophysical measurements and FMS and UBI images suggest that the section drilled during Expedition 309 may be separated into subsections, continuous with the three logging intervals distinguished during Leg 206 (see Wilson, Teagle, Acton, et al., 2003):

- Logging Interval I (base of casing to 346 mbsf) is characterized by high resistivity (up to 100 Ω·m) and monotonous FMS and UBI images and corresponds to the massive ponded lava.

- Logging Interval II (346–532 mbsf) is marked by a sharp increase in NGR log values, variable geophysical properties, and distinctive electrical and acoustic images that indicate the presence of pillow lavas intercalated with sheet and massive flows and hyaloclastites.

- Logging Interval III (532–920 mbsf) was identified during Leg 206 down to 752 mbsf by a decrease in the range of variation of physical properties and electrical images that agree with the petrological interpretation of this zone as a sequence of massive and sheet flows. In the section drilled during Expedition 309, this interval

has moderate resistivity values (commonly between 10 and 100 Ω·m) with very high, short-wavelength frequency variability. Natural radioactivity is highly variable in this interval but is usually >2 gAPI. Intervals of high natural radioactivity (>8 gAPI) are present between 770 and 774, 784 and 796, and 842 and 878 mbsf. An extremely high value (37 gAPI) of natural radioactivity is recorded at 886 mbsf. Between 785 and 843 and 853 and 920 mbsf, electrical resistivity increases with depth from 8.6 to 770 Ω·m and 9.1 to 106 Ω·m, respectively. Similar trends are recorded with the FMS-sonic tool where compressional velocities increase from 4 km/s to up to 6 km/s. Logging interval III is characterized by alternating layers of thin flows, breccias, and massive units.

- Logging Interval IV extends from 920 to 1061 mbsf. This interval is characterized by long-wavelength, large-amplitude resistivity variations. Within this interval, low-resistivity zones are generally associated with high natural radioactivity values. The lowest resistivity values are recorded between 919 and 927, 1028 and 1032, and 1047 and 1054 mbsf. The interval between 919 and 927 mbsf shows perturbations in the temperature profile that may indicate a highly fractured or faulted zone where fluids are circulating. The interval 1028–1032 mbsf is associated with an increase in the natural radioactivity and can confidently be correlated with the mineralized volcanic breccia (Cores 309-1256D-122R through 123R; Unit 1256D-42). Logging interval IV coincides with volcanic breccias interbedded within sheet flows as described in cores.

- Logging Interval V extends from 1061 mbsf to the bottom of the hole and corresponds to the sheeted intrusives. This interval is characterized by high electrical resistivities (generally >100 Ω·m) up to 2500 Ω·m at 1161 mbsf. Furthermore, extremely low (<2 gAPI) and constant natural radioactivity is recorded in this interval. Below 1028 mbsf, *P*-wave values increase and velocities higher than 6 km/s become common. In this interval, density is generally in the range 2.8–2.9 g/cm^3. FMS and UBI images show the common presence of subvertical, highly conductive features that dip steeply (~80°–85°) to the northeast and are interpreted to be dike margins. These regions have abundant horizontal fractures and veins.

During postdrilling logging, the temperature of Hole 1256D was recorded using the TAP tool (Fig. F52). The temperature record from the TAP tool clearly does not record the equilibrium thermal state of the crust because of ~33 days of fluid circulation during drilling, but it does provide important information on the cooling of the Site 1256 lithosphere. The maximum temperature in the hole is 60°C—much cooler than the equilibrium temperature of 105°C predicted from heat flow and temperatures mea-

sured during predrilling operation (see **"Predrilling Logging Operations"**). A temperature of 60°C is also significantly cooler than the equilibrium temperature measured in Hole 1256D at 724 mbsf before the commencement of coring during Expedition 309. There are clear perturbations in the temperature profile, with three intervals at ~691, 796, and 928 mbsf displaying negative temperature excursions that indicate a slower return toward the predicted equilibrium temperature (Fig. **F52**). In the same figure, the resistivity log and the FMS images (917–934 mbsf) show that these intervals have very low resistivity. The 928 mbsf perturbation corresponds to a change in rock type in the recovered cores from massive aphyric basalt to a cryptocrystalline to fine-grained sheet flow (Units 1256D-34b through 35a). The transient temperature anomaly probably indicates that this interval is a zone of high permeability that was preferentially invaded by the cold drilling fluids and is consequently recovering more slowly.

Digital Imaging

Rotary coring generally returns azimuthally unoriented samples, but cores can potentially be oriented by matching features observed in the core to features imaged by wireline logging of the borehole wall. For the purpose of obtaining orientation, all whole-round core pieces that were longer than ~80 mm and that could be rotated smoothly through 360° were imaged on the Deutsche Montan Technologie Digital Color CoreScan system. Because of limited time between the collection of downhole logging data and the end of the cruise, only a few preliminary attempts at matching core images to logging images have been made. Some of these attempts show potentially good matches between the unrolled core images and the FMS and UBI data from Hole 1256D. Figure **F53** shows an example using the largest piece recovered during Expedition 309, from Section 309-1256D-85R-1. Although it is hard to trace fractures as sinusoids through all four panels from the FMS pads, the spacing and dip of the fractures can be matched convincingly between the core images and the FMS images with the cutting line on the north side of the core.

CONCLUSIONS

Expedition 309 is the second scientific ocean drilling cruise in a multiphase mission to Site 1256 to recover, for the first time, a complete section of the upper oceanic crust from extrusive lavas down through the dikes and into the uppermost gabbros. Expedition 309, Superfast Spreading Rate Crust 2, successfully deepened Hole 1256D (6.736°N, 91.934°W) by 503 m to a total depth of 1255.1 mbsf (1005.1 msb). At the

end of Expedition 309, Hole 1256D had penetrated a total of >800 m of extrusive lavas and entered a region dominated by intrusive rocks. Hole 1256D is now the fourth deepest hole drilled into oceanic basement since the inception of scientific ocean drilling in 1968 and the second deepest penetration into in situ ocean crust behind Hole 504B. Following the completion of a comprehensive wireline logging program, the hole was successfully exited and left clear of equipment with only minor unconsolidated fill at the bottom of the hole. Hole 1256D is in excellent condition and ready for deepening.

The principal achievements of Expedition 309 are as follows:

- Hole 1256D was deepened by 503.1 m to a total depth of 1255.1 mbsf or 1005.1 msb, penetrating 810.9 m thick extrusives and 194.1 m into sheeted intrusives, with an average recovery of 36% and penetration rate of 15 m per coring day. At 1255 mbsf, Hole 1256D is tantalizingly close to the predicted minimum estimated depth to the frozen axial magma chambers.

- The upper oceanic crust so far drilled in Hole 1256D is subdivided into the lava pond (250–350 mbsf), sheet and massive flows (534–1004 mbsf), transition zone (1004–1061 mbsf), and sheeted intrusives (>1060 mbsf). The basalts show evidence of fractionation and replenishment downhole. Trace element concentrations are within one standard deviation of the average EPR MORB, albeit on the relatively trace element–depleted side.

- Hole 1256D is only the second penetration of the transition from low-temperature alteration to high-temperature hydrothermal alteration in a continuous section of oceanic crust, and this occurs at ~1000 mbsf. Prior to Expedition 309, this transition had only been described in Hole 504B. The rocks at Site 1256 are less altered compared to most other basement sites (e.g., Sites 417 and 418 and Holes 504B and 896A), and there is not a steady decrease in the effects of seawater alteration with depth. Instead, alteration is most commonly associated with well-developed steeply dipping vein networks. Although pyrite is abundant in the Expedition 309 cores, stockwork mineralization, such as that present in Hole 504B, has not been penetrated in the transition from extrusive to intrusive rocks or the change from low-temperature to hydrothermal alteration.

- Dike intrusion, brecciation, and hydrothermal alteration are intimately associated, and these features become more common downhole below 1000 msb. Fractures and veins are generally steeply dipping in the section of Hole 1256D drilled during Expedition 309, in contrast to both gentle and steep dips in the upper hole drilled during Leg 206. Subvertical dike margins imaged by FMS and UBI in the sheeted

intrusives suggest that the steeply inclined (>75°) chilled margins observed in the cores have true dips toward the northeast, consistent with the paleoridge axis orientation and slight tilting toward the ridge axis.

- Physical properties show marked changes across the lithologic transition zone. The porosity of massive lavas decreases from 4% to 2% at the base of the transition zone, and *P*-wave velocities increase from <5.5 to >6 km/s at 1240 mbsf. The average TC in the sheet and massive flows is 1.8 ± 0.2 W/(m·K), but there is a significant increase in TC starting in the transition zone and a distinct steplike increase to 2.1 ± 0.1 W/(m·K) at the top of the sheeted intrusives.

- A full sequence of downhole logs, including pre- and postdrilling temperature profiles and multiple triple combo passes and FMS and UBI imaging runs were recorded. Wireline logs confirm that Hole 1256D is in very good condition. Calipers on the triple combo and FMS tool strings indicate hole diameters typically between 11 and 14 inches. However, comparison of the pre- and postdrilling hole caliper of the upper 500 m of basement does indicate enlargement of Hole 1256D due to drilling, with a number of intervals quite strongly eroded.

Expedition 309 (July–August 2005) will be followed closely by Expedition 312 (November–December 2005). Despite our grueling pace of advance (15 m/day), progress with deepening Hole 1256D was steady. Optimistically anticipating the same benign drilling conditions and good fortune and assured of highly astute rig floor operations, Expedition 312, with 37 days of drilling operations, is set to deepen Hole 1256D by a further 500 m, well beyond the depths where geophysical interpretations predict gabbros to occur.

PRELIMINARY ASSESSMENTS

Preliminary Operational Assessment

Accomplished versus Planned Drilling

The drilling objective of Expedition 309 was to deepen Hole 1256D as much as possible during the operating time allowed. The target depth of 1350 mbsf was based on an rate of penetration of 1.5 m/h. This was to be accomplished while leaving the hole free of junk so that it could be reentered again during Expedition 312. Hole 1256D was reentered for the first time on 16 July 2005. After an initial water sample was taken with the WSTP, logging runs with the triple combo and FMS-sonic tool strings were completed to determine the condition of the hole. During Expedition 309 the

hole was cored to a depth of 1255.1 mbsf, a total of 503.1 m penetration using nine CC-9 coring bits. There was an overall recovery rate of 36.3%, with the recovery for the final bit run at 73.2%. On two occasions while coring, drops in pump pressure were noticed by the Transocean crew and the drill string was pulled out of the hole. On both occasions, cracks were found, once in the bit sub, and once in the 5 inch drill pipe. Quick action and good decisions by the crew averted junking the hole on both occasions. After coring, the hole was again logged using the triple combo, FMS-sonic, and UBI tool strings. An attempt to do a seismic study using Schlumberger's WST tool was not successful because the tool could not be lowered to the bottom of the hole. Operations ended in Hole 1256D on 25 August at 1300 h.

Preliminary Scientific Assessment

The primary operational objective of Expedition 309 and upcoming Expedition 312 (November 2005–January 2006) is to drill Hole 1256D as deeply and as cleanly as possible to attain the first continuous sampling of the uppermost ocean crust. Despite >30 y of scientific ocean drilling, this fundamental objective remains an unattained ambition. Such a section will provide hitherto unavailable knowledge about the geological, geochemical, and geophysical structure of the oceanic crust and the processes responsible for its accretion and evolution. This drilling campaign will confirm the nature of axial low-velocity zones, thought to be high-level magma chambers, as well as establish the relationships between such magma chambers and the overlying dikes and eruptive lavas. It will provide critical samples to understand the interactions between axial and ridge flank magmatic, hydrothermal, and tectonic processes and ground-truth regional seismic and magnetic measurements.

As the critical middle leg of this combined mission, Expedition 309 was highly successful in all respects. Hole 1256D has now been deepened to a total depth of 1255 mbsf (1005 msb) and, following a comprehensive program of wireline logging, was exited cleanly. Hole 1256D is in good condition, clear of junk and ready for deepening during Expedition 312. The bottom of Hole 1256D is now in a region of sheeted intrusives (below 1061 mbsf), having sampled ~754 m of eruptive lavas and a ~57 m thick lithologic transition zone. Reconsideration of cores recovered during Leg 206 identified two lava subdivisions that appear to have been erupted on the flanks of the ridge axis with a ~100 m thick massive ponded lava overlying ~184 m of lava flows with rare inflation textures that require eruption onto a subhorizontal surface. This total thickness of ~284 m of off-axis lavas is very close to our preferred estimate (~300 m; see Table T1) for the lavas that buried the axial magma chamber on the ridge flanks

and agrees well with geophysical interpretations (e.g., Hooft et al., 1996; Carbotte et al., 1997a). Accounting for this thickness of off-axis lavas and 250 m of sediments, our best estimate of the depth where gabbros occur is between 1275 and 1550 mbsf (Table **T1**). At a total depth of 1255 mbsf, Hole 1256D is nearing a depth where gabbros are predicted to occur if our precruise predictions remain valid. Gabbros are certainly within range of drilling during Expedition 312, assuming progress similar to Expedition 309. A relatively thick extrusive sequence (~470 m of on-axis lavas; the sheet and massive flows) (Table **T4**) and thin sheeted intrusive complex with a predicted thickness of between 215 and 490 m (from Expedition 309 drilling combined with the estimated depths to gabbro) is in agreement with theoretical models of the accretion of fast spreading rate ocean crust (Phipps Morgan and Chen, 1993; Wilson, Teagle, Acton et al., 2003).

Core recovery during Expedition 309 was 36%, although the final bit run sampled 40 m of massive basalts at a recovery rate of 73%. The overall recovery rate of 36% is less than that achieved in the upper portion of Hole 1256D drilled during Leg 206 (48%), but that figure is skewed by very high rates of recovery in the ponded lava flow (93%; 250–350 mbsf); recovery of lavas beneath this unit (39%) was similar to that of Expedition 309. These recovery rates are far superior to those achieved in DSDP/ODP Hole 504B with average core recovery of ~30% in volcanic rocks and a miserly 14% from the dikes. Poor core recovery of hard, fractured formations such as mid-ocean ridge basalts continues to be a major operational obstacle to scientific progress by ocean drilling. Many critical questions require high recovery, continuous cores such as can be obtained on land. Presently, the integration of incomplete core with wireline logs remains extremely difficult and time consuming.

As expected for crust formed at a fast spreading rate (>80 mm/y), sheet and massive flows are the dominant extrusive rocks drilled during both Leg 206 and Expedition 309. However, deeper in the drilled section, the exact nature of the sheeted intrusives may be open to debate. Subvertical chilled margins are common from ~1061 mbsf (Fig. **F16**), and wireline acoustic and electric images indicate numerous steeply dipping fractures suggestive of dike margins in this zone. Our preferred interpretation is that the lower part of Hole 1256D (below 1061 m) has entered a sheeted dike complex. However, because of only partial recovery of core inherent to upper crustal ocean drilling (~36%), there is the possibility that some of the massive basalts sampled from this zone could be subvolcanic sills crosscut by thin dikes. The absence of recovered subhorizontal chilled contacts weighs against the presence of sills, but the possibility exists that such contacts were preferentially lost due to low core recovery.

Further close inspection of wireline images postcruise should validate our interpretation that these rocks are sheeted dikes.

The intimate association of brecciation, dike intrusion, hydrothermal alteration, and mineralization becomes increasingly common below ~1000 mbsf and is a new observation. In these cores, there is a clear linkage between the intrusion of magmas and the penecontemporaneous incursion of mineralizing fluids during dike injection at a magmatically robust spreading ridge, as has been suggested from recent seismic anisotropy experiments undertaken at 9°N on the EPR (Tong et al., 2004). Together with the forthcoming observations from Expedition 312, these cores will enable significant progress toward understanding the interdependency of magmatic and hydrothermal processes in crust formed at fast spreading rates.

Establishment of the contribution of different layers of the oceanic crust to marine magnetic anomalies is a primary objective of Expeditions 309 and 312. Unfortunately, all cores recovered to date from Hole 1256D suffer from very strong magnetic overprints and measurement of true paleomagnetic vectors and intensities remains extremely difficult. A nonmagnetic BHA (bit and bit sub for example) may reduce magnetic overprinting during drilling, and that concept should be investigated. Also essential is a functioning, gyroscopically oriented, three-component wireline magnetometer with a temperature endurance ($\geq 100°C$) that allows it to be deployed in deep basement drill holes. Such a tool would enable the magnetic properties of the ocean crust to be measured in situ.

The wireline logging program generally returned good data, although only preliminary results were available onboard ship and for this report. Drilling-induced hole enlargement due to the transit of the drill string has led to the erosion of the borehole walls in places, resulting in inferior data for tools that require eccentralization and good contact with the borehole wall (accelerator porosity sonde, hostile environment lithodensity sonde, UBI, and FMS). The WST failed to enter Hole 1256D past the casing, and the vertical seismic profiling experiment could not be conducted. The deployment of this short, light tool should probably not have been risked in this deep basement hole, particularly when superior wireline vertical seismic profiling tools are available.

REFERENCES

Alt, J.C., 1995. Subseafloor processes in mid-ocean ridge hydrothermal systems. *In* Humphris, Zierenberg, R., Mullineaux, L., and Thomson, R. (Eds.), *Seafloor Hydrothermal Systems: Physical, Chemical, Biological and Geological Interactions within Hydrothermal Systems.* Geophys. Monogr., 91:85–114.

Alt, J.C., 1999. Very low grade hydrothermal metamorphism of basic igneous rocks. *In* Frey, M., and Robinson, D. (Eds.), *Very Low Grade Metamorphism:* Cambridge (Blackwell), 169–201.

Alt, J.C., 2004. Alteration of the upper oceanic crust: mineralogy, chemistry, and processes. *In* Elderfield, H., and Davis, E. (Eds.), *Hydrogeology of the Oceanic Lithosphere:* New York (Cambridge Univ. Press), 456–488.

Alt, J.C., Davidson, G., Teagle, D.A.H., and Karson, J., 2003. The isotopic composition of gypsum in the Macquarie Island ophiolite: implications for the sulfur cycle and the subsurface biosphere in oceanic crust. *Geology,* 31:549–552. **doi:10.1130/0091-7613(2003)031<0549:ICOGIT>2.0.CO;2**

Alt, J.C., Kinoshita, H., Stokking, L.B., et al., 1993. *Proc. ODP, Init. Repts.,* 148: College Station, TX (Ocean Drilling Program).

Alt, J.C., Laverne, C., Vanko, D.A., Tartarotti, P., Teagle, D.A.H., Bach, W., Zuleger, E., Erzinger, J., Honnorez, J., Pezard, P.A., Becker, K., Salisbury, M.H., and Wilkens, R.H., 1996. Hydrothermal alteration of a section of upper oceanic crust in the eastern equatorial Pacific: a synthesis of results from Site 504 (DSDP Legs 69, 70, and 83, and ODP Legs 111, 137, 140, and 148.) *In* Alt, J.C., Kinoshita, H., Stokking, L.B., and Michael, P.J. (Eds.), *Proc. ODP, Sci. Results,* 148: College Station, TX (Ocean Drilling Program), 417–434.

Alt, J.C., and Teagle, D.A.H., 1999. The uptake of carbon during alteration of ocean crust. *Geochim. Cosmochim. Acta,* 63(10):1527–1535. **doi:10.1016/S0016-7037(99)00123-4**

Alt, J.C., and Teagle, D.A.H., 2000. Hydrothermal alteration and fluid fluxes in ophiolites and oceanic crust. *In* Dilek, Y., Moores, E., Elthon, D., and Nicolas, A. (Eds.), *Ophiolites and Oceanic Crust: New Insights from Field Studies and the Ocean Drilling Program.* Spec. Pap.— Geol. Soc. Am., 349:273–282.

Autio, L.K., and Rhodes, J.M., 1983. Costa Rica Rift Zone basalts: geochemical and experimental data from a possible example of multistage melting. *In* Cann, J.R., Langseth, M.G., Honnorez, J., Von Herzen, R.P., White, S.M., et al., *Init. Repts. DSDP,* 69: Washington (U.S. Govt. Printing Office), 729–745.

Bach, W., Peucker-Ehrenbrink, B., Hart, S.R., and Blusztajn, J.S., 2003. Geochemistry of hydrothermally altered oceanic crust: DSDP/ODP Hole 504B—implications for seawater-crust exchange budgets and Sr- and Pb-isotopic evolution of the mantle. *Geochem., Geophys., Geosyst.,* 4(3). **doi:10.1029/2002GC000419**

Banerjee, N.R., and Muehlenbachs, K., 2003. Tuff life: bioalteration in volcaniclastic rocks from the Ontong Java Plateau. *Geochem., Geophys., Geosyst.,* 4. **doi:10.1029/2002GC000470**

Bascom, W., 1961. *A Hole in the Bottom of the Sea:* New York (Doubleday).

Becker, K., Foss, G., et al., 1992. *Proc. ODP, Init. Repts.,* 137: College Station, TX (Ocean Drilling Program).

Bickle, M.J., and Teagle, D.A.H., 1992. Strontium alteration in the Troodos ophiolite: implications for fluid fluxes and geochemical transport in mid-ocean ridge hydrothermal systems. *Earth Planet. Sci. Lett.,* 113:219–237. **doi:10.1016/0012-821X(92)90221-G**

Blake, R.E., Alt, J.C., and Martini, A.M., 2001. Oxygen isotope ratios of PO_4: an inorganic indicator of enzymatic activity and P metabolism and a new biomarker in the search for life. *Proc. Natl. Acad. Sci. U. S. A.,* 98(5):2148–2153. **doi:10.1073/pnas.051515898**

Böhlke, J.K., Honnorez, J., Honnorez-Guerstein, B.-M., Muehlenbachs, K., and Petersen, N., 1981. Heterogeneous alteration of the upper oceanic crust: correlation of rock chemistry, magnetic properties, and O-isotope ratios with alteration patterns in basalts from Site 396B, DSDP. *J. Geophys. Res.,* 86:7935–7950.

Cande, S.C., and Kent, D.V., 1995. Revised calibration of the geomagnetic polarity timescale for the Late Cretaceous and Cenozoic. *J. Geophys. Res.,* 100:6093–6095. **doi:10.1029/94JB03098**

Cannat, M., Karson, J.A., Miller, D.J., et al., 1995. *Proc. ODP, Init. Repts.,* 153: College Station, TX (Ocean Drilling Program).

Carbotte, S., Mutter, C., Mutter, J., and Ponce-Correa, G., 1997a. Influence of magma supply and spreading rate on crustal magma bodies and emplacement of the extrusive layer: insights from the East Pacific Rise at lat 16°N. *Geology,* 26:455–458. **doi:10.1130/0091-7613(1998)026<0455:IOMSAS>2.3.CO;2**

Carbotte, S.M., Mutter, J.C., and Xu, L., 1997b. Contribution of volcanism and tectonism to axial and flank morphology of the southern East Pacific Rise, 17°10′ –17°40′ S, from a study of Layer 2A geometry. *J. Geophys. Res.,* 102(B5):10165–10184. **doi:10.1029/96JB03910**

Coogan, L.A., Jenkin, G.R.T., and Wilson, R.N., 2002a. Constraining the cooling rate of the lower oceanic crust: a new approach applied to the Oman ophiolite. *Earth Planet. Sci. Lett.,* 199(1–2):127–146. **doi:10.1016/S0012-821X(02)00554-X**

Coogan, L.A., Thompson, G., and McLeod, C.J., 2002b. A textural and geochemical investigation of high level gabbros from the Oman ophiolite: implications for the role of the axial magma chamber at fast-spreading ridges. *Lithos,* 63:67–82. **doi:10.1016/S0024-4937(02)00114-7**

COSOD II, 1987. *Rep. 2nd Conf. Scientific Ocean Drilling:* Washington/Strasbourg (JOIDES/European Sci. Found.).

Detrick, R., Collins, J., Stephen, R., and Swift, S., 1994. In situ evidence for the nature of the seismic Layer 2/3 boundary in oceanic crust. *Nature (London, U. K.),* 370:288–290. **doi:10.1038/370288a0**

Detrick, R.S., Toomey, D.R., and Collins, J.A., 1998. Three-dimensional upper crustal heterogeneity and anisotropy around Hole 504B from seismic topography. *J. Geophys. Res.,* 103(B12):30485–30504. **doi:10.1029/98JB02409**

Dick, H.J.B., and Mével, C., 1996. *The Oceanic Lithosphere and Scientific Drilling into the 21st Century:* Woods Hole, MA (ODP-InterRidge-IAVCEI).

Dick, H.J.B., Natland, J.H., Miller, D.J., et al., 1999. *Proc. ODP, Init. Repts.,*176 [Online]. Available from World Wide Web: <**http://www-odp.tamu.edu/publications/176_IR/176TOC.HTM**>.

Edmond, J.M., Measures, C., Magnum, B., Grant, B., Sclater, F.R., Collier, R., Hudson, A., Gordon, L.I., and Corliss, J.B., 1979. On the formation of metal-rich deposits at ridge crests. *Earth. Planet. Sci. Lett.,* 46:19–30. **doi:10.1016/0012-821X(79)90062-1**

Elderfield, H., and Schultz, A., 1996. Mid-ocean ridge hydrothermal fluxes and the chemical composition of the ocean. *Annu. Rev. Earth Planet. Sci.,* 24(1):191–224. **doi:10.1146/annurev.earth.24.1.191**

Elderfield, H., Wheat, C.G., Mottl, M.J., Monnin, C., and Spiro, B., 1999. Fluid and geochemical transport through oceanic crust: a transect across the eastern flank of the Juan de Fuca Ridge. *Earth Planet. Sci. Lett.,* 172(1–2):151–165. **doi:10.1016/S0012-821X(99)00191-0**

Expedition 304 Scientists, 2005. Oceanic core complex formation, Atlantis Massif—oceanic core complex formation, Atlantis Massif, Mid-Atlantic Ridge: drilling into the footwall and hanging wall of a tectonic exposure of deep, young oceanic lithosphere to study deformation, alteration, and melt generation. *IODP Prel. Rept.,* 304. **doi:10.2204/iodp.pr.304.2005**

Expedition 305 Scientists, 2005. Oceanic core complex formation, Atlantis Massif—oceanic core complex formation, Atlantis Massif, Mid-Atlantic Ridge: drilling into the footwall and hanging wall of a tectonic exposure of deep, young oceanic lithosphere to study deformation, alteration, and melt generation. *IODP Prel. Rept.,* 305. **doi:10.2204/iodp.pr.305.2005**

Farrell, J.W., Raffi, I., Janecek, T.C., Murray, D.W., Levitan, M., Dadey, K.A., Emeis, K.-C., Lyle, M., Flores, J.-A., and Hovan, S., 1995. Late Neogene sedimentation patterns in the eastern equatorial Pacific Ocean. *In* Pisias, N.G., Mayer, L.A., Janecek, T.R., Palmer-Julson, A., and van Andel, T.H. (Eds.), *Proc. ODP, Sci. Results,* 138: College Station, TX (Ocean Drilling Program), 717–756.

Furnes, H., and Staudigel, H., 1999. Biological mediation in ocean crust alteration: how deep is the deep biosphere? *Earth Planet. Sci. Lett.,* 166:97–103. **doi:10.1016/S0012-821X(99)-00005-9**

Gillis, K., Mével, C., Allan, J., et al., 1993. *Proc. ODP, Init. Repts.,* 147: College Station, TX (Ocean Drilling Program).

Gillis, K.M., Coogan, L.A., and Pedersen, R., 2005. Strontium isotope constraints on fluid flow in the upper oceanic crust at the East Pacific Rise. *Earth Planet. Sci. Lett.,* 232(1–2):83–94. **doi:10.1016/j.epsl.2005.01.008**

Gillis, K.M., Muehlenbachs, K., Stewart, M., Gleeson, T., and Karson, J., 2001. Fluid flow patterns in fast spreading East Pacific Rise crust exposed at Hess Deep. *J. Geophys. Res.,* 106:26311–26329. **doi:10.1029/2000JB000038**

Gillis, K.M., and Roberts, M.D., 1999. Cracking at the magma–hydrothermal transition: evidence from the Troodos ophiolite, Cyprus. *Earth Planet. Sci. Lett.,* 169:227–244. **doi:10.1016/S0012-821X(99)00087-4**

Hallenborg, E., Harding, A.J., Kent, G.M., and Wilson, D.S., 2003. Seismic structure of 15 Ma oceanic crust formed at an ultrafast spreading East Pacific Rise: evidence for kilometer-scale fracturing from dipping reflectors. *J. Geophys. Res.,* 108(B11):2532. **doi:10.1029/2003JB002400**

Honnorez, J., 1981. The aging of the oceanic crust at low temperature. *In* Emiliani, C. (Ed.), *The Sea* (Vol. 7): *The Oceanic Lithosphere:* New York (Wiley), 525–587.

Hooft, E.E.E., Schouten, H., and Detrick, R.S., 1996. Constraining crustal emplacement processes from variation in seismic Layer 2A thickness at the East Pacific Rise. *Earth Planet. Sci. Lett.,* 142(3–4):289–309. **doi:10.1016/0012-821X(96)00101-X**

Hosford, A., Tivey, M., Matsumoto, T., Dick, H., Schouten, H., and Kinoshita, H., 2003. Crustal magnetization and accretion at the Southwest Indian Ridge near the Atlantis II Fracture Zone, 0–25 Ma. *J. Geophys. Res.,* 108(B3). **doi:10.1029/2001JB000604**

International Working Group, 2001. *Earth, Oceans, and Life: Scientific Investigation of the Earth System Using Multiple Drilling Platforms and New Technologies—Integrated Ocean Drilling Program Initial Science Plan, 2003–2013.* Washington (International Working Group Support Office).

Karson, J.A., 2002. Geologic structure of the uppermost oceanic crust created at fast- to intermediate-rate spreading centers. *Annu. Rev. Earth Planet. Sci.,* 30:347–384. **doi:10.1146/annurev.earth.30.091201.141132**

Karson, J.A., Klein, E.M., Hurst, S.D., Lee, C.E., Rivizzigno, P.A., Curewitz, D., Morris, A.R., and Hess Deep 1999 Scientific Party, 2002. Structure of uppermost fast-spread oceanic

crust exposed at the Hess Deep Rift: implications for subaxial processes at the East Pacific Rise, *Geochem., Geophys., Geosyst.,* 3. doi:10.1029/2001GC000155

Kelemen, P.B., Kikawa, E., Miller, D.J., et al., 2004. *Proc. ODP, Init. Repts.,* 209 [Online]. Available from World Wide Web: <http://www-odp.tamu.edu/publications/209_IR/ 209ir.htm>.

Kelemen, P.B., Koga, K., and Shimizu, N., 1997. Geochemistry of gabbro sills in the crust–mantle transition zone of the Oman ophiolite: implications for the origin of the oceanic lower crust. *Earth Planet Sci. Lett.,* 146:475–488. doi:10.1016/S0012-821X(96)00235-X

Kempton, P.D., Autio, L.K., Rhodes, J.M., Holdaway, M.J., Dungan, M.A., and Johnson, P., 1985. Petrology of basalts from Hole 504B, Deep Sea Drilling Project, Leg 83. *In* Anderson, R.N., Honnorez, J., Becker, K., et al., *Init. Repts. DSDP,* 83: Washington (U.S. Govt. Printing Office), 129–164.

Laverne, C., 1993. Occurrence of siderite and ankerite in young basalts from the Galapagos Spreading Center (DSDP Holes 506G and 507B). *Chem. Geol.,* 106(1–2):27–46. doi:10.1016/0009-2541(93)90164-E

Laverne, C., Agrinier, P., Hermitte, D., and Bohn, M., 2001. Chemical fluxes during hydrothermal alteration of a 1200-m long section of dikes in the oceanic crust, DSDP/ODP Hole 504B. *Chem. Geol.,* 181:73–98. doi:10.1016/S0009-2541(01)00277-7

Macdonald, K.C., Fox, P.J., Alexander, R.T., Pockalny, R., and Gente, P., 1996. Volcanic growth faults and the origin of Pacific abyssal hills. *Nature (London, U. K.),* 380:125–129. doi:10.1038/380125a0

Macdonald, K.C., Haymon, R., and Shor, A., 1989. A 220 km² recently erupted lava field on the East Pacific Rise near lat 8°S. *Geology,* 17:212–217. doi:10.1130/0091-7613(1989)017<0212:AKRELF>2.3.CO;2

MacLeod, C.J., and Yaouancq, G., 2000. A fossil melt lens in the Oman ophiolite: implications for magma chamber processes at fast spreading ridges. *Earth Planet. Sci. Lett.,* 176:357–373. doi:10.1016/S0012-821X(00)00020-0

Manning, C.E., MacLeod, C.J., and Weston, P.E., 2000. Lower-crustal cracking front at fast spreading ridges: evidence from the East Pacific Rise and the Oman ophiolite. *In* Dilek, Y., Moores, E.M., Elthon, D., and Nicolas, A. (Eds.), *Ophiolites and Oceanic Crust: New Insights from Field Studies and the Ocean Drilling Program.* Spec. Pap.—Geol. Soc. Am., 349:261–272.

Menard, H.W., 1964. *Marine Geology of the Pacific:* New York (McGraw-Hill).

Murray, R.W., Schrag, D.P., and Wheat, C.G., 2002. *Opportunities in Geochemistry for Post-2003 Ocean Drilling:* Washington (Joint Oceanographic Institutions, Inc.).

Natland, J.H., and Dick, H.J.B., 1996. Melt migration through high-level gabbroic cumulates of the East Pacific Rise at Hess Deep: the origin of magma lenses and the deep crustal structure of fast-spreading ridges. *In* Mével, C., Gillis, K.M., Allan, J.F., and Meyer, P.S. (Eds.), *Proc. ODP, Sci. Results,* 147: College Station, TX (Ocean Drilling Program), 21–58.

Natland, J.H., Adamson, A.C., Laverne, C., Melson, W.G., and O'Hearn, T., 1983. A compositionally nearly steady-state magma chamber at the Costa Rica Rift: evidence from basalt glass and mineral data, Deep Sea Drilling Project Sites 501, 504, and 505. *In* Cann, J.R., Langseth, M.G., Honnorez, J., Von Herzen, R.P., White, S.M., et al., *Init. Repts. DSDP,* 69: Washington (U.S. Govt. Printing Office), 811–858.

Ocean Drilling Program, 1996. *Understanding Our Dynamic Earth through Ocean Drilling: Ocean Drilling Program Long Range Plan Into the 21st Century:* Washington (Joint Oceanographic Institutions).

Parsons, B., and Sclater, J.G., 1977. An analysis of the variation of ocean floor bathymetry and heat flow with age. *J. Geophys. Res.,* 82:803–827.

Petersen, N., Eisenach, P., and Bleil, U., 1979. Low temperature alteration of the magnetic minerals in ocean floor basalts. *In* Talwani, M., Harrison, C.G., and Hayes, D. (Eds.), *Deep*

Drilling Results in the Atlantic Ocean: Ocean Crust. Am. Geophys. Union, Maurice Ewing Ser., 2:169–209.

Phipps Morgan, J., and Chen, Y.J., 1993. The genesis of oceanic crust: magma injection, hydrothermal circulation, and crustal flow. *J. Geophys. Res.,* 98:6283–6297.

Pisias, N.G., and Delaney, M.L. (Eds.), 1999. *Conference on Multiple Platform Exploration of the Ocean (COMPLEX):* Washington (Joint Oceanographic Institutions, Inc.).

Purdy, G.M., Kong, L.S.L., Christeson, G.L., and Solomon, S.C., 1992. Relationship between spreading rate and the seismic structure of mid-ocean ridges. *Nature (London, U. K.),* 355:815–872. **doi:10.1038/355815a0**

Raitt, R.W., 1963. The crustal rocks. *In* Hill, M.N. (Ed.), *The Sea—Ideas and Observations on Progress in the Study of the Seas* (Vol. 3): *The Earth Beneath the Sea:* New York (Wiley-Interscience), 85–102.

Richardson, C.J., Cann, J.R., Richards, H.G., and Cowan, J.G., 1987. Metal-depleted root zones of the Troodos ore-forming hydrothermal systems, Cyprus. *Earth Planet. Sci. Lett.,* 84:243–253. **doi:10.1016/0012-821X(87)90089-6**

Schiffman, P., and Smith, B.M., 1988. Petrology and oxygen isotope geochemistry of a fossil seawater hydrothermal system within the Solea Graben, northern Troodos ophiolite, Cyprus. *J. Geophys. Res.,* 93:4612–4624.

Shor, E.N., 1985. A chronology from Mohole to JOIDES. *In* Drake, E.T., and Jordan, W.M. (Eds.), *Geologists and Ideas: A History of North American Geology.* Geol. Soc. Spec. Publ., 4:391–399.

Singh, S.C., Kent, G.M., Collier, J.S., Harding, A.J., and Orcutt, J.A., 1998. Melt to mush variations in crustal magma properties along the ridge crest at the southern East Pacific Rise. *Nature (London, U. K.),* 394:874–878. **doi:10.1038/29740**

Stewart, M.A., Karson, J.A., and Klein, E.M., 2005. Four-dimensional upper crustal construction at fast-spreading mid-ocean ridges: a perspective from an upper crustal cross-section at the Hess Deep Rift. *J. Volcanol. Geotherm. Res.,* 144:287–309. **doi:10.1016/j.jvolgeores.2004.11.026**

Su, Y., and Langmuir, C.H., 2003. Global MORB chemistry compilation at segment scale [Ph.D. dissert.]. Columbia Univ. Available from World Wide Web: <**http://petdb.ldeo.columbia.edu/documentation/morbcompilation/**>.

Teagle, D.A.H., Alt, J.C., and Halliday, A.N., 1998. Tracing the chemical evolution of fluids during hydrothermal recharge: constraints from anhydrite recovered in ODP Hole 504B. *Earth Planet. Sci. Lett.,* 155:167–182. **doi:10.1016/S0012-821X(97)00209-4**

Teagle, D.A.H., Bickle, M.J., and Alt, J.C., 2003. Recharge flux to ocean-ridge black smoker systems: a geochemical estimate from ODP Hole 504B. *Earth Planet. Sci. Lett.,* 210:81–89. **doi:10.1016/S0012-821X(03)00126-2**

Tong, C.H., White, R.S., Warner, M.R., and ARAD Working Group, 2004. Effects of tectonism and magmatism on crack structure in oceanic crust: a seismic anisotropy study. *Geology,* 32(1):25–28. **doi:10.1130/G19962.1**

Umino S., Miyashita, S., Hotta, F., and Adachi, Y., 2003. Along-strike variation of the sheeted dike complex in the Oman ophiolite: insights into subaxial ridge segment structures and the magma plumbing system. *Geochem., Geophys., Geosyst.,* 4. **doi:10.1029/2001GC000233**

Umino, S., Obata, S., Lipman, P., Smith, J.R., Shibata, T., Naka, J., and Trusdell, F., 2002. Emplacement and inflation structures of submarine and subaerieal pahoehoe lavas from Hawaii. *In* Takahashi, E., et al. (Eds.), *Hawaiian Volcanoes: Deep Underwater Perspectives.* Geophys. Monogr., 128:85–101.

Umino, S., Obata, S., and Lipman, P.W., 2000. Subaqueous lava flow lobes, observed on ROV *KAIKO* dives off Hawaii. *Geology,* 28:503–506. **doi:10.1130/0091-7613(2000)028<0503:SLFLOO>2.3.CO;2**

Vanko, D., and Laverne, C., 1998. Hydrothermal anorthitization of plagioclase within the magmatic/hydrothermal transition at mid-ocean ridges: examples from deep sheeted dikes (Hole 504B, Costa Rica Rift) and a sheeted dike root zone (Oman ophiolite). *Earth Planet. Sci. Lett.,* 162:27–43. **doi:10.1016/S0012-821X(98)00155-1**

Varne, R., Brown, A.V., and Fallon, T., 2000. Macquarie Island: its geology, structural history, and the timing and tectonic setting of its N-MORB to E-MORB magnetism. *In* Dilek, Y., Moores, E.M., Elthon, D., and Nicolas, A. (Eds.), *Ophiolites and Oceanic Crust: New Insights from Field Studies and the Ocean Drilling Program.* Spec. Pap.—Geol. Soc. Am., 349:301–320.

Vine, F.J., and Matthews, D.H., 1963. Magnetic anomalies over oceanic ridges. *Nature (London, U. K.),* 199:947–949.

White, S.M., Hayman, R.M., Fornari, D.J., Perfit, M.R., and Macdonald, K.C., 2002. Correlation between volcanic and tectonic segmentation of fast-spreading ridges: Evidence from volcanic structures and lava flow morphology on the East Pacific Rise at 9°–10°N. *J. Geophys. Res.,* 107:2173. **doi:10.1029/2001JB000571**

White, S.M., Macdonald, K.C., and Haymon, R.M., 2000. Basaltic lava domes, lava lakes, and volcanic segmentation on the southern East Pacific Rise. *J. Geophys. Res.,* 105:23519–23536. **doi:10.1029/2000JB900248**

Wilson, D.S., 1996. Fastest known spreading on the Miocene Cocos-Pacific plate boundary. *Geophys. Res. Lett.,* 23:3003–3006. **doi:10.1029/96GL02893**

Wilson, D.S., Hallenborg, E., Harding, A.J., and Kent, G.M., 2003. Data report: Site survey results from cruise EW9903. *In* Wilson, D.S., Teagle, D.A.H., Acton, G.D., *Proc. ODP, Init. Repts.,* 206, 1–49 [CD-ROM]. Available from: Ocean Drilling Program, Texas A&M University, College Station TX 77845-9547, USA. [**HTML**]

Wilson, D.S., Teagle, D.A.H., Acton, G.D., et al., 2003. *Proc. ODP, Init. Repts.,* 206 [Online]. Available from World Wide Web: <**http://www-odp.tamu.edu/publications/206_IR/206ir.htm**>.

Table T1. Predicted depths to gabbros, Site 1256.

	Depth to axial low-velocity zone		100 m of off-axis lavas		300 m of off-axis lavas	
	msb	mbsf	msb	mbsf	msb	mbsf
Minimum:	725	975	825	1075	1025	1275
Maximum:	1000	1250	1100	1350	1300	1550

Notes: msb = meters subbasement. Depths to the axial low-velocity zone are estimated from the relationship with spreading rate shown in Figure **F3** (following Purdy et al., 1992; Carbotte et al., 1997b) for ocean crust spreading at 200 mm/y. Depth in mbsf includes the 250 m thick sediment cover at Site 1256.

Table T2. Operations conducted during Expedition 309, Hole 1256D. (**See table notes.** Continued on next page.)

Operation in hole	Local time (h)	Date (2005)	Time on hole (h)	Time on site (h)	Time on site (days)	Comments
Arrive on site, lower all thrusters	1030	16 Jul				
Reentry number 1	1945	16 Jul	9.25	9.25	0.39	
Begin WSTP run	0030	17 Jul	4.75	14.00	0.58	
End WSTP	0430	17 Jul	4.00	18.00	0.75	
Begin APCT run	0430	17 Jul	0.00	18.00	0.75	
End APCT run	0630	17 Jul	2.00	20.00	0.83	
Begin second WSTP run	0630	17 Jul	0.00	20.00	0.83	
End second WSTP run	0830	17 Jul	2.00	22.00	0.92	
Rig up logging equipment	1015	17 Jul	1.75	23.75	0.99	
End triple combo	2045	17 Jul	10.50	34.25	1.43	
End FMS	0530	18 Jul	8.75	43.00	1.79	Clear seafloor at 0615 h on 18 July
Clear cone	0615	18 Jul	0.75	43.75	1.82	
Deploy RCB bit number 1	1500	18 Jul	8.75	52.50	2.19	
Reentry number 2	2325	18 Jul	8.42	60.92	2.54	
Begin coring with bit number 1	1200	19 Jul	12.58	73.50	3.06	
End Coring with bit number 1	0145	22 Jul	61.75	135.25	5.64	Clear seafloor at 0410 h on 22 July
Bit number 1 on deck	1000	22 Jul	8.25	143.50	5.98	
Deploy bit number 2	1200	22 Jul	2.00	145.50	6.06	
Start-slip and cut drilling line	1645	22 Jul	4.75	150.25	6.26	
End-slip and cut drilling line	1745	22 Jul	1.00	151.25	6.30	
Reentry number 3	1911	22 Jul	1.43	152.68	6.36	
Begin coring with bit number 2	2230	22 Jul	3.32	156.00	6.50	
End coring with bit number 2	0010	26 Jul	73.67	229.67	9.57	Clear seafloor at 0300 h on 26 July
Bit number 2 on deck	0830	26 Jul	8.33	238.00	9.92	
Deploy bit number 3	1000	26 Jul	1.50	239.50	9.98	
Reentry number 4	1610	26 Jul	6.17	245.67	10.24	
Begin coring with bit number 3	2045	26 Jul	4.58	250.25	10.43	
End coring with bit number 3	1530	29 Jul	66.75	317.00	13.21	Clear seafloor at 1800 h on 29 July
Bit number 3 on deck	0000	30 Jul	8.50	325.50	13.56	
Deploy bit number 4	0000	30 Jul	0.00	325.50	13.56	
WSTP sample	1000	30 Jul	10.00	335.50	13.98	
Reentry number 5	1015	30 Jul	0.25	335.75	13.99	
Begin coring with bit number 4	1445	30 Jul	4.50	340.25	14.18	Cracked bit sub
End coring with bit number 4	1745	31 Jul	27.00	367.25	15.30	Clear seafloor at 2215 h on 31 July
Bit number 4 on deck	0300	1 Aug	9.25	376.50	15.69	
Deploy bit number 5	0630	1 Aug	3.50	380.00	15.83	
Reentry number 6	1415	1 Aug	7.75	387.75	16.16	
Start-slip and cut drilling line	1430	1 Aug	0.25	388.00	16.17	
End-slip and cut drilling line	1530	1 Aug	1.00	389.00	16.21	
Begin coring with bit number 5	1945	1 Aug	4.25	393.25	16.39	
End coring with bit number 5	1845	4 Aug	71.00	464.25	19.34	Clear seafloor at 2115 h on 4 Aug

Table T2 (continued).

Operation in hole	Local time (h)	Date (2005)	Time on hole (h)	Time on site (h)	Time on site (days)	Comments
Bit number 5 on deck	0200	5 Aug	7.25	471.50	19.65	
Deploy bit number 6	0215	5 Aug	0.25	471.75	19.66	
Reentry number 7	0951	5 Aug	7.60	479.35	19.97	
Begin coring with bit number 6	1430	5 Aug	4.65	484.00	20.17	
End coring with bit number 6	0930	8 Aug	67.00	551.00	22.96	Clear seafloor at 0400 h on 8 Aug
Bit number 6 on deck	1800	8 Aug	8.50	559.50	23.31	
Deploy bit number 7	1815	8 Aug	0.25	559.75	23.32	
Reentry number 8	0145	9 Aug	7.50	567.25	23.64	
Begin coring with bit number 7	0815	9 Aug	6.50	573.75	23.91	
End coring with bit number 7	1415	11 Aug	54.00	627.75	26.16	Clear seafloor at 1350 h on 12 Aug
NDT inspect DC	0405	12 Aug	13.83	641.58	26.73	
Bit number 7 on deck	0415	12 Aug	0.17	641.75	26.74	
Deploy bit number 8	0415	12 Aug	0.00	641.75	26.74	
Check drill string for cracks	1345	12 Aug	9.50	651.25	27.14	
Change out 2 stands 5 inch drill pipe	2030	12 Aug	6.75	658.00	27.42	
Reentry number 9	0230	13 Aug	6.00	664.00	27.67	
Begin coring with bit number 8	0730	13 Aug	5.00	669.00	27.88	
End coring with bit number 8	1045	16 Aug	75.25	744.25	31.01	Clear seafloor at 1340 h on 16 Aug
Bit number 8 on deck	1945	16 Aug	9.00	753.25	31.39	
Deploy bit number 9	2000	16 Aug	0.25	753.50	31.40	
Reentry number 10	0340	17 Aug	7.67	761.17	31.72	
Begin coring with bit number 9	0730	17 Aug	3.83	765.00	31.88	
End coring with bit number 9	1040	20 Aug	75.17	840.17	35.01	
Begin wiper trip	1040	20 Aug	0.00	840.17	35.01	
End wiper trip	1800	20 Aug	7.33	847.50	35.31	Clear seafloor at 1640 h on 20 Aug
Bit number 9 on deck	0200	21 Aug	8.00	855.50	35.65	
Make up/deploy logging BHA	0200	21 Aug	0.00	855.50	35.65	
Reentry number 11	0800	21 Aug	6.00	861.50	35.90	
Run in hole to casing shoe	0830	21 Aug	0.50	862.00	35.92	
Rig up logging equipment	1200	21 Aug	3.50	865.50	36.06	
Triple combo completed	2315	21 Aug	11.25	876.75	36.53	Not able to get WST downhole
FMS-sonic completed	1100	22 Aug	11.75	888.50	37.02	
UBI experiment completed	0400	23 Aug	17.00	905.50	37.73	Clear seafloor at 0600 h on 24 Aug
WST experiment completed	1315	23 Aug	9.25	914.75	38.11	
FMS-sonic completed	0500	24 Aug	15.75	930.50	38.77	
Beacon recovered	1200	24 Aug	7.00	937.50	39.06	
Rig for departure	1300	24 Aug	1.00	938.50	39.10	Beacon recovered after 39 days
Depart location	1300	24 Aug	0.00	938.50	39.10	

Notes: WSTP = Water Sampling Temperature Probe, APCT = Advanced Piston Corer Temperature, FMS = Formation MicroScanner, RCB = Rotary Core Barrel, NDT = nondestructive testing, DC = drill collar, BHA = bottom-hole assembly, WST = Well Seismic Tool, UBI = Ultrasonic Borehole Imager.

Table T3. Summary of coring bits used during Expedition 309.

Bit number	Manufacturer	Serial number	Bit type	Size	Number of cores	Interval cored (m)	Recovered (m)	Recovery (%)	Coring time (h)	Rate of penetration (m/h)
Log bit					Logging				43.8	
1256D-1	RBI	BF-739	CC-9	$9^7/_8$	11	69.1	25.20	36.5	51.7	1.34
1256D-2	RBI	BF-852	CC-9	$9^7/_8$	11	76.8	18.02	23.5	52.1	1.47
1256D-3	RBI	BF-854	CC-9	$9^7/_8$	11	61.1	14.85	24.3	52.8	1.16
1256D-4	RBI	BF-856	CC-9	$9^7/_8$	4	20.4	9.52	46.7	17.8	1.14
1256D-5	RBI	BF-858	CC-9	$9^7/_8$	15	72.1	20.56	28.5	50.1	1.44
1256D-6	RBI	BF-741	CC-9	$9^7/_8$	12	57.6	21.45	37.2	50.8	1.13
1256D-7	RBI	BF-742	CC-9	$9^7/_8$	8	36.3	17.70	48.8	42.5	0.85
1256D-8	RBI	BF-853	CC-9	$9^7/_8$	12	58.6	17.74	30.3	57.8	1.01
1256D-9	RBI	CL-540	CC-9	$9^7/_8$	12	51.3	37.57	73.2	53.1	0.97
Log bit					Logging				76.0	
				Totals:	96	503.3	182.61			1.17

Table T4. Key parameters for Hole 1256D and preliminary subdivisions of the upper oceanic crust, Site 1256.

Location: 6°44.163′ N, 91°56.061′ W

Water depth (m): 3634.7

Sediment thickness (m): 250

16 inch casing string (m): 269.5

Interval in Hole 1256D drilled during

  ODP Leg 206: 752 mbsf (502 msb)

  IODP Expedition 309: 1255.1 mbsf (1005.1 msb)

Subdivision	Core, section, interval (cm)	Igneous unit	Depth (mbsf)	Criteria
Lava pond	206-1256D-2R-1, 0 cm	1256D-1 (1256C-1 through 18)	~250	Massive ponded lava and overlying sheet flows
Inflated flows	206-1256D-13R-1, 0 cm	1256D-2	350.3	Massive, sheet, and pillowed flows with inflation features
Sheet and massive flows	206-1256D-43R-1, 0 cm	1256D-16	533.9	Sheet flows with subordinate massive flows
Transition zone	309-1256D-117R-1, 85 cm	1256D-40	1004.2	Sheet flows with breccias, rare dikes, and alteration at (sub-)greenschist facies conditions
Sheeted intrusives	309-1256D-129R-1, 0 cm	1256D-44a	1060.9	Massive basalts, common subvertical intrusive contacts. Elevated V_P and TC.
Expedition 309 maximum depth	309-1256D-170R-3, 89 cm	1256D-65	1255.5	(n.b. curated depth)

Notes: msb = meters subbasement. V_P = P-wave velocity. TC = thermal conductivity, n.b.

Table T5. Igneous unit and contact log, Hole 1256D. (**See table note.** Continued on next page.)

Unit/ Subunit	Upper contact		Nature of contact/ Rationale for boundary	Minimum thickness (m)	Rock type
	Core, section, piece, interval	Depth (mbsf)			
	309-1256D-				
27	75R-1 (Piece 1, 0 cm)	752.0	Chilled margin	3.17	Aphyric cryptocrystalline to microcrystalline basaltic sheet flow
28	77R-1 (Piece 16, 66 cm)	759.4	Chilled margin	3.69	Sparsely to moderately phyric cryptocrystalline to fine-grained basaltic sheet flow
29a	78R-3 (Piece 2, 10 cm)	766.5	Breccia and chilled margin	3.53	Aphyric cryptocrystalline to microcrystalline basaltic sheet flow
29b	80R-1 (Piece 2, 3 cm)	779.2	Breccia and chilled margin	8.59	Aphyric cryptocrystalline to fine-grained basaltic sheet flow
30	84R-2 (Piece 10, 60 cm)	803.9	Textural change	3.16	Massive aphyric fine-grained basalt
31	85R-3 (Piece 3, 24 cm)	814.6	Chilled margin	11.27	Massive aphyric fine-grained basalt
32	88R-1 (Piece 9, 49 cm)	840.7	Textural change	0.93	Aphyric fine-grained sheet flow
33a	89R-1 (Piece 1, 0 cm)	849.8	Different style of eruption	9.19	Aphyric microcrystalline sheet flow
33b	99R-1(Piece 1, 0 cm)	907.4	Textural change (more massive and coarse grained)	2.45	Aphyric fine-grained basaltic sheet flow
34a	100R-1 (Piece 2, 6 cm)	910.7	Breccia (containing clasts with chilled margin)	2.72	Massive aphyric microcrystalline to fine-grained basalt
34b	101R-2 (Piece 7, 33 cm)	918.8	Rubble, change in fracturation and alteration features	2.49	Massive aphyric fine-grained basalt
35a	102R-3 (Piece 6, 24 cm)	929.8	Textural change	2.71	Aphyric cryptocrystalline to fine grained basaltic sheet flow
35b	106R-1 (Piece 16, 67 cm)	951.1	Phenocrysts (sparsely olivine-clinopyroxene-plagioclase phyric)	0.32	Sparsely phyric cryptocrystalline to microcrystalline sheet flow
35c	106R-1 (Piece 24, 108 cm)	951.5	Return to aphyric texture	2.14	Aphyric cryptocrystalline to microcrystalline basaltic sheet flow
36a	108R-2 (Piece 11, 61 cm)	960.9	Breccia, textural change	3.56	Massive aphyric microcrystalline basalt
36b	110R-1 (Piece 3, 26 cm)	969.9	Textural change	2.85	Massive aphyric microcrystalline basalt
36c	111R-1 (Piece 2, 25 cm)	974.7	Textural change	1.39	Massive aphyric microcrystalline basalt
37	112R-1 (Piece 10, 75 cm)	980.0	Textural change, phenocrysts (sparsely cpx-plag phyric)	0.89	Sparsely phyric cryptocrystalline to microcrystalline sheet flow
38	113R-1 (Piece 10, 38 cm)	984.4	Breccia (containing clasts with chilled margin)	2.15	Aphyric microcrystalline to fine-grained sheet flow
39a	114R-1 (Piece 12, 112 cm)	989.9	Moderate vesicular, breccia with cryptocrystalline clasts	0.81	Massive sparsely phyric moderately vesicular microcrystalline basalt
39b	114R-2 (Piece 10, 66 cm)	990.9	Textural change (disappearance of vesicles)	3.38	Massive aphyric microcrystalline basalt
40	117R-1 (Piece 6, 85 cm)	1004.1	Textural change, brecciation	1.67	Cataclastic-massive basaltic unit
41	118R-1 (Piece 8, 66 cm)	1008.7	Textural change	3.87	Aphyric microcrystalline basaltic sheet flow
42a	122R-1 (Piece 7, 25 cm)	1027.6	Textural change (volcanic breccia)	1.30	Mineralized volcanic breccia
42b	122R-2 (Piece 4, 30 cm)	1029.1	Volcanic breccia is interbedded with sheet flow	1.47	Mineralized volcanic breccia intercalated with aphyric cryptocrystalline basaltic sheet flow
43	123R-1 (Piece 24, 109 cm)	1033.2	Textural change	4.40	Aphyric microcrystalline basaltic sheet flow
44a	129R-1 (Piece 1, 0 cm)	1060.9	Textural change	1.96	Massive aphyric microcrystalline basalt
44b	130R-1 (Piece 1, 0 cm)	1065.7	Breccia, textural change	2.34	Massive aphyric microcrystalline basalt
44c	131R-1 (Piece 1, 0 cm)	1070.5	Textural change	4.41	Massive aphyric microcrystalline basalt
44d	133R-1 (Piece 5, 108 cm)	1081.2	Textural change	3.54	Massive aphyric microcrystalline basalt

Table T5 (continued).

Unit/ Subunit	Upper contact		Nature of contact/ Rationale for boundary	Minimum thickness (m)	Rock type
	Core, section, piece, interval	Depth (mbsf)			
45	135R-1 (Piece 10, 101 cm)	1090.7	Breccia	2.83	Massive aphyric microcrystalline basalt
46a	137R-1 (Piece 16, 105 cm)	1100.4	Textural change	2.24	Massive aphyric microcrystalline basalt
46b	139R-1 (Piece 2, 8 cm)	1109.0	Textural change and possible contact	1.63	Massive aphyric microcrystalline basalt
47	140R-1 (Piece 4, 19 cm)	1113.9	Complex brecciated intrusive contact	0.90	Intrusive contact breccia and aphyric fine-grained basalt
48	141R-1 (Piece 2, 9 cm)	1118.6	Brecciated chilled margin	3.59	Massive aphyric microcrystalline to fine-grained basalt
49	143R-1 (Piece 12, 56 cm)	1128.7	Breccia, dike contact	0.94	Aphyric microcrystalline basalt
50	143R-2 (Piece 6, 22 cm)	1129.8	Change of phenocryst content (olivine + clinopyroxene)	9.61	Massive sparsely phyric microcrystalline basalt
51	147R-1 (Piece 5, 19 cm)	1145.4	Textural change (more coarse grained)	0.97	Doleritic basalt
52a	148R-1 (Piece 1, 0 cm)	1151.1	Textural change	3.77	Massive aphyric microcrystalline basalt
52b	149R-1	–	Intrusive contact	–	Aphyric cryptocrystalline basalt
52c	151R-1	–	Intrusive contact	–	Aphyric cryptocrystalline basalt
53a	152R-1 (Piece 1, 0 cm)	1169.9	Textural change	3.00	Massive aphyric fine-grained basalt
53b	153R-2	–	Intrusive contact	–	Aphyric cryptocrystalline basalt
54	154R-1 (Piece 1, 0 cm)	1179.6	Textural change	4.68	Massive aphyric microcrystalline basalt
55a	156R-1 (Piece 1, 0 cm)	1189.4	Textural change	6.06	Massive aphyric microcrystalline basalt
55b	157R-1	–	Intrusive contact	–	Aphyric microcrystalline basalt
56a	159R-1 (Piece 16, 93 cm)	1204.7	Textural change	3.94	Massive aphyric cryptocrystalline to microcrystalline basalt
56b	161R-1	–	Intrusive contact	–	Aphyric cryptocrystalline basalt
57a	162R-1 (Piece 9, 65 cm)	1214.1	Textural change	4.93	Massive aphyric cryptocrystalline-microcrystalline basalt
57b	162R-3	1216.4	Intrusive contact	–	Aphyric cryptocrystalline basalt
57c	163R-2	1219.5	Textural change and intrusive contact	–	Aphyric cryptocrystalline basalt
58	163R-3 (Piece 1, 0 cm)	1221.0	Textural change	2.83	Massive aphyric cryptocrystalline to microcrystalline basalt
59	164R-2 (Piece 9, 45 cm)	1225.0	Textural change	0.98	Massive aphyric microcrystalline basalt
60a	164R-3 (Piece 3, 16 cm)	1226.2	Textural change	3.69	Massive aphyric microcrystalline basalt
60b	165R-3	–	Intrusive contact	–	Aphyric cryptocrystalline dike
61a	166R-1 (Piece 1, 0 cm)	1232.6	Textural change	3.56	Massive aphyric microcrystalline basalt
61b	166R-1	–	Intrusive contact	–	Aphyric cryptocrystalline dike
62	167R-1 (Piece 1, 0 cm)	1236.4	Textural change	3.01	Massive aphyric-sparsely phyric microcrystalline basalt
63	167R-3 (Piece 11, 73 cm)	1239.8	Breccia, textural change	6.37	Massive aphyric microcrystalline basalt
64	169R-1 (Piece 9, 60 cm)	1247.6	Textural change	4.32	Massive aphyric microcrystalline basalt
65	170R-2 (Piece 12, 104 cm)	1254.2	Textural change	1.15	Massive aphyric microcrystalline basalt

Note: cpx = clinopyroxene, plag = plagioclase.

Figure F1. A. Basement age versus depth of basement penetration for scientific drill holes deeper than 50 m drilled into in situ ocean crust formed at the mid-ocean ridges. **B.** Depth of penetration of drill holes into in situ basement clustered by broad spreading rate subdivisions where slow < 40 mm/y < moderate < 80 mm/y < fast. Note that the boundaries between erupted lavas, the dike–lava transition zone, and the sheeted dike complex/upper gabbro boundary are placed at arbitrary depths based loosely on Hole 504B stratigraphy. Predictions based on marine seismic reflection studies indicate that the combined thickness of the lava–dike sequences should decrease with spreading rate but are yet to be tested, and whether it is the dikes or lavas that are thinned is so far unknown. Black lines = DSDP drill holes, dark blue lines = ODP drill holes, red lines = Holes 1256C and 1256D drilled into basement during Leg 206 and Expedition 309. For complete discussion see Wilson, Teagle, Acton, et al. (2003).
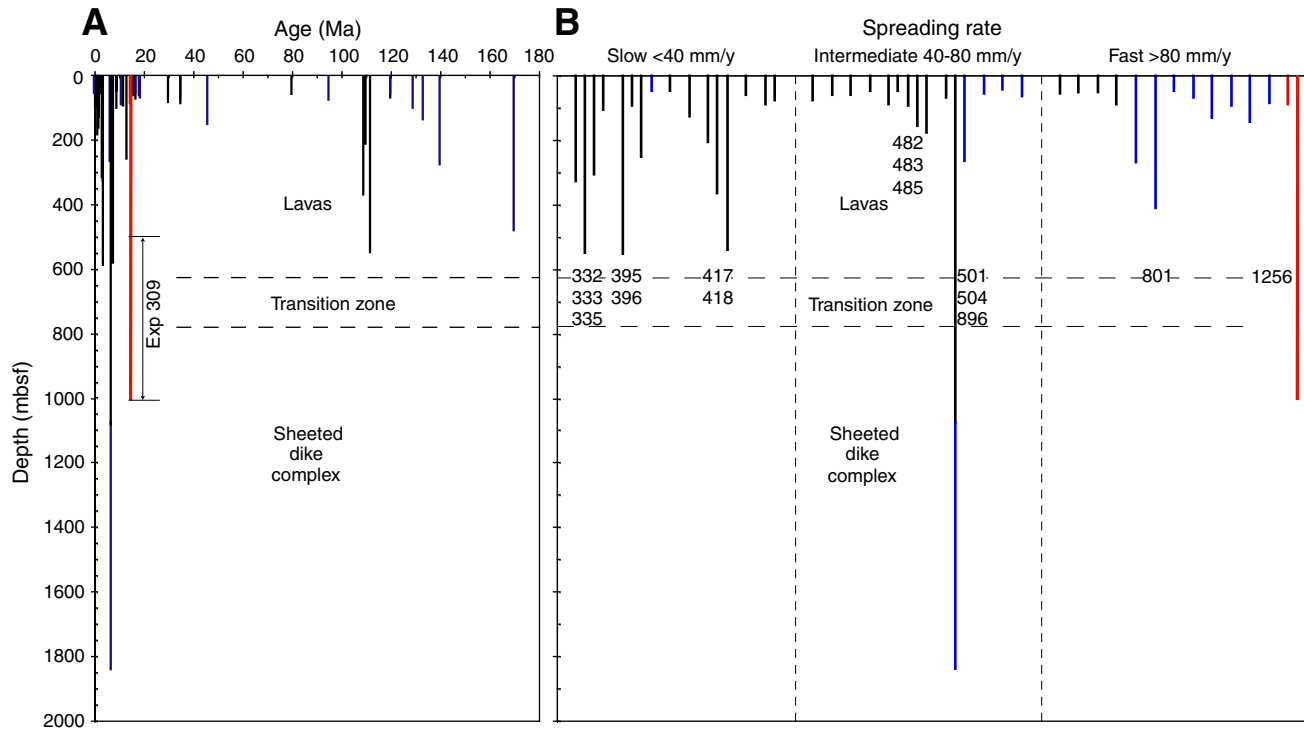
Figure F2. Age map of the Cocos plate and corresponding regions of the Pacific plate. Isochrons at 5 m.y. intervals have been converted from magnetic anomaly identifications according to the timescale of Cande and Kent (1995). Selected DSDP and ODP sites that reached basement are indicated. The wide spacing of 10–20 m.y. isochrons to the south reflects the extremely fast (200–220 mm/y) full spreading rate (modified from Wilson, Teagle, Acton, et al., 2003). FZ = fracture zone.
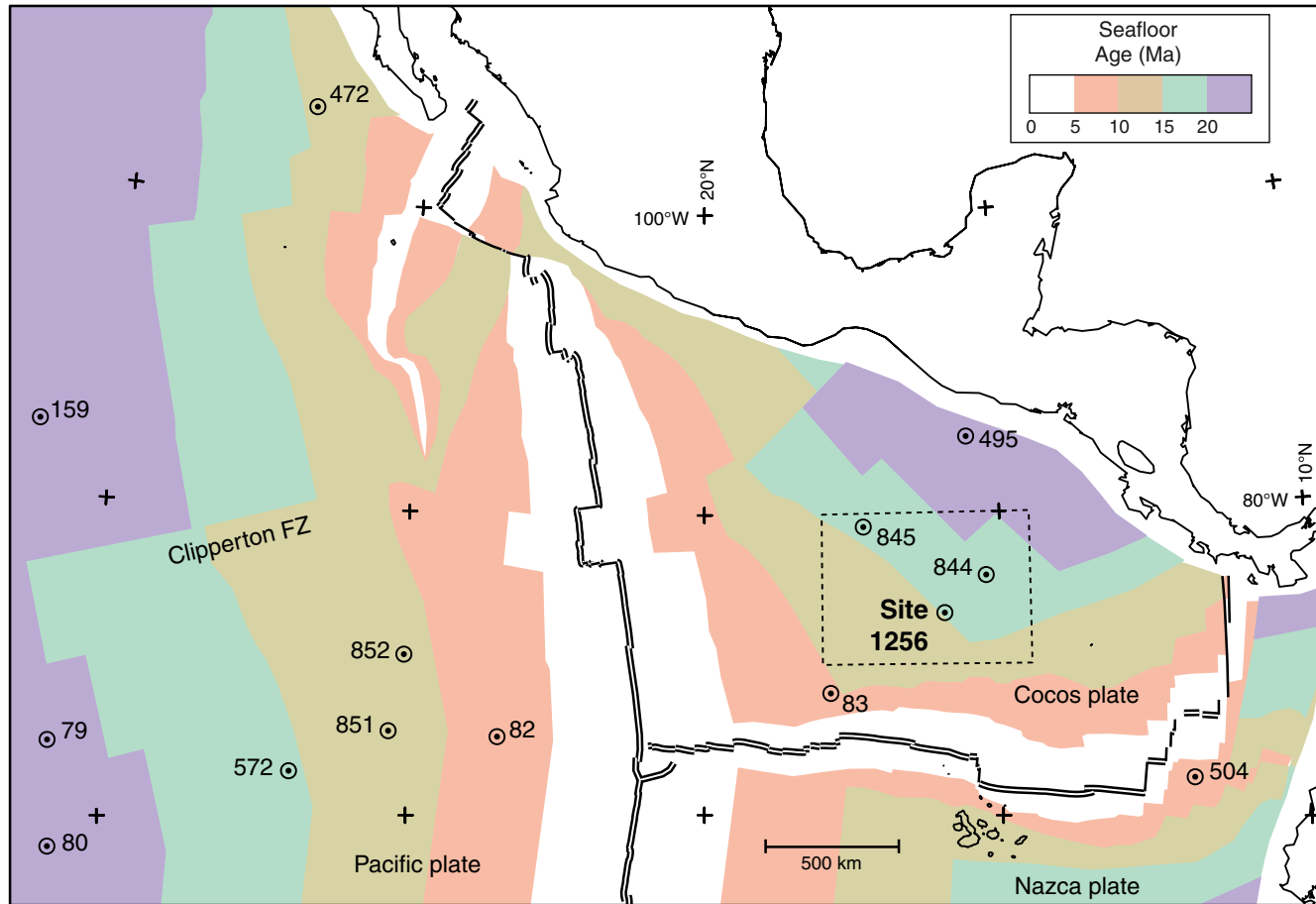
Figure F3. Depth to axial low-velocity zone plotted against spreading rate (modified from Purdy et al., 1992, and Carbotte et al., 1997b). Depth versus rate predictions from two models of Phipps Morgan and Chen (1993) are shown, extrapolated subjectively to 200 mm/y (dashed lines). Penetration to date in Holes 504B and 1256D is shown by solid vertical lines, and planned deepening for Expeditions 309 and 312 is indicated. MAR = Mid-Atlantic Ridge, EPR = East Pacific Rise, JdF = Juan de Fuca Ridge, Lau = Valu Fa Ridge in Lau Basin, CRR = Costa Rica Rift.
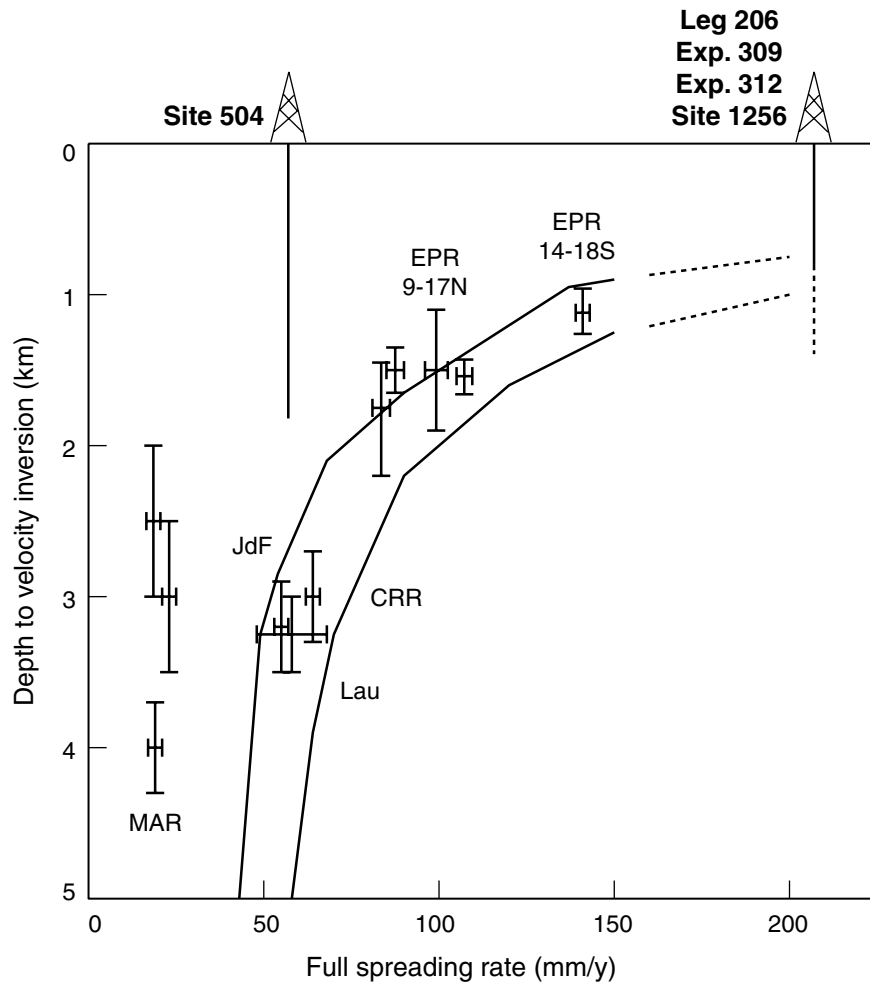
Figure F4. Reconstruction of Site 1256 and vicinity at 14 Ma, ~1 m.y. after formation of the site at the East Pacific Rise. Positions and plate velocities (arrows labeled in millimeters per year) are relative to the Antarctic plate, which is reasonably fixed relative to the spin axis and hotspots. Bars = reconstructed positions of mapped magnetic Anomalies 5B, 5C, and 6 (ages 15–20 Ma), circles = existing DSDP/ODP drill sites.
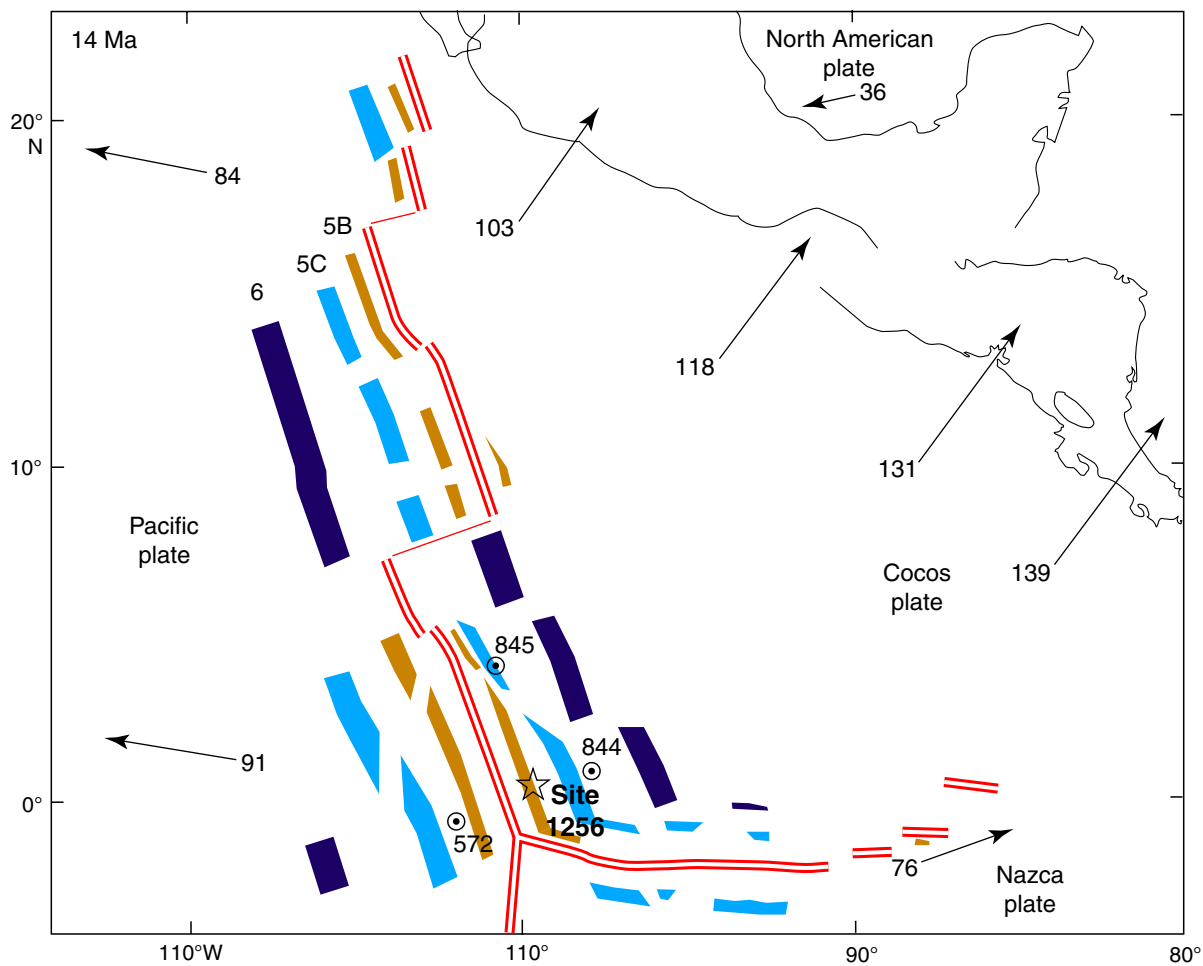
Figure F5. A. Details of isochrons inferred from magnetic anomalies near Site 1256. Shading shows normal magnetic polarity based on digitized reversal boundaries (small circles; after Wilson, 1996). Bold line shows location of Guatemala Basin (GUATB) multichannel seismic (MCS) tracklines from the site survey Cruise EW9903 conducted in March–April 1999 (Wilson et al., 2003). Anomaly ages: 5A = ~12 Ma, 5B = 15 Ma, and 5D = ~17 Ma. **B.** Bathymetry and site survey track map for Site 1256 (proposed Site GUATB-03C). Abyssal hill relief of up to 100 m is apparent in the southwest part of the area; relief to the northeast is lower and less organized. Line numbers 21–28 identify MCS lines from the site survey. OBH = ocean bottom hydrophone.
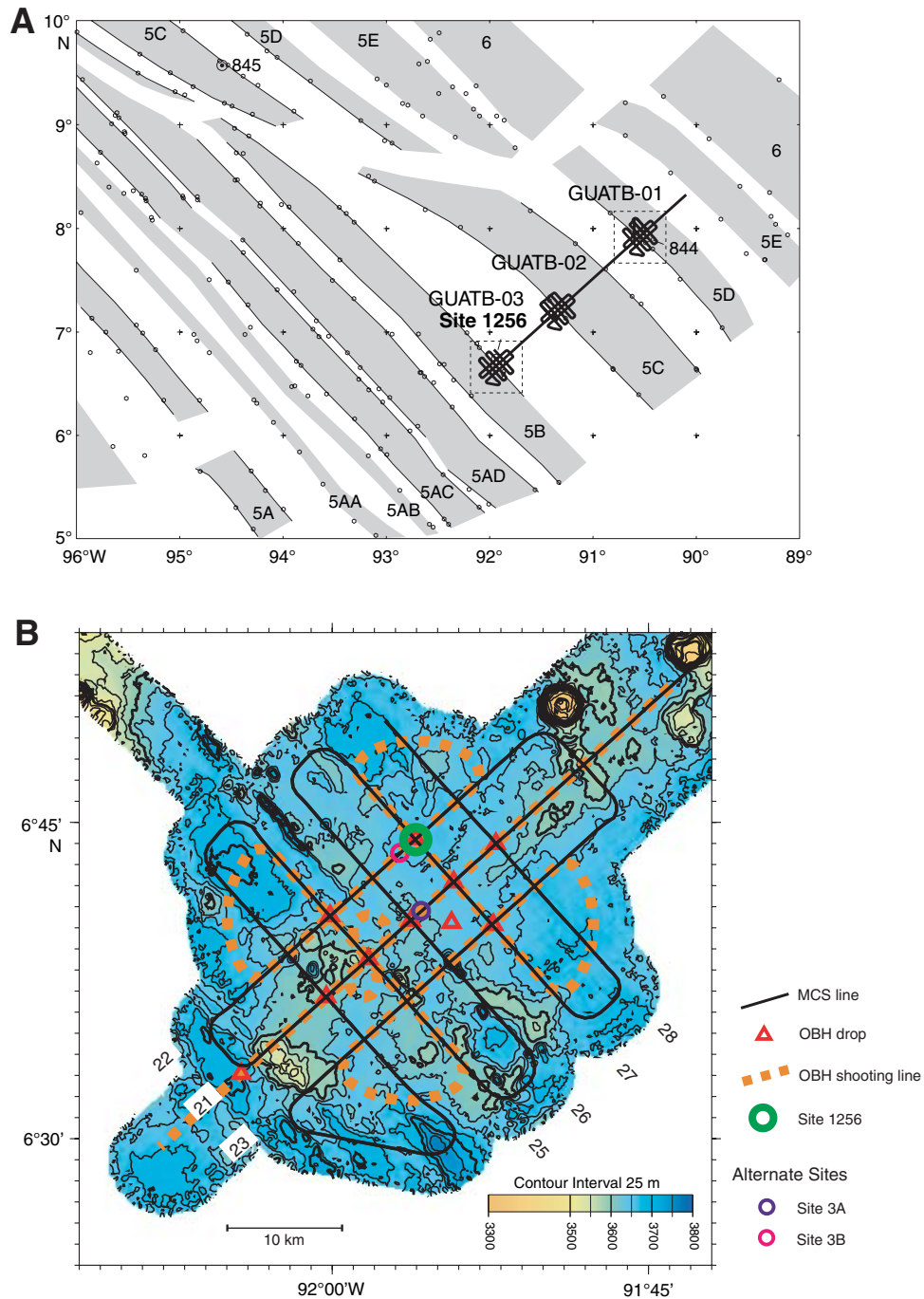
Figure F6. Site survey MCS data (Hallenborg et al., 2003) from the lines that cross at Site 1256, with penetration as of the end of Expedition 309 scaled approximately to travel time. Distances are in kilometers. Horizontal reflectors in the upper basement to travel times of 5.5 s appear to result from contrasts between lava flow sequences, corresponding to depths of at least 800 meters subbasement.
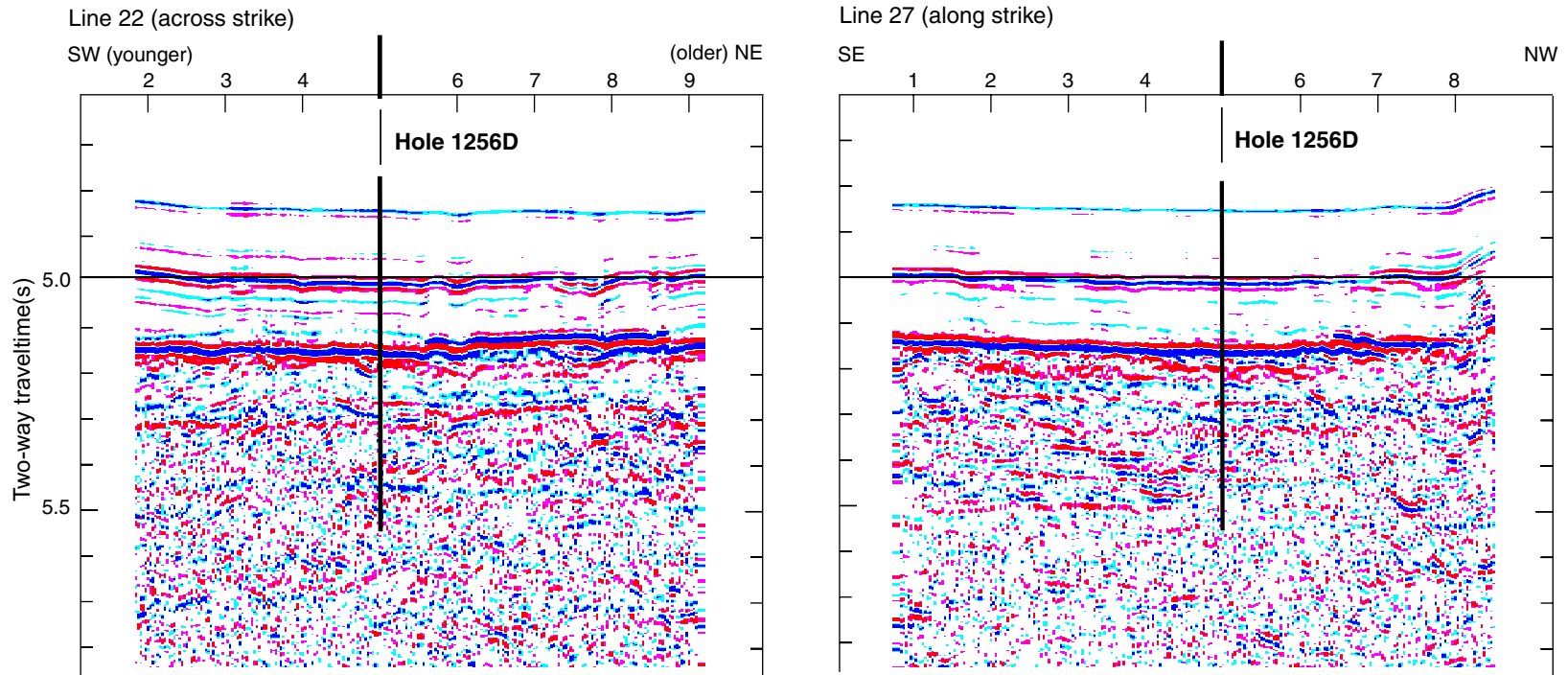
Figure F7. One-dimensional velocity model based on inversion of refraction data. At shallow depths, separate inversions were performed on northeast and southwest data subsets, with slightly faster velocities found to the northeast where abyssal hill topography is very subdued. The Layer 2/3 boundary is present in the depth range 1.2–1.5 km. The velocity model of Detrick et al. (1998) for Site 504, also based on ocean bottom hydrophone refraction, is shown for comparison. Apparent differences are dominated by differences in the inversion techniques, but the differences at 1.3–1.7 km may be barely above uncertainty.
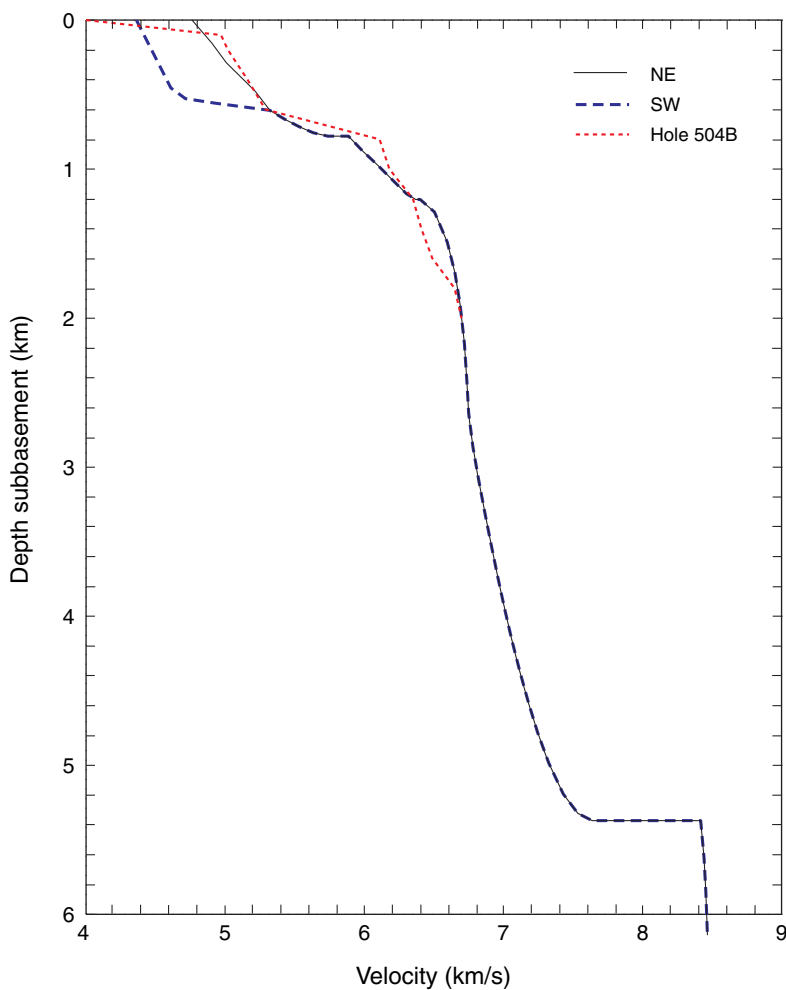
Figure F8. A. Contour map of seismic *P*-wave velocity at the top of basement, based on tomographic inversion of seismic refraction data (A. Harding, unpubl. data). The low-velocity area southwest of the center may reflect pillow lavas or other porous formation. The high-velocity area extending southeast from Site 1256 may reflect the extent of the ponded lava sequence drilled at the top of basement in Holes 1256C and 1256D. **B.** Geological map of Site 1256 area (GUATB-03) showing bathymetry, alternate site locations, and selected top-of-basement velocity contours from A. The larger velocity contour line partially encloses velocity >4.82 km/s, which we interpret as a plausible proxy for the presence of thick ponded lava flows, as encountered at Site 1256. The smaller contour encloses velocities <4.60 km/s, possibly reflecting a greater portion of pillow lavas than elsewhere in the region. Alternate reentry Sites 3D and 3E are 0.5–1.0 km from Site 1256.
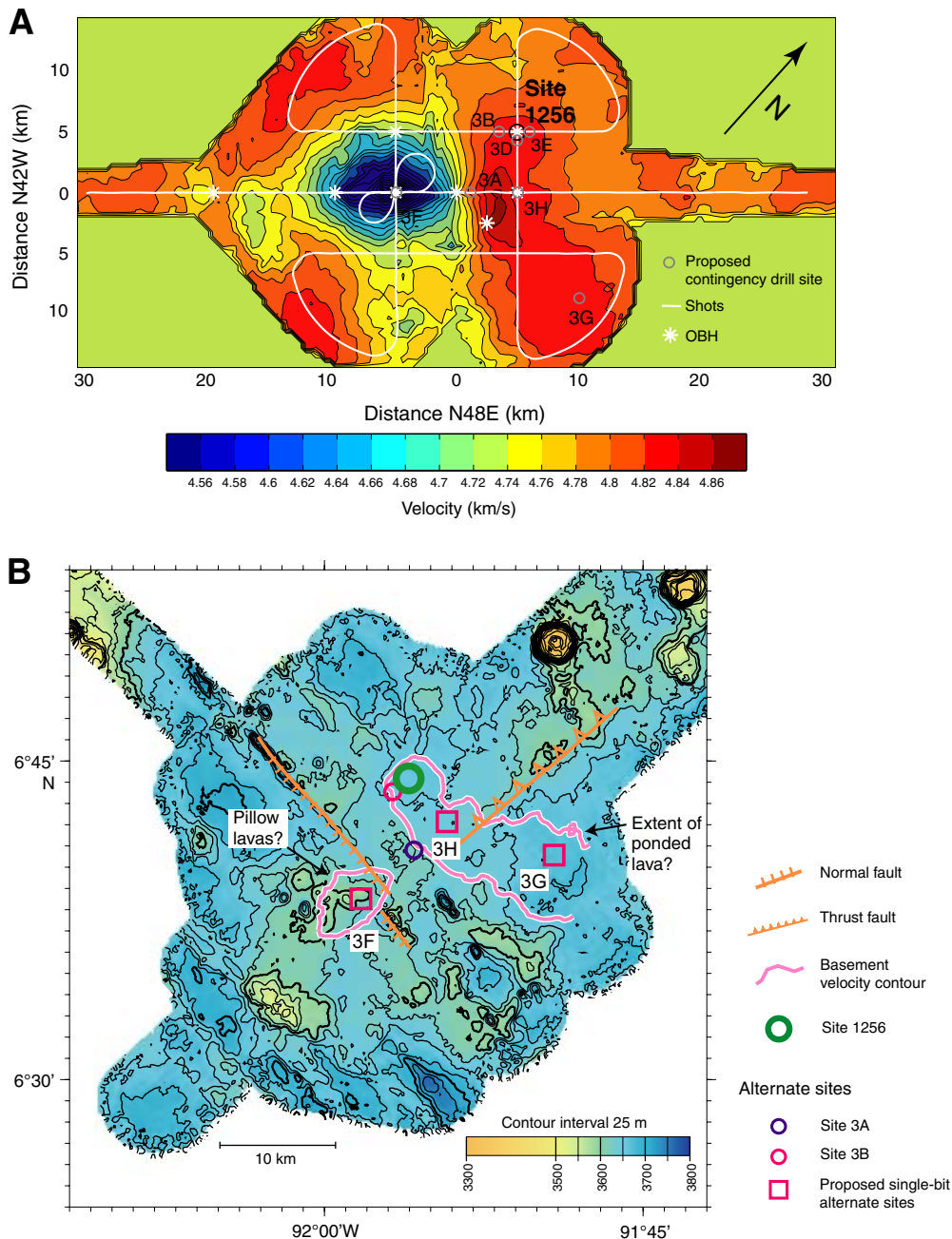
Figure F9. Recovery and lithology schematics and selected chemical and logging results for basement in Holes 1256C and 1256D during Leg 206 (Wilson, Teagle, Acton, et al., 2003).
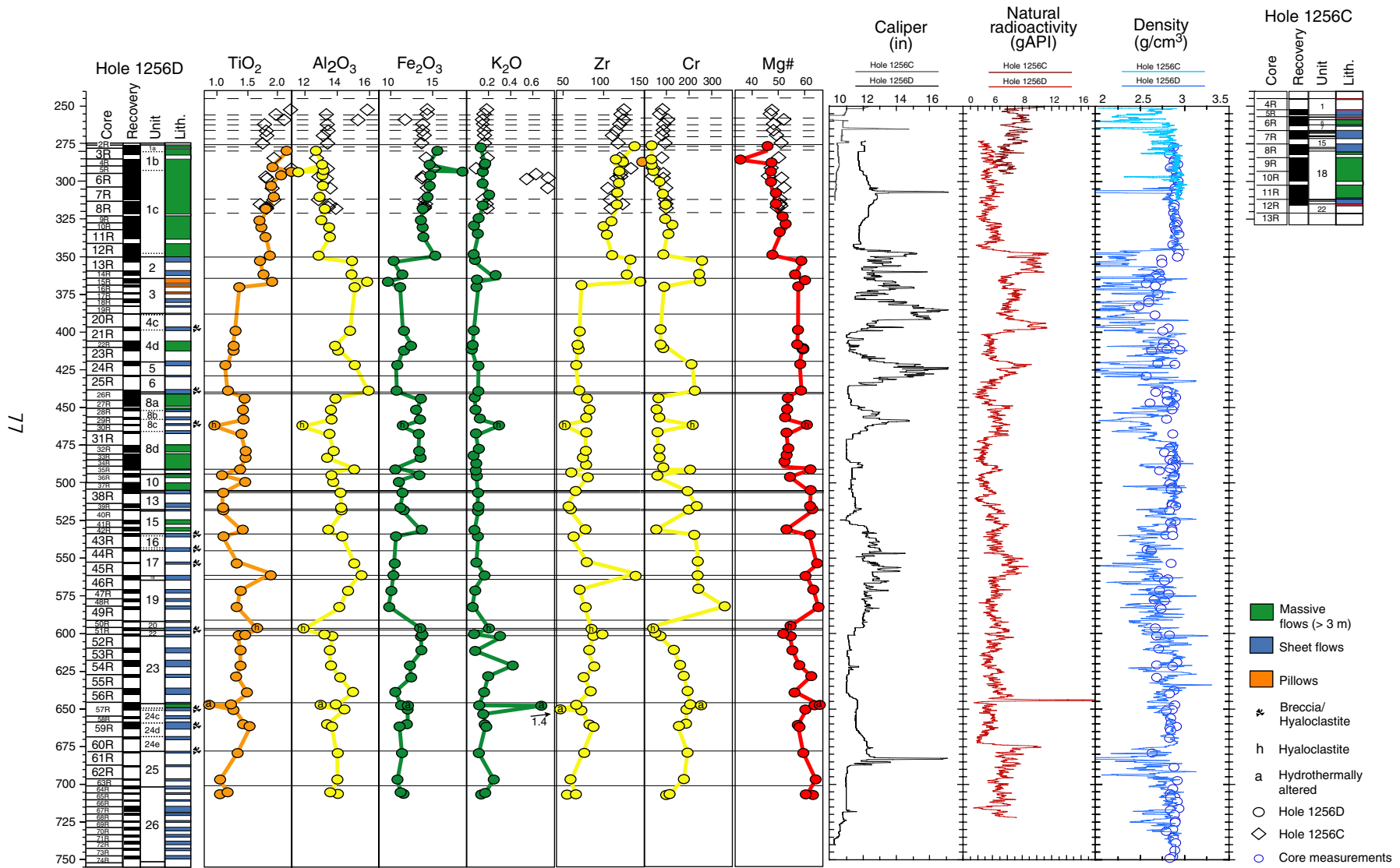
Figure F10. Distribution of alteration zones with depth in selected ODP basement sections compared to Hole 1256D.
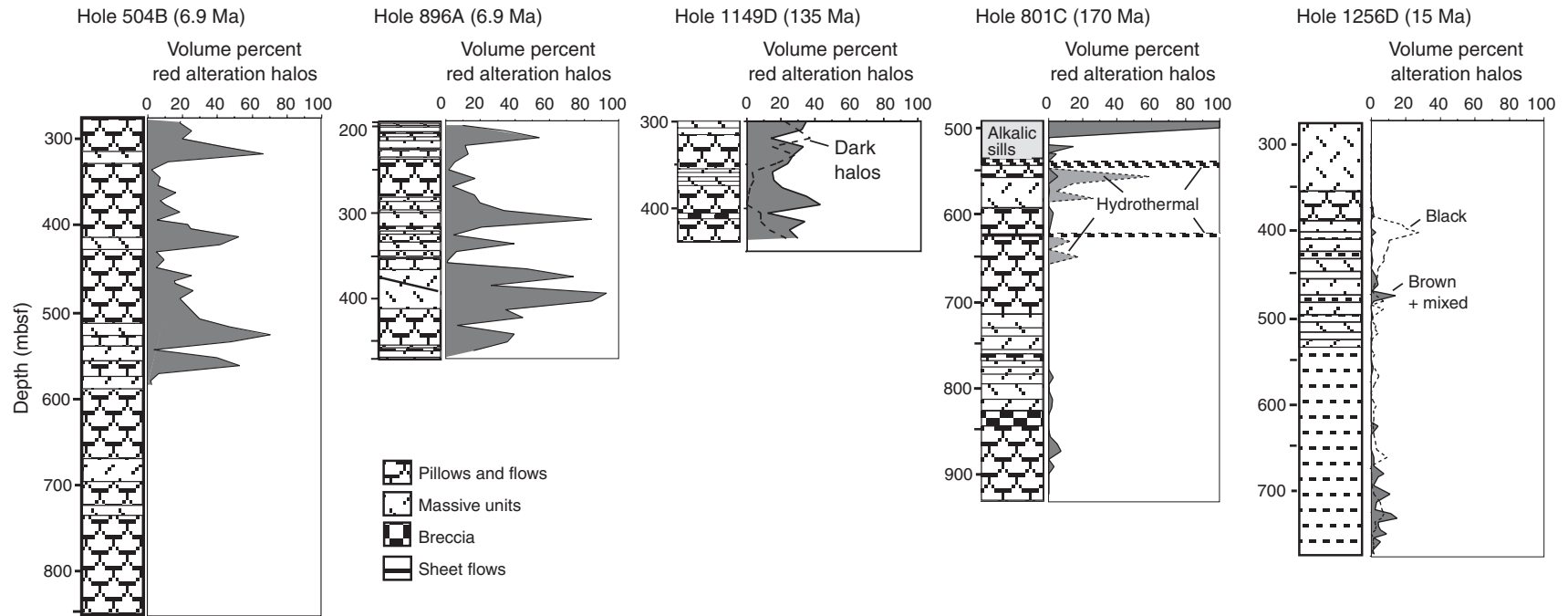
Figure F11. Depth versus time predicted for drilling and wireline logging operations for Expeditions 309 and 312. Black line = depth of Hole 1256D before operations during Expedition 309. Horizontal lines = range of depths at which axial low-velocity zones, now frozen as gabbros, should be present, assuming 300 m of off-axis lavas (see Table T1). RCB = rotary core barrel.
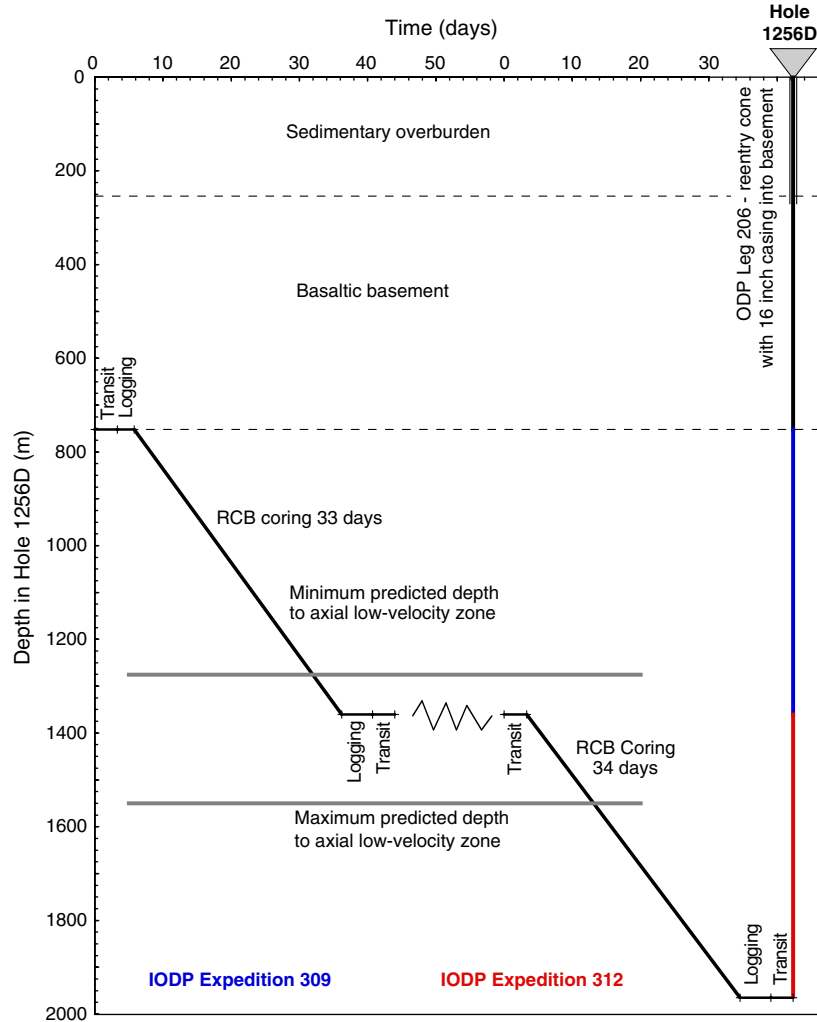
Figure F12. Bit sub under tension on the rotary table. Note the large crack that extends most of the way around the circumference.

Figure F13. Crack found in the 5 inch drill pipe. The ends of the crack are splayed with curved edges, whereas the central portion is planar.

Figure F14. Drilling progress in Hole 1256D during Expedition 309. Black line = actual drilling progress versus time, compared to precruise estimates of progress based on penetration rates of 1 (red) and 1.5 (blue) m/h with 54 h rotation time per CC-9 RCB. Bit changes and drill string withdrawals because of equipment damage are indicated. The minimum and maximum predicted target depth to gabbros is shown (see Fig. F11). WSTP = Water Sampling Temperature Probe. ROP = rate of penetration.
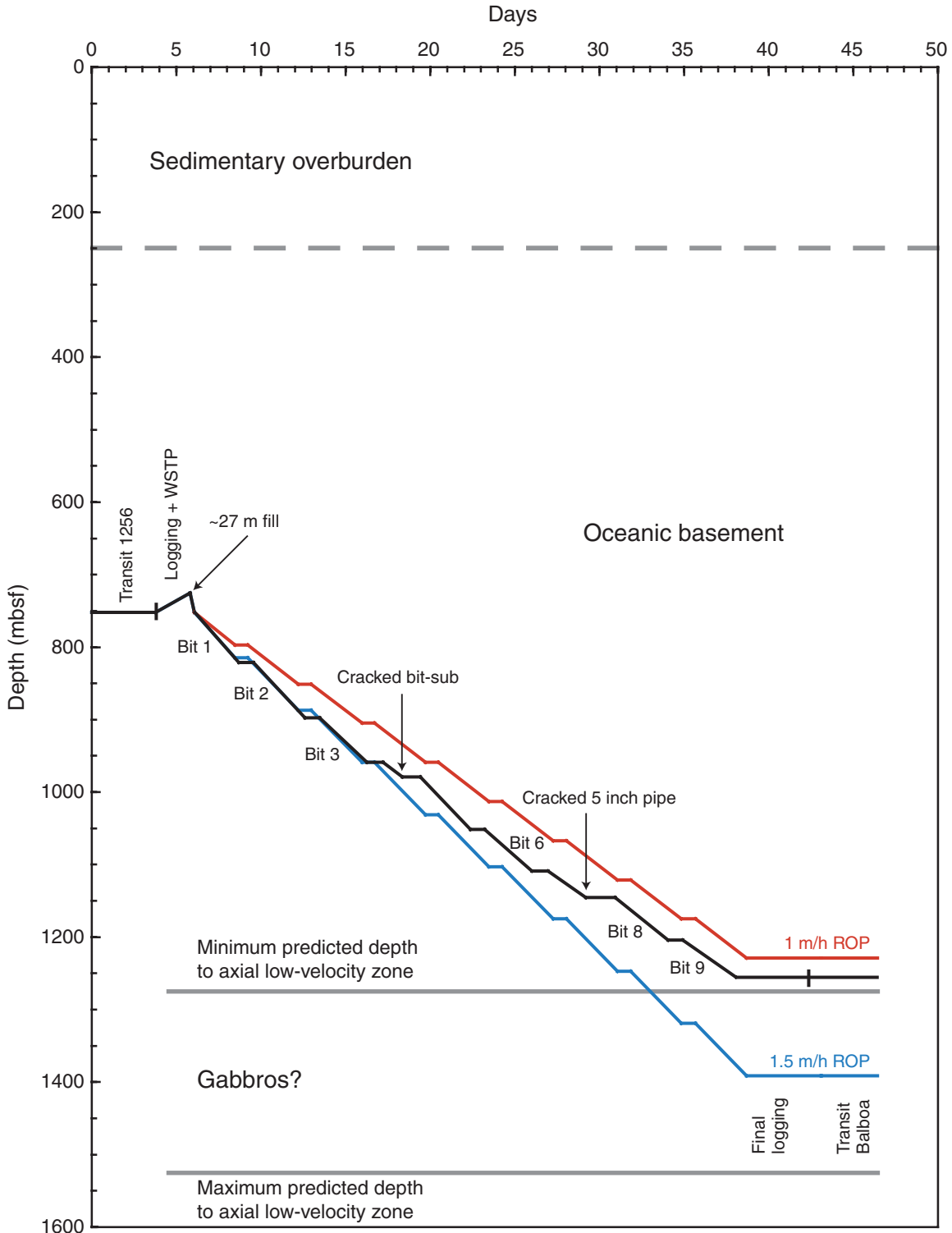
Figure F15. Boreholes >200 m deep drilled into in situ ocean crust by DSDP, ODP, and IODP compared to Hole 1256D. Hole 504B is the only other basement hole to sample a complete extrusive sequence and penetrate into the sheeted dikes. ODP Hole 735B and IODP Hole U1309D, which drilled deeply into gabbros tectonically exposed near ridge-transform intersections on the Southwest Indian Ridge and Mid-Atlantic Ridge respectively, are shown for comparison. L.p. = lava pond, Inflate = inflated flows, Sheet and mass flows = sheet and massive flows, T.z. = transition zone, S. intru. = sheeted intrusives. msb = meters subbasement. See Table T4 for description and basis for these subdivisions.
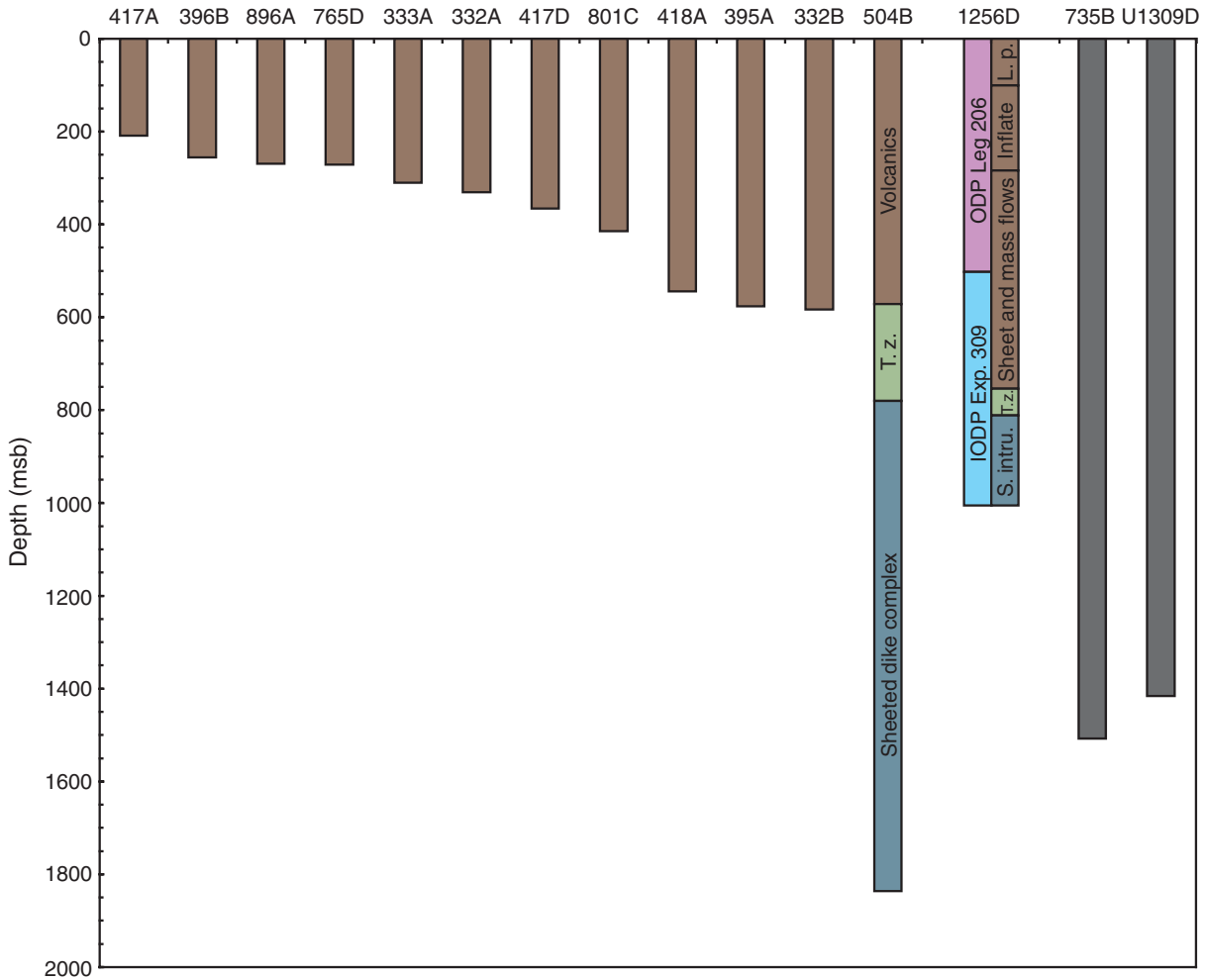
Figure F16. Simplified igneous stratigraphy of Hole 1256D, showing the dominant rock types and the preliminary subdivisions of the upper crust.
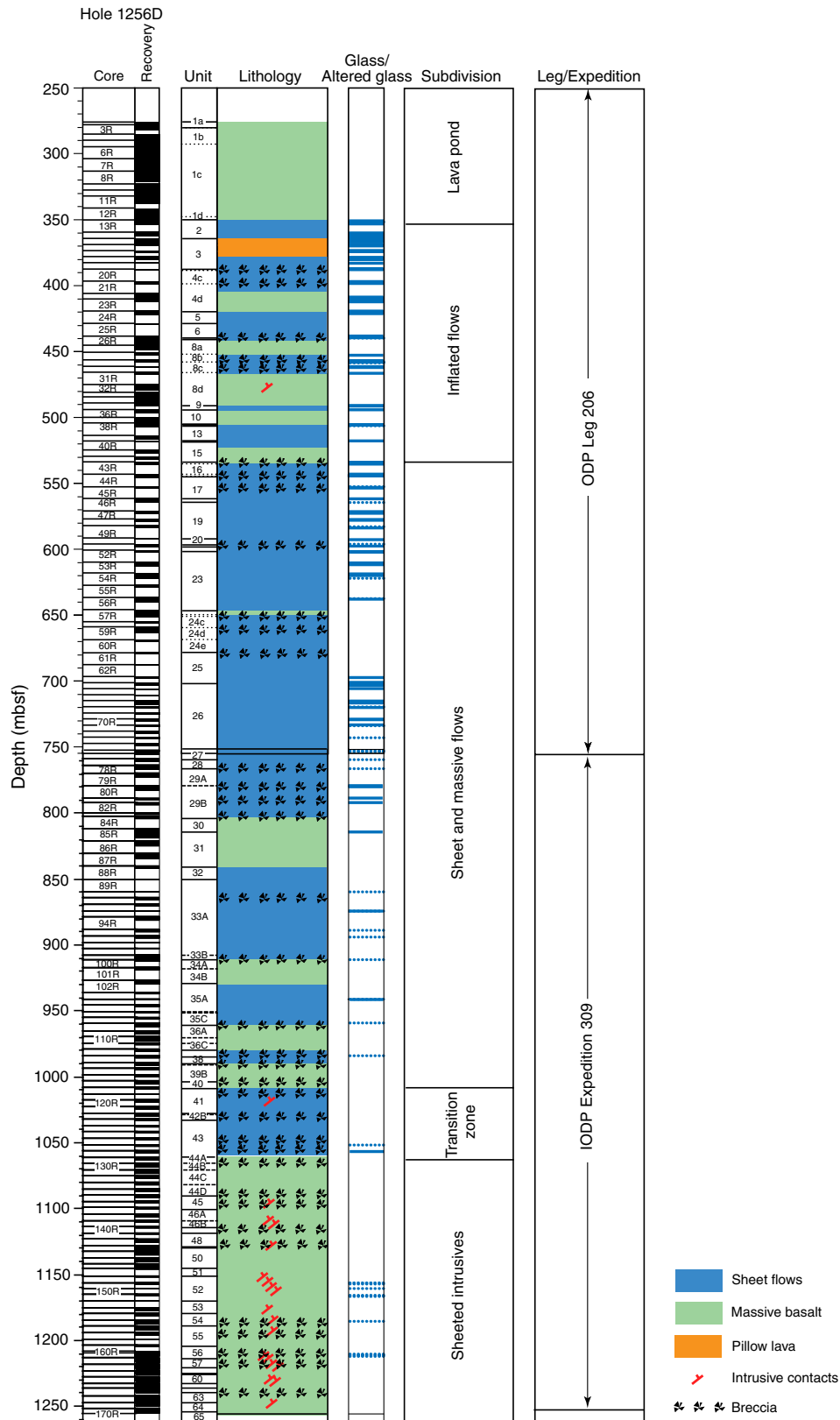
Figure F17. Summary of basement stratigraphy in Hole 1256D, cored during Expedition 309, showing (from left) a depth scale, core numbers, recovered intervals, unit and subunit boundaries, igneous lithology, locations of glass and altered glass (solid/stippled line), groundmass grain size, and phenocryst percentage based on thin section descriptions. cx = cryptocrystalline, µx =microcrystalline, fg = fine grained, ol = olivine, plag = plagioclase, cpx = clinopyroxene. The Leg 206 stratigraphy is slightly revised according to the Leg 206 VCD records.
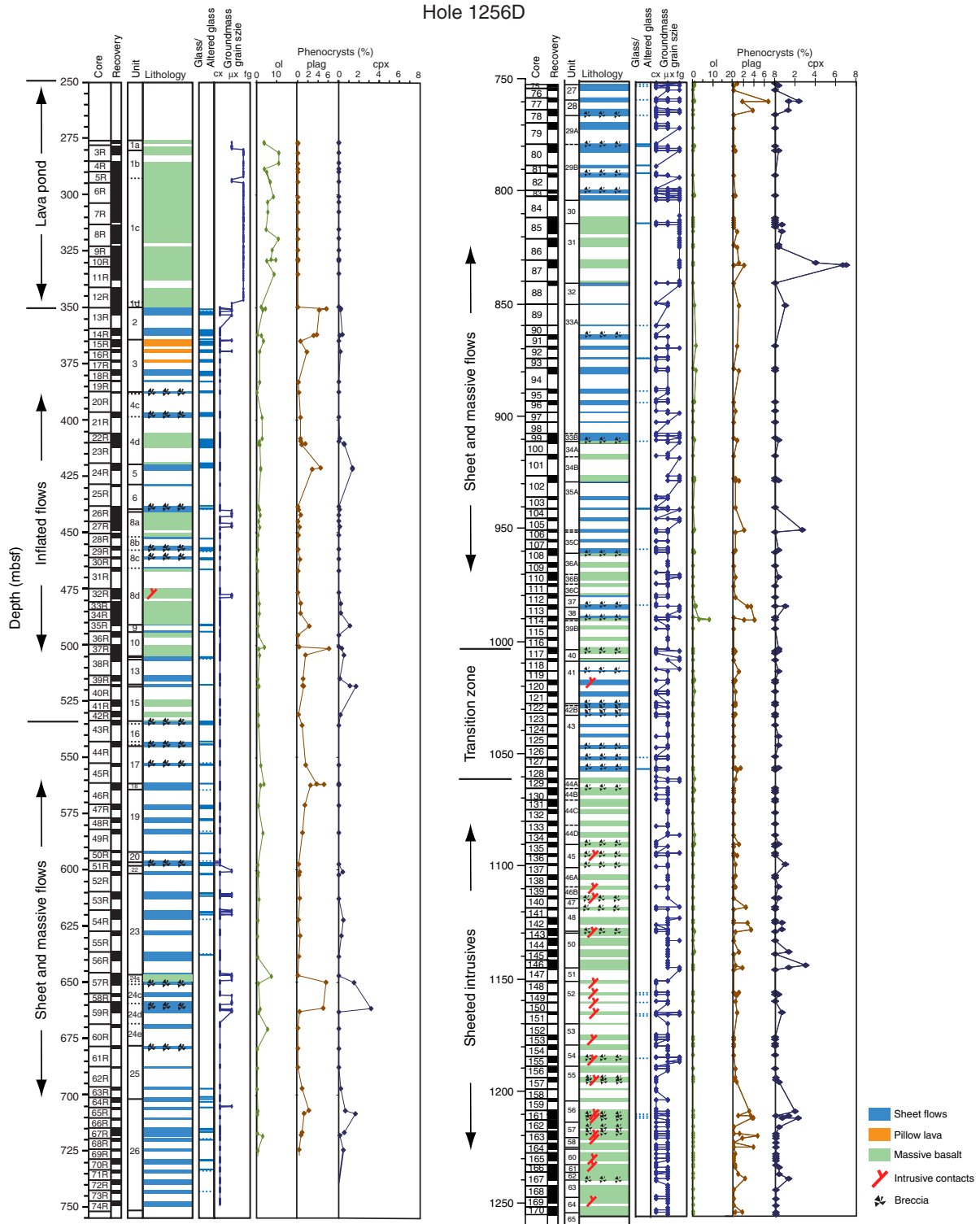
Figure F18. Aphyric cryptocrystalline to microcrystalline basalt typical for the interior of sheet flows (Subunit 1256D-29a) (interval 309-1256D-79R-2, 37–50 cm).

Figure F19. Sparsely olivine-clinopyroxene-plagioclase phyric microcrystalline basalt sheet flow (Unit 1256D-28) (interval 309-1256D-77R-2, 20–32 cm).
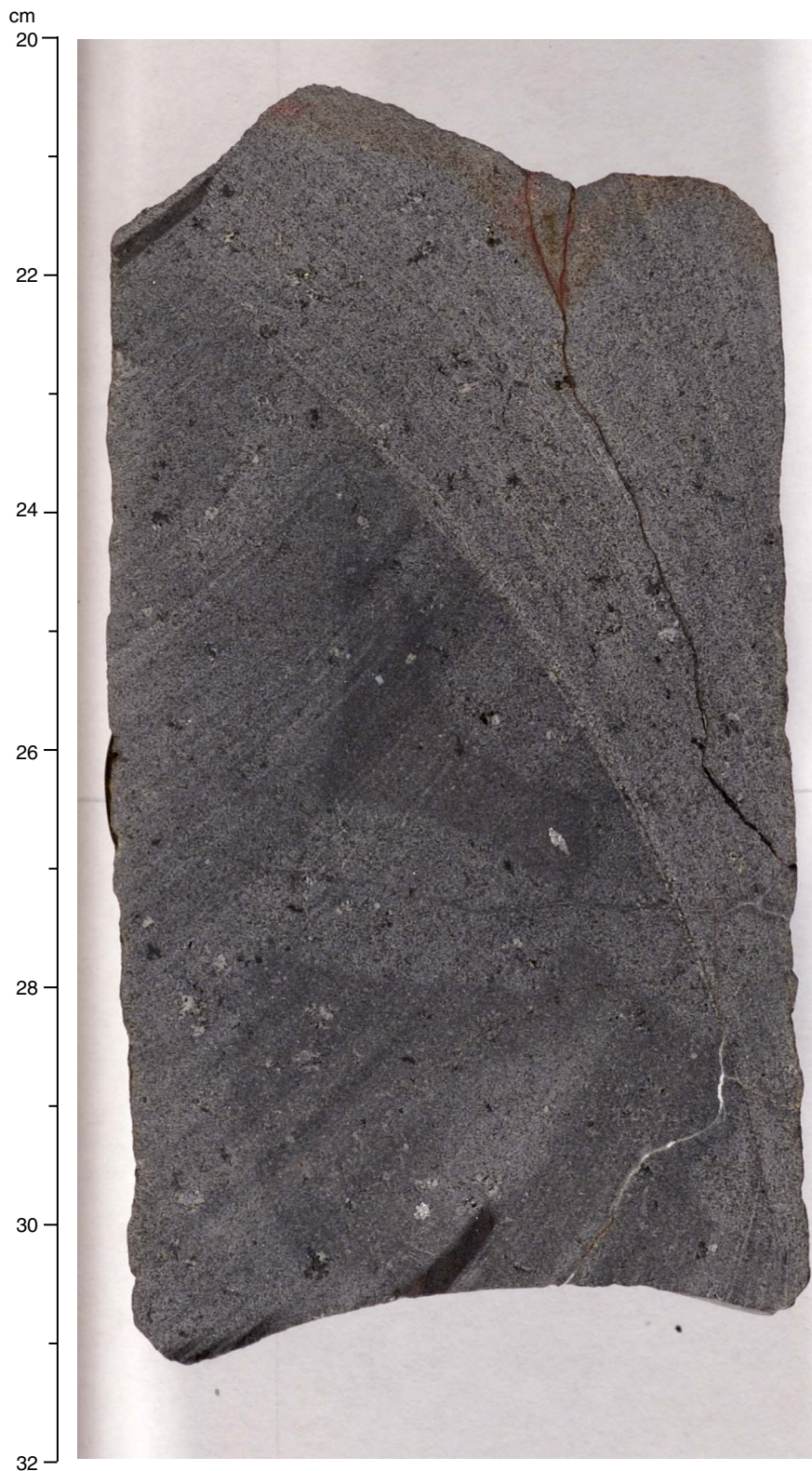
Figure F20. Holocrystalline fine-grained gabbroic xenolith in an aphyric microcrystalline basaltic sheet flow (Subunit 1256D-35c) (interval 309-1256D-108R-1, 30–36 cm). The xenolith consists of olivine, plagioclase, and clinopyroxene minerals. Cavities within the xenolith are filled with the aphyric microcrystalline basalt of the host rock.
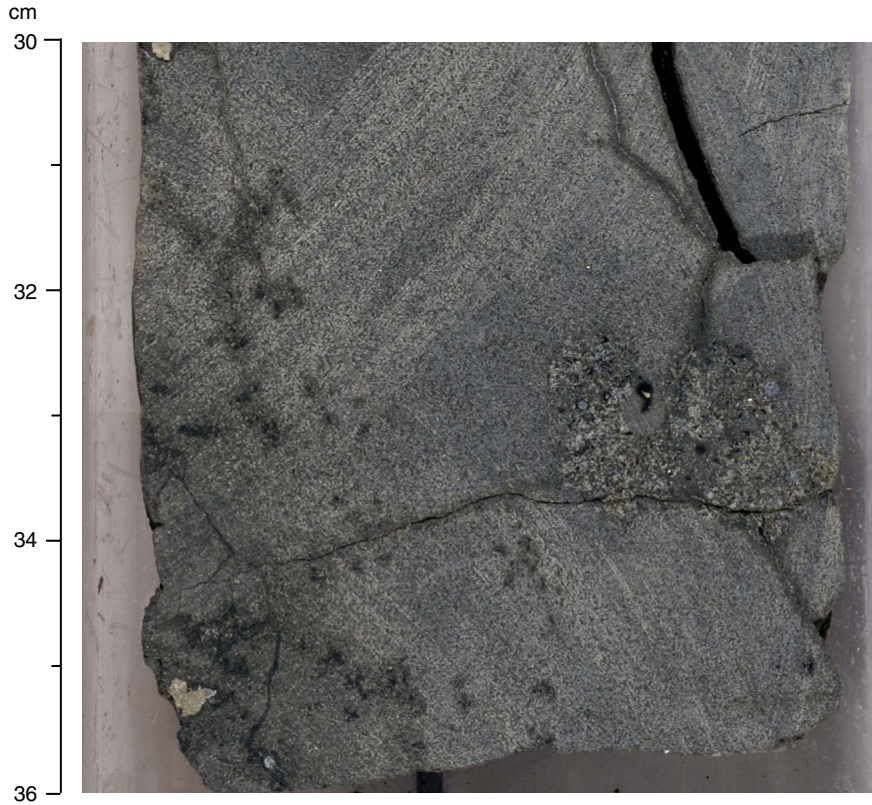
Figure F21. Typical aphyric fine-grained massive basalt (Unit 1256D-30) (interval 309-1256D-85R-1, 120–139 cm).

Figure F22. Sparsely plagioclase-olivine phyric moderately vesicular microcrystalline basalt (Subunit 1256D-39a) (interval 309-1256D-114R-1, 128–143 cm). Note the dark olivine phenocrysts and the spherical vesicle, filled with saponite.

Figure F23. Intergranular texture in massive fine-grained basalt (cross-polarized light; field of view = 5.0 mm) (Sample 309-1256D-86R-3, 94–97 cm).
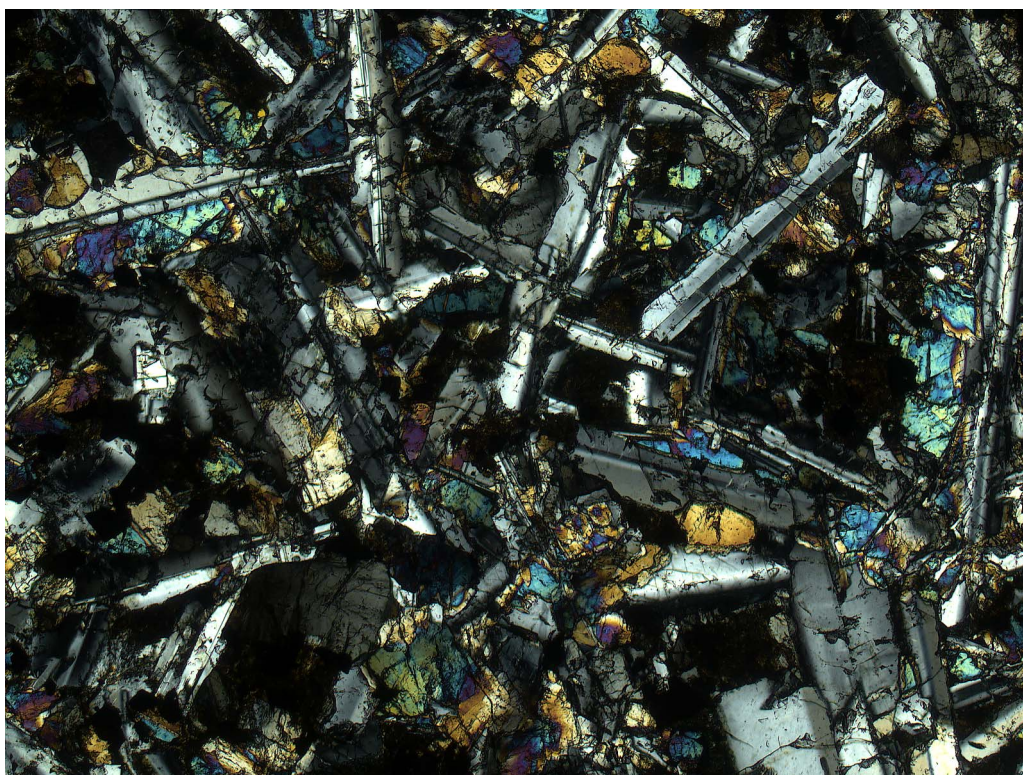
Figure F24. Cryptocrystalline basalt clasts (right edge) embedded in fine- to medium-grained cataclastic massive unit (Unit 1256D-40) (interval 309-1256D-117R-1, 121–131 cm).
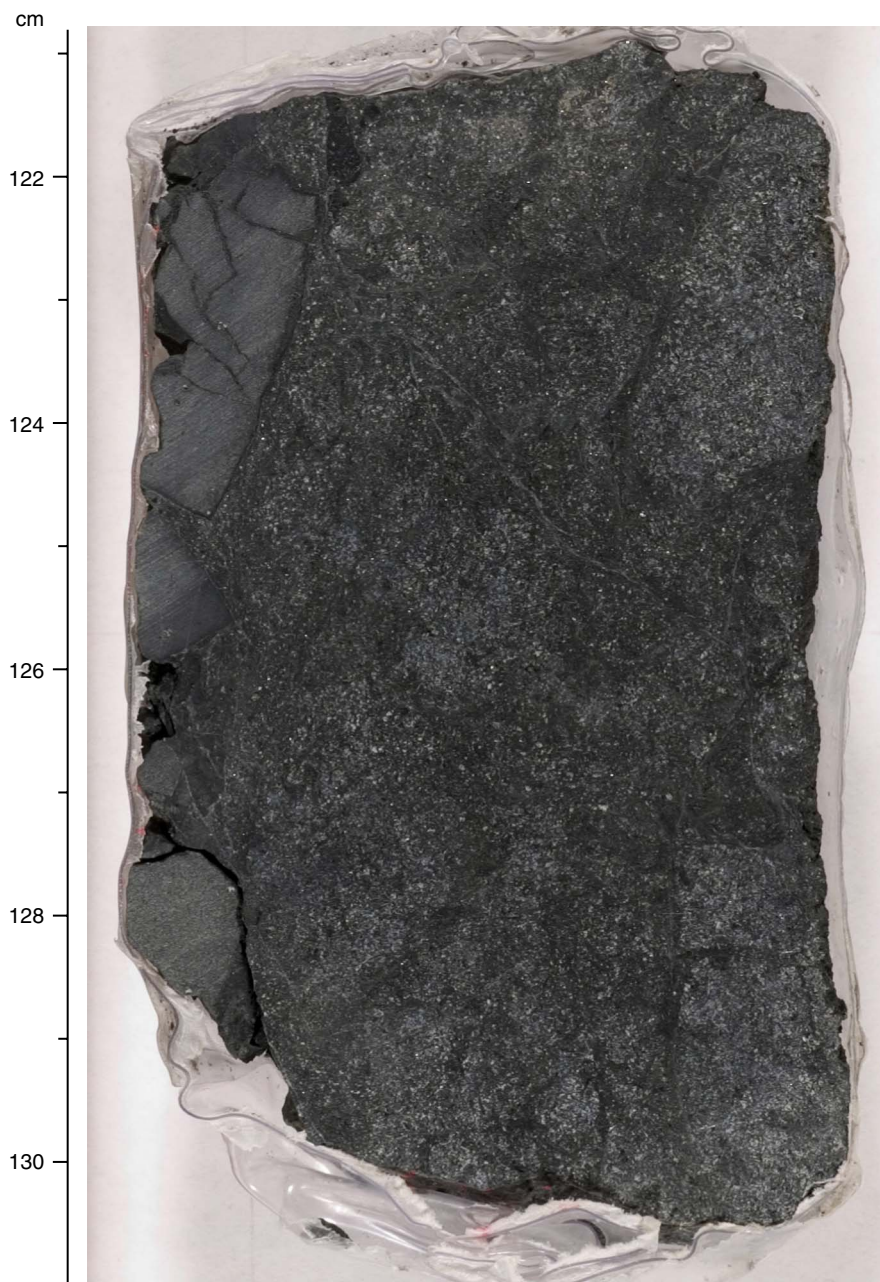
Figure F25. Mineralized volcanic breccia (Subunit 1256D-42a) and volcanic breccia interbedded with sheet flow (Subunit 1256D-42b). The breccia consists of angular fragments of glassy to cryptocrystalline basalt embedded in altered glass, sulfides, and late carbonate. Pieces indicated by arrows in Subunit 1256D-42b are brecciated. **A.** Interval 309-1256D-122R-1 (Piece 12, 50–66 cm). **B.** Interval 309-1256D-122R-1 (Piece 13, 67–80 cm). **C.** Interval 309-1256D-123R-1 (Piece 4, 15–20 cm). **D.** Interval 309-1256D-122R-2 (Pieces 2 and 3, 15–30 cm).
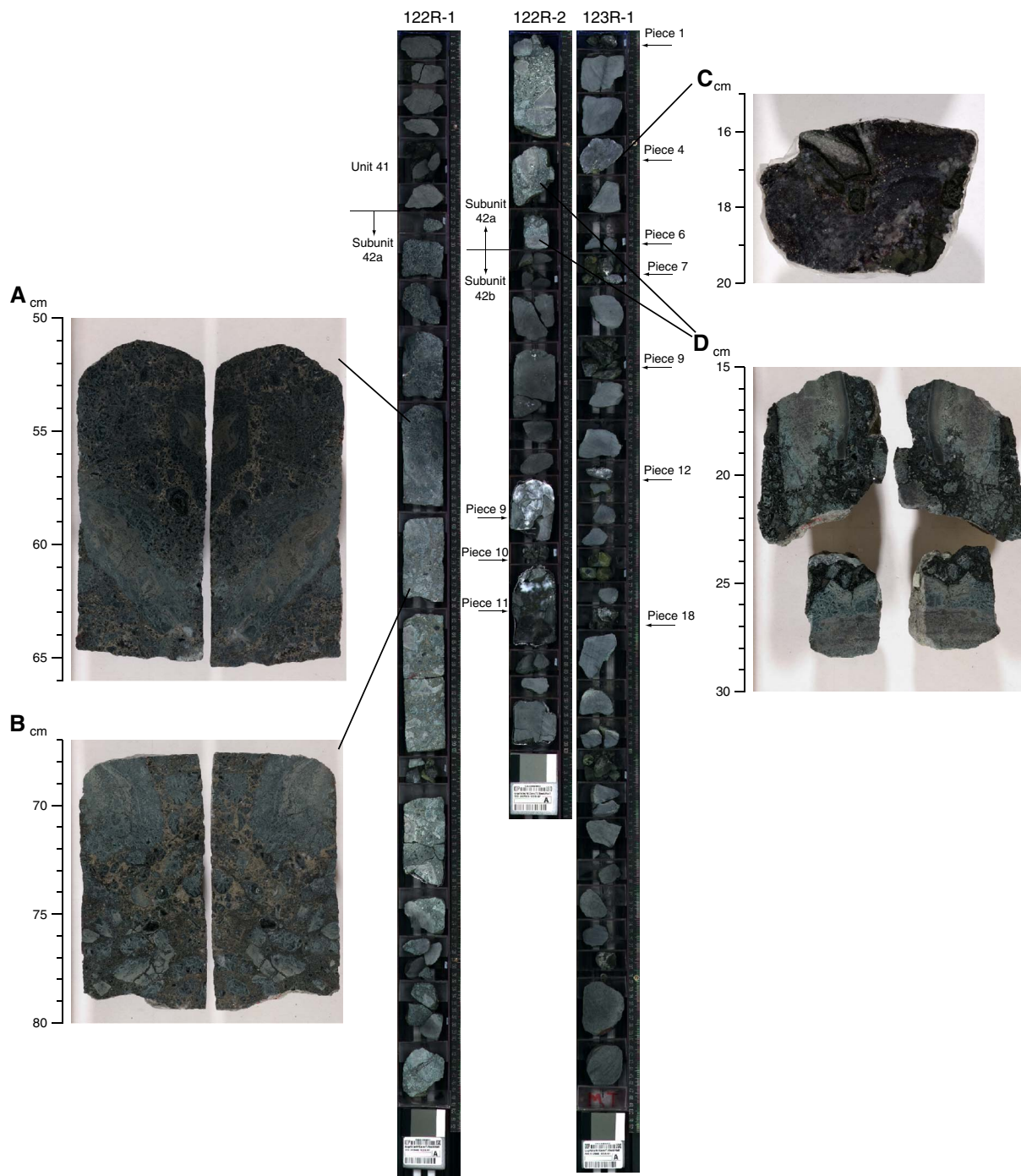
Figure F26. Holocrystalline, intergranular texture in a fine-grained dolerite of massive basalt in sheeted intrusives (field of view = 2.5 mm) (Sample 309-1256D-130R-2, 38–41 cm).
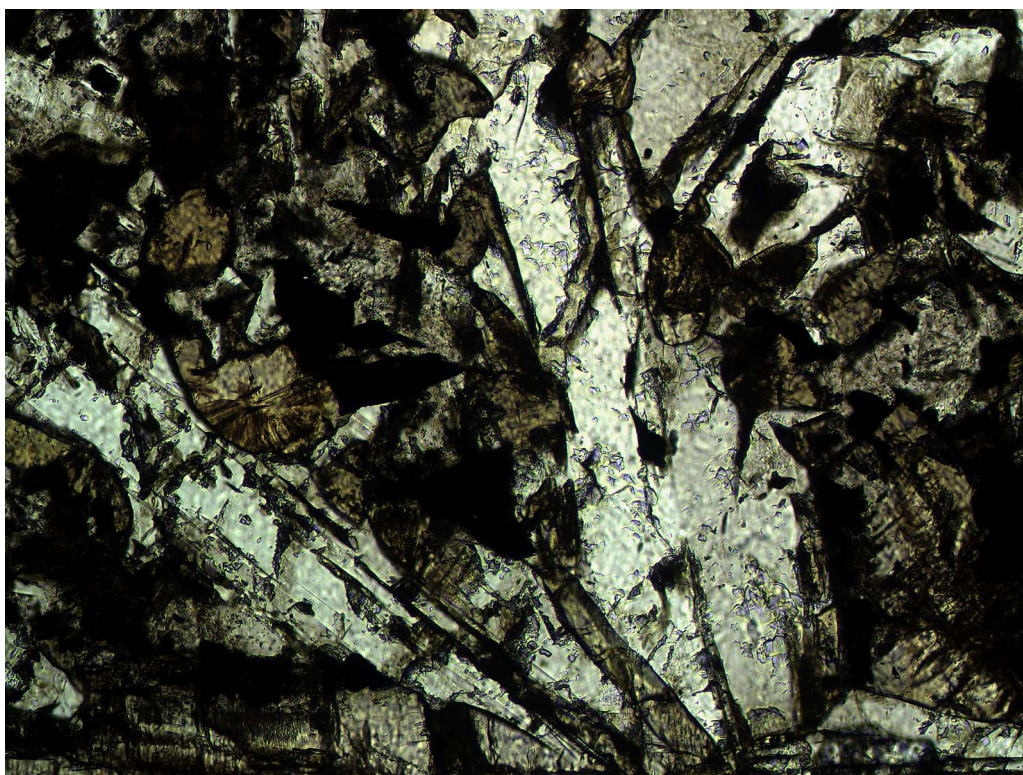
Figure F27. Sulfide-impregnated dike margin breccia (interval 309-1256D-140R-1, 42–58 cm).
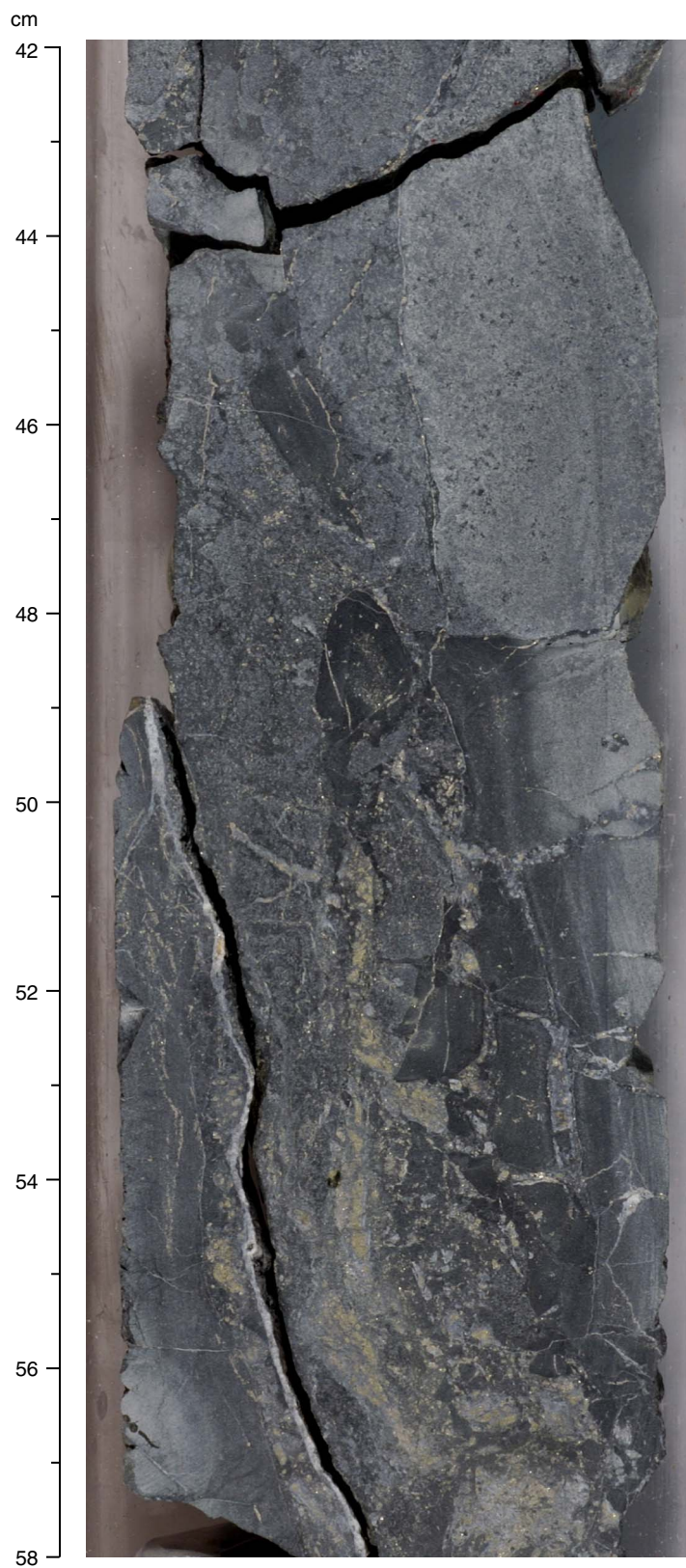
Figure F28. Three complex intrusive contacts. **A.** Composite dike. The chilled margin forms a convex lobe, indicating that the host rock was still ductile during the intrusion (interval 309-1256D-155R-1, 83–90 cm). **B.** An inner sparsely phyric dike intrudes a sparsely phyric spherulitic chilled margin, which is different from the aphyric host rock. Therefore, in this piece, two subsequent intrusive contacts are recorded (interval 309-1256D-161R-2, 0–8 cm). **C.** Lobate contact with brecciation of the external chilled margin and dispersion of the small clasts in the host rock observed (interval 309-1256D-163R-1, 112–122 cm).
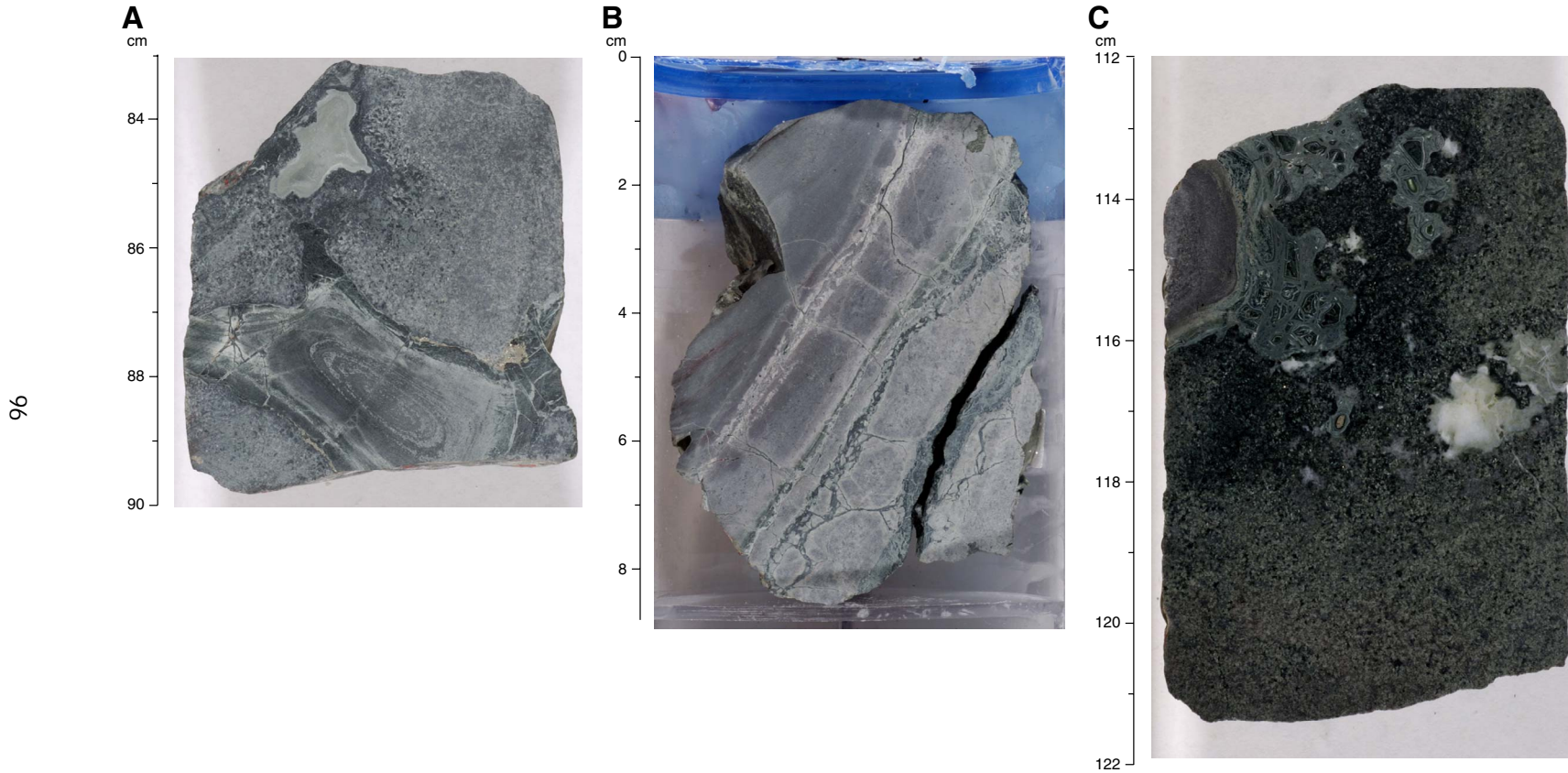
Figure F29. Expedition 309 phenocryst content compared with Leg 206 phenocryst data. **A.** Frequency of modal abundance of phenocrysts in basalt from Leg 206 and Expedition 309. **B.** Proportion of plagioclase-clinopyroxene-olivine phenocrysts in basalt from Leg 206 and Expedition 309. Pl = plagioclase, Cpx = clinopyroxene, Ol = olivine. **C.** Pie charts depicting relative abundance of plagioclase-clinopyroxene-olivine phenocrysts in basalts from Leg 206 and Expedition 309.
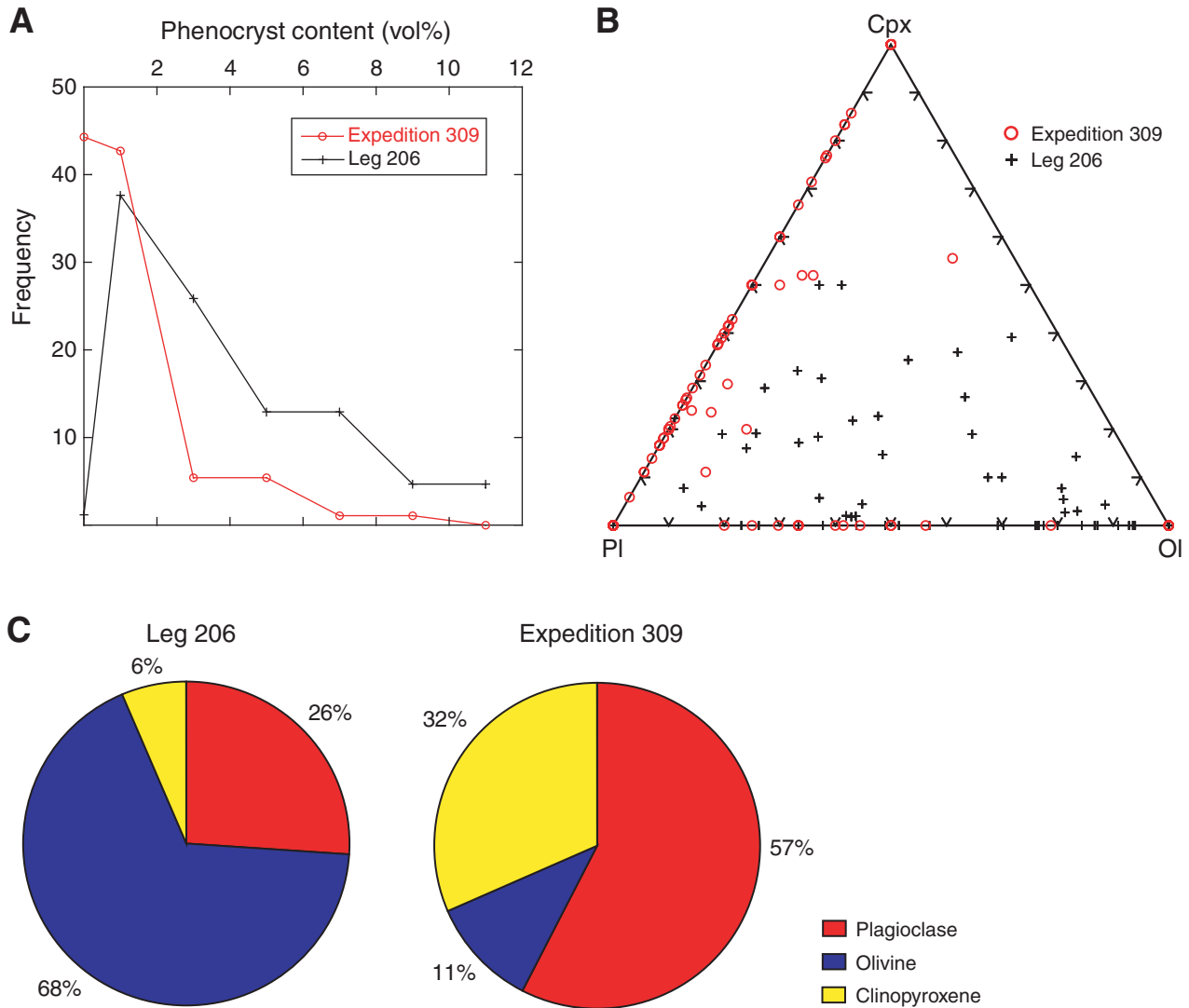
Figure F30. Plots of whole-rock chemical composition (shipboard ICP-AES analyses) versus depth with igneous stratigraphy and units. Error bar indicates the analytical precision. (Continued on next three pages.)
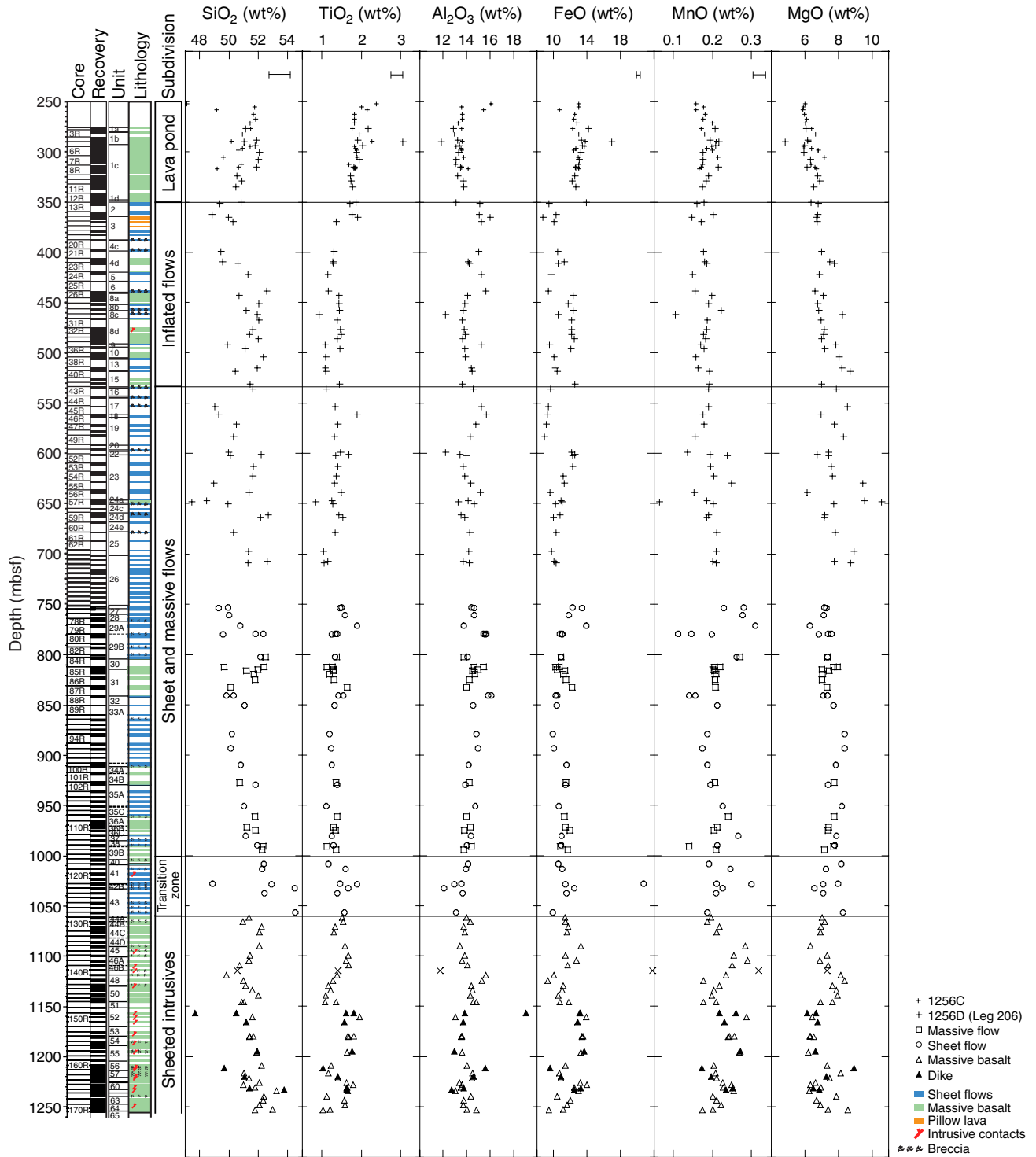
Figure F30 (continued).
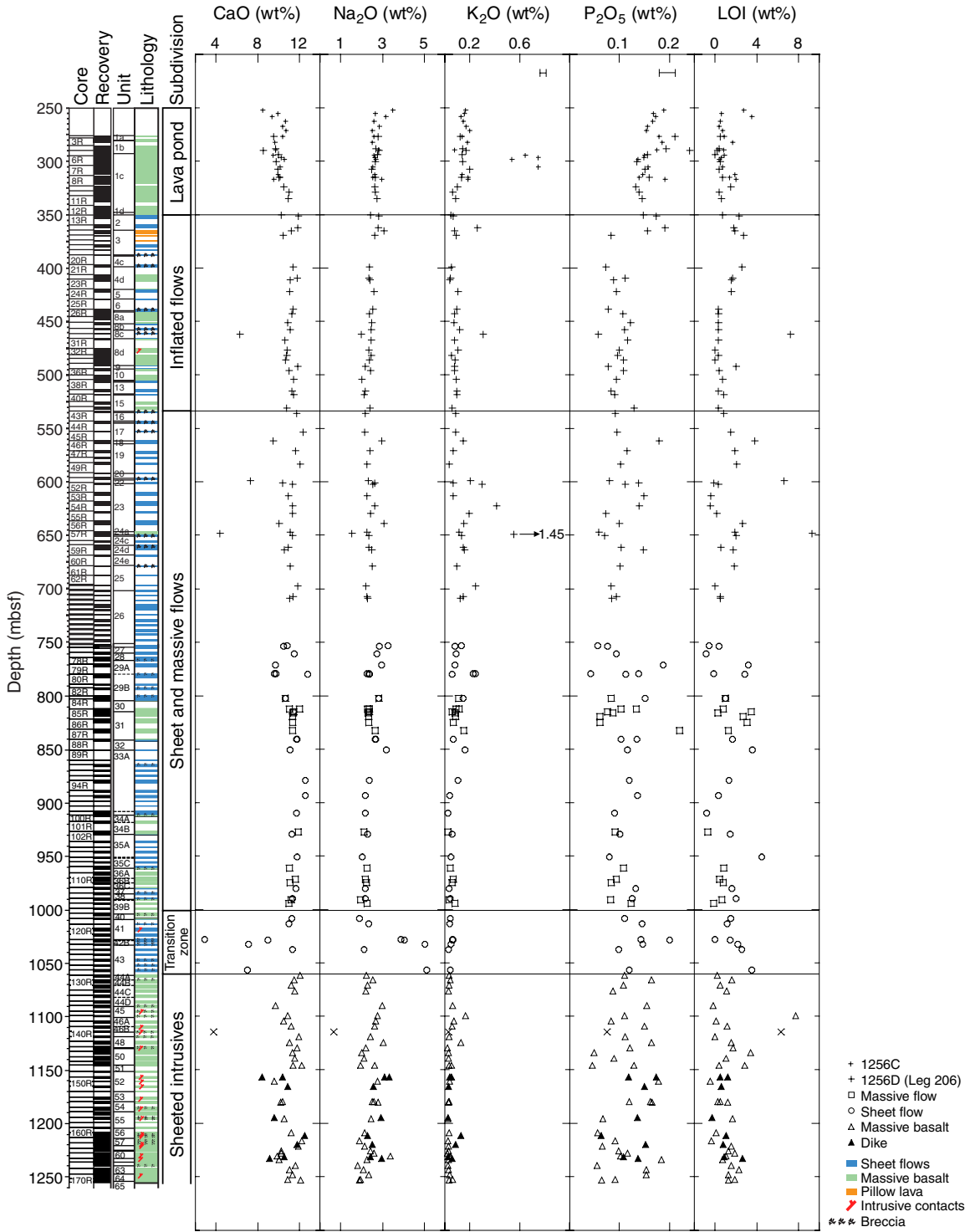
Figure F30 (continued).
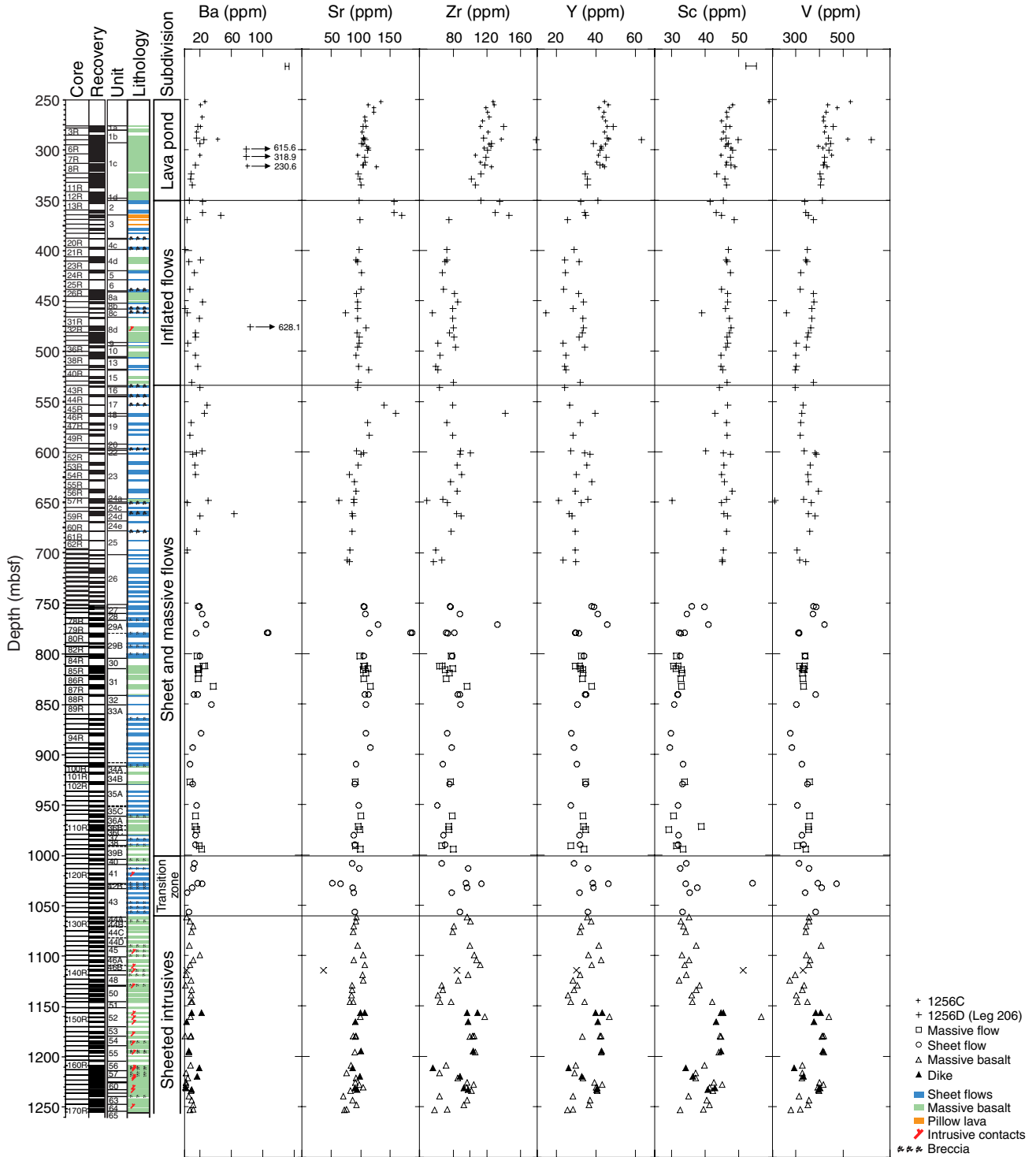
Figure F30 (continued).
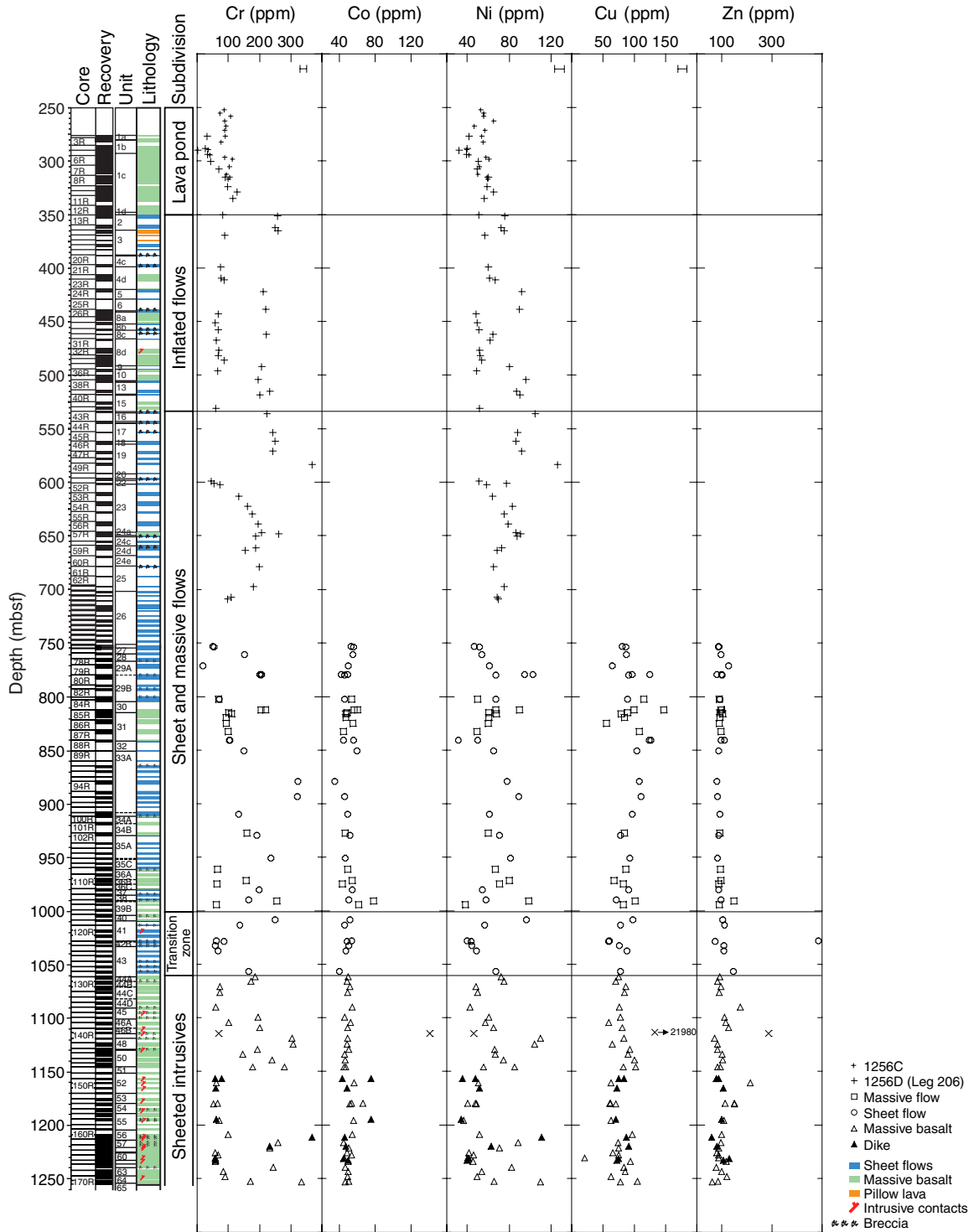
Figure F31. Plots of all elements versus MgO for all whole-rock shipboard analyses. Error bar indicates the analytical precision. (Continued on next page.)
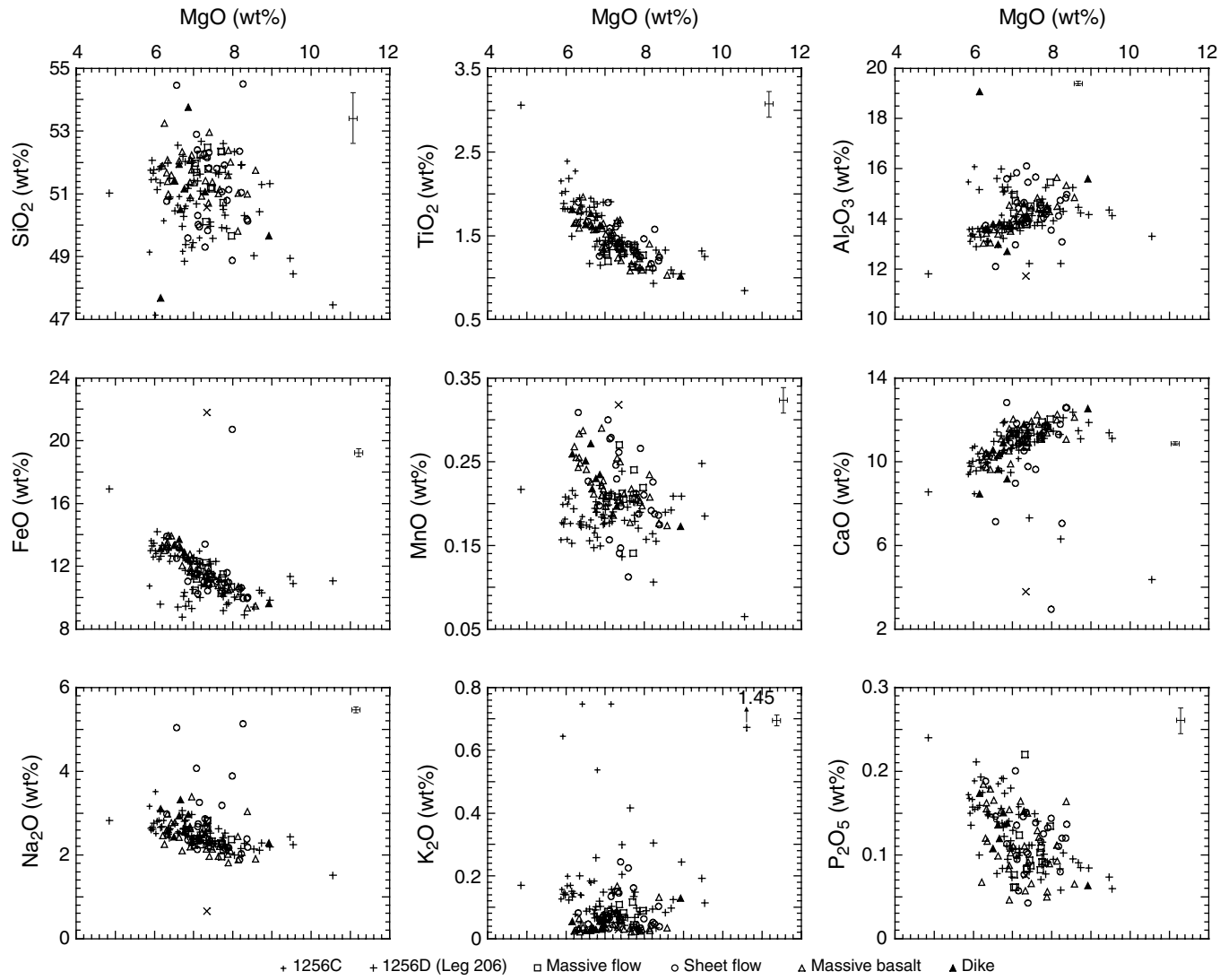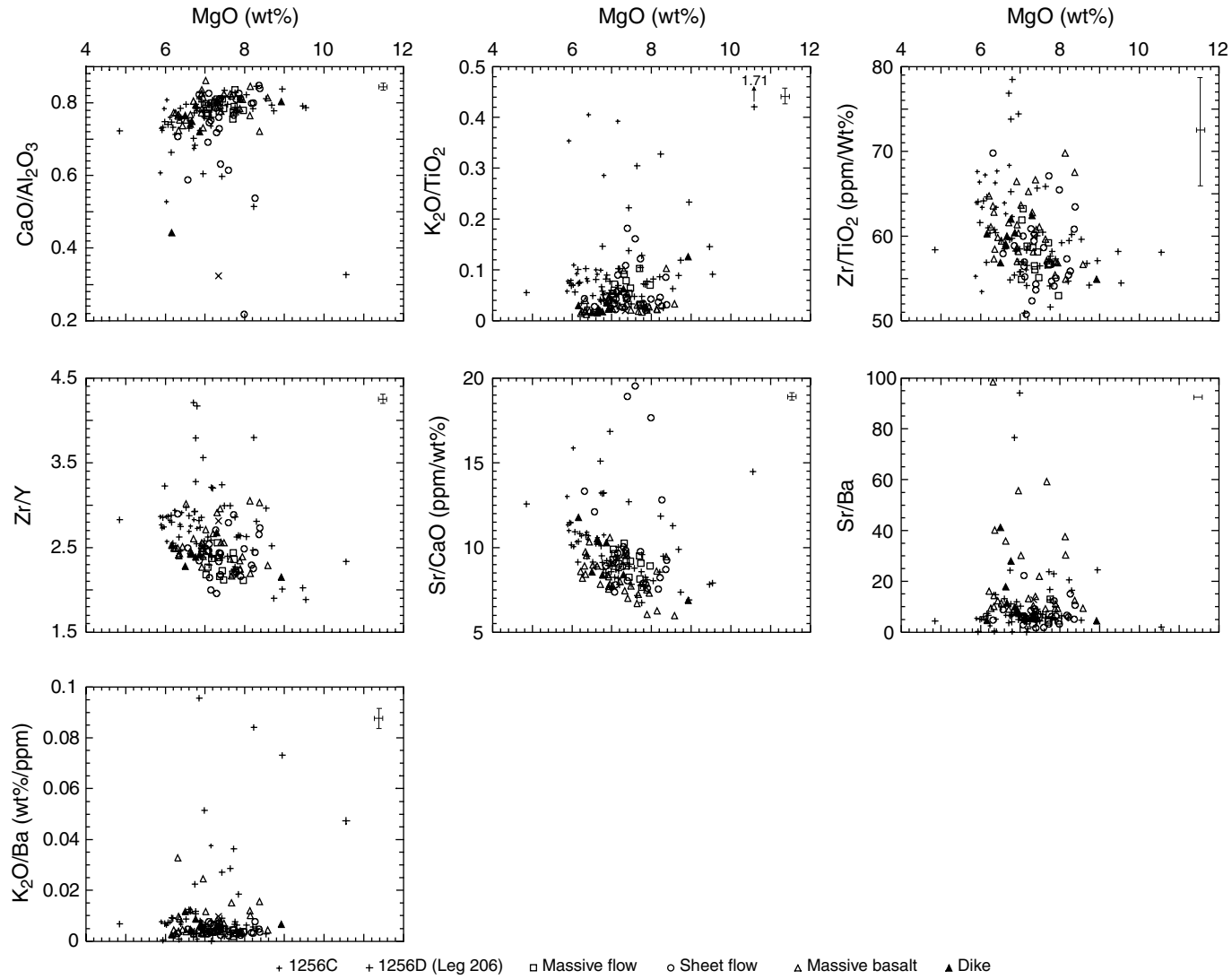
Figure F32. Zr versus Y and Zr versus TiO$_2$ for basalts from Site 1256.
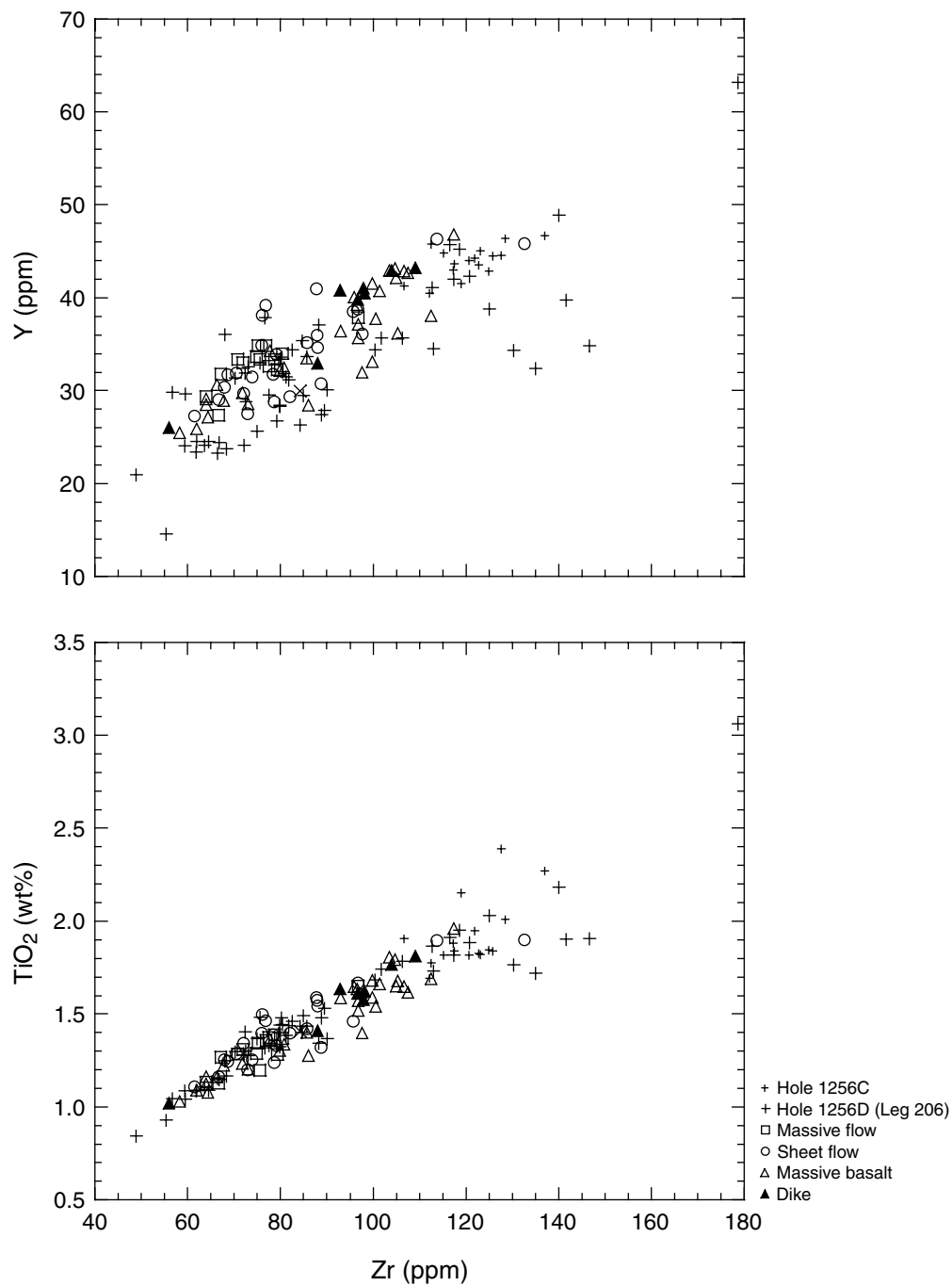
Figure F33. East Pacific Rise (EPR) mid-ocean-ridge basalt (MORB) normalized multielement plot of the average of different lithologic subdivisions from Hole 1256D. LP = lava pond, IF = inflated flows, SMF = sheet and massive flows, TZ = transition zone, and SI = sheeted intrusives. The values of Ba, Y, Sr, Zr, and TiO_2 are taken from Su and Langmuir et al. (2003). Other elements are compiled from PETDB (**www.petdb.org**) for basalts with MgO >6.0 wt%.
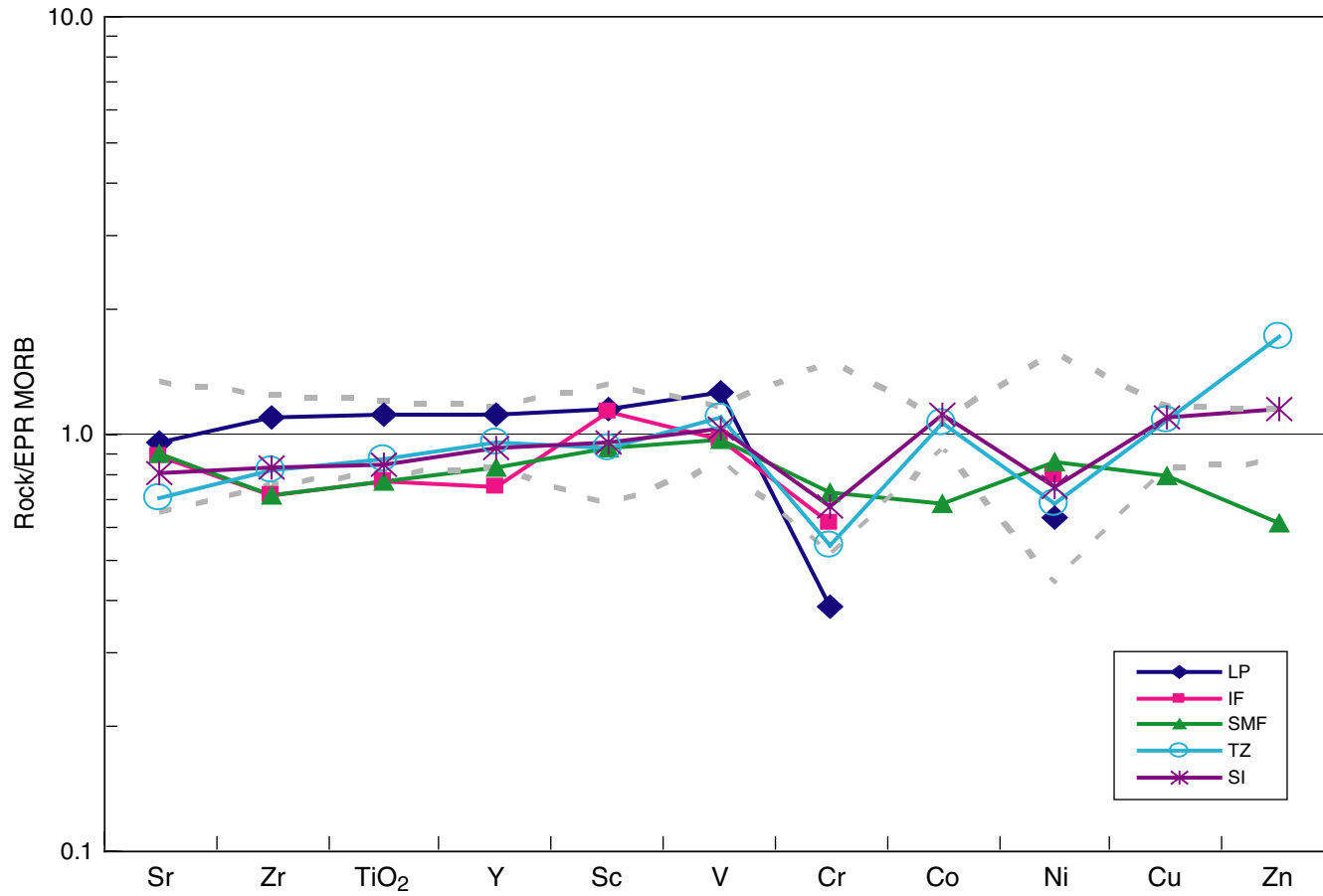
Figure F34. Comparison of incompatible element ratio (Zr/TiO$_2$, Zr/Y) versus MgO and basalt from Hole 504B. Hole 504B basalts from Autio and Rhodes (1983), Kempton et al. (1985), Natland et al. (1983), Expedition 304 Scientists (2005), and Expedition 305 Scientists (2005).
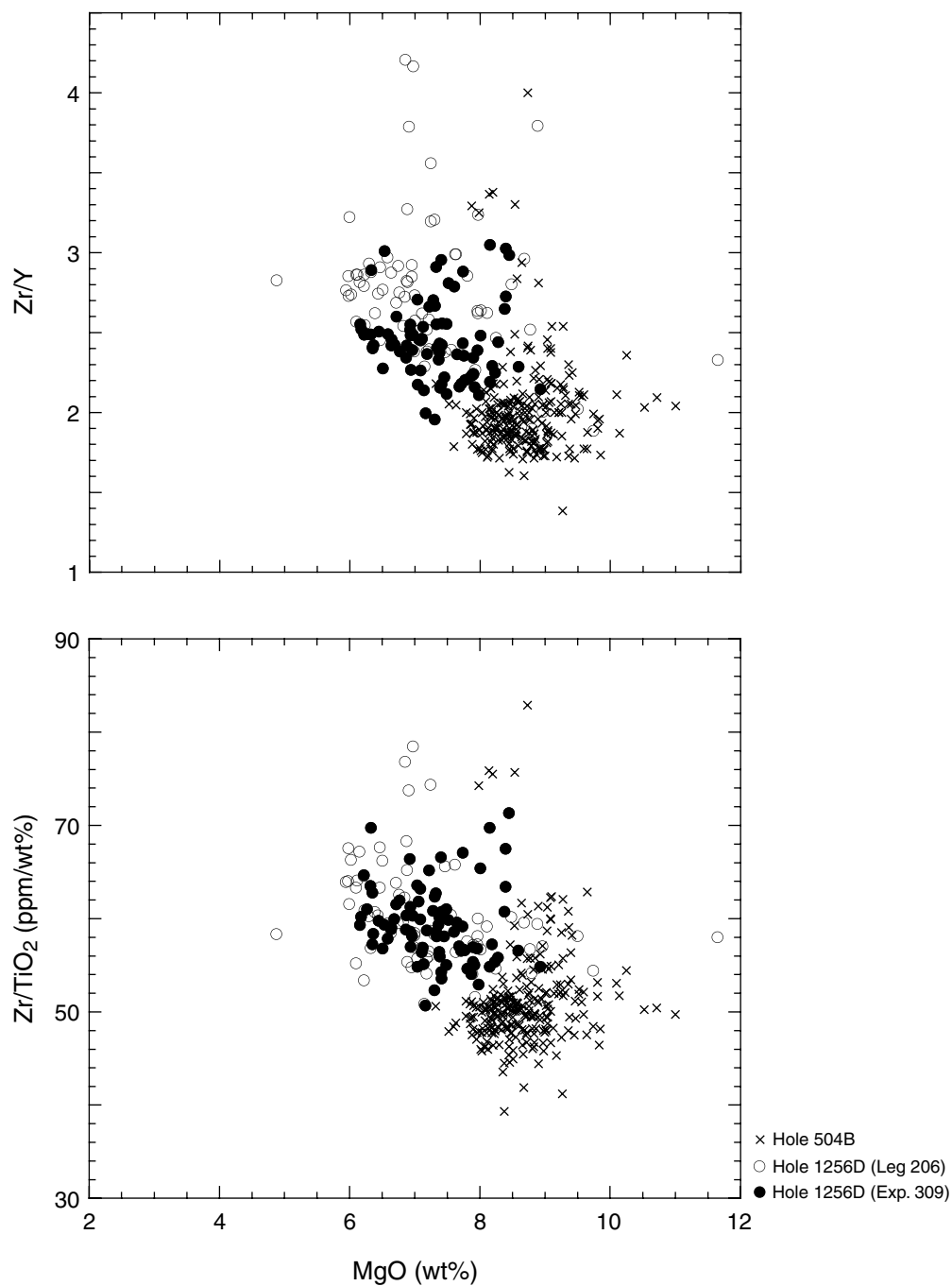
Figure F35. Zr/TiO$_2$ and Zr/Y ratios for first-order mid-ocean-ridge segments along EPR from 14°N to 19°S and Site 1256. Zr and Y data are taken from PETDB (**www.petdb.org**), and the plotted values are the average of segment centers. Error bars are 1σ. The spreading rate of each segment is calculated by the Online Ridge Spreading rate calculator (**www.ldeo.columbia.edu/users/menke/plates.html**). The spreading rate of Site 1256 is given by Wilson (1996). The range of latitude of each segment center is indicated by the labels underneath the x-axis, and numbers above the x-axis are the spreading rate (full rate) of each segment.
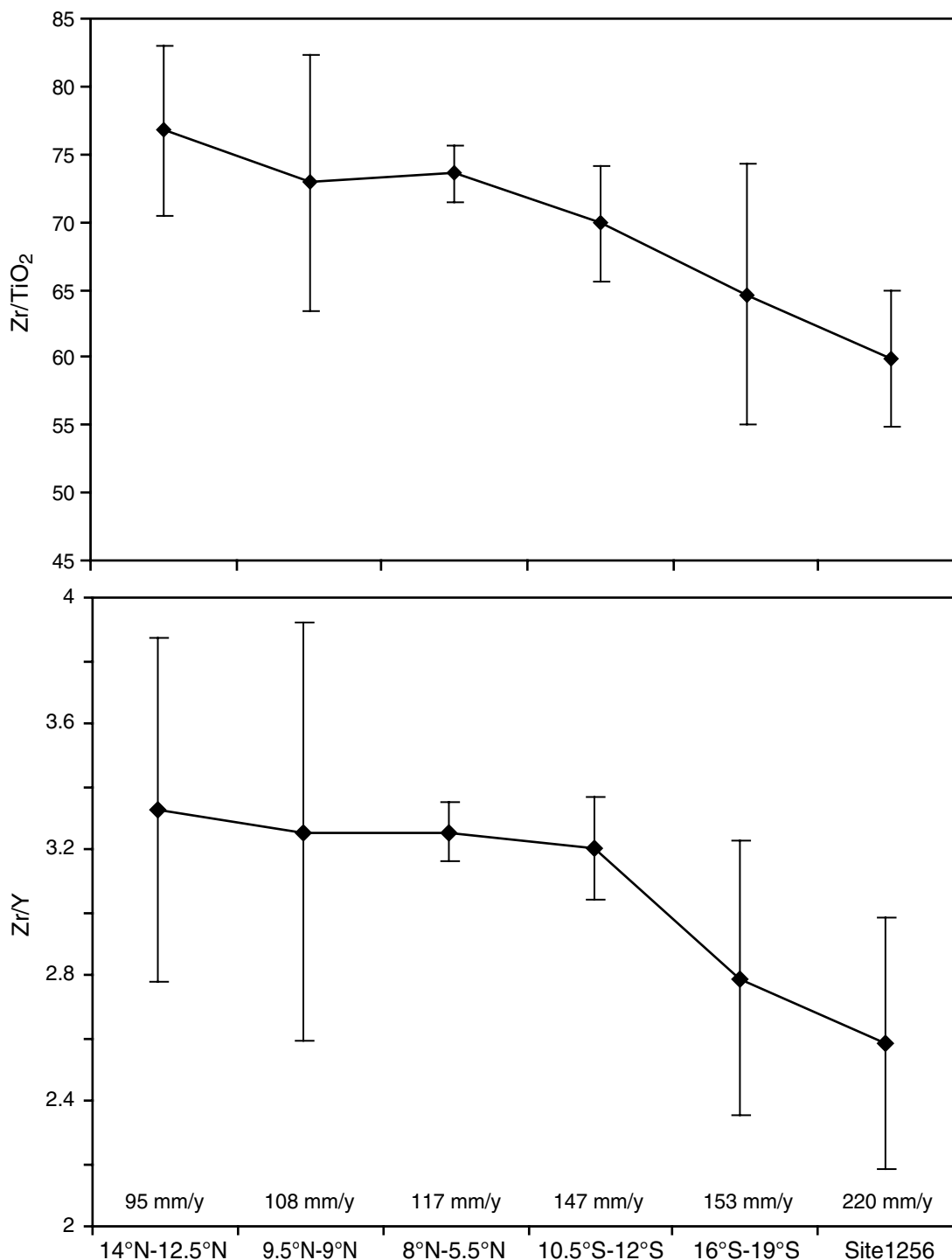
Figure F36. Alteration style and intensity (given as percentage per core) down Hole 1256D for the section drilled during Expedition 309. Percentages are normalized to amount of recovered material per core (per meter) and plotted versus depth.
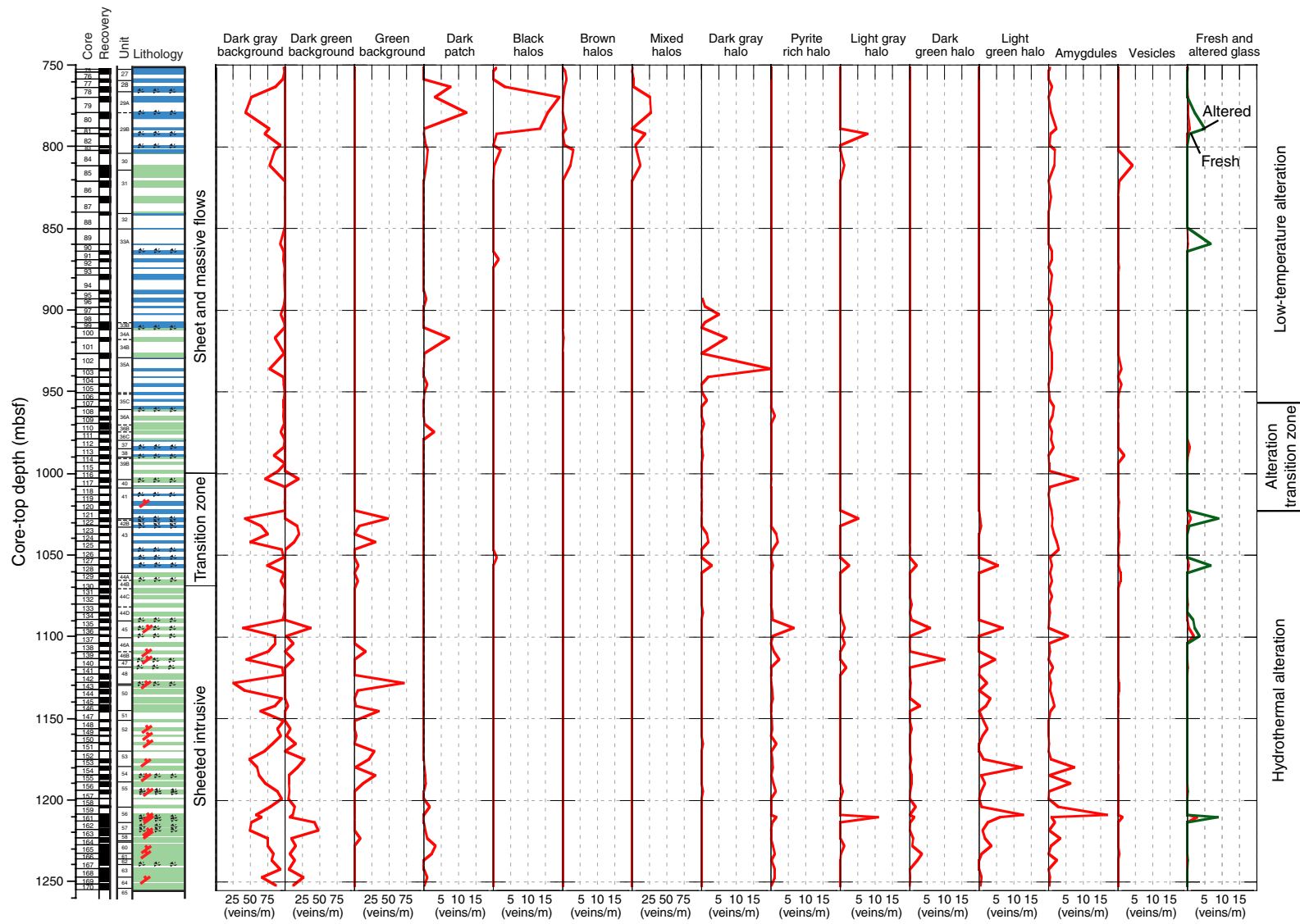
Figure F37. Total volume percent of secondary minerals contained within veins with depth in Hole 1256D for the section drilled during Expedition 309. Percentages are normalized to amount of recovered material per core (per meter) and plotted versus depth to top of core.
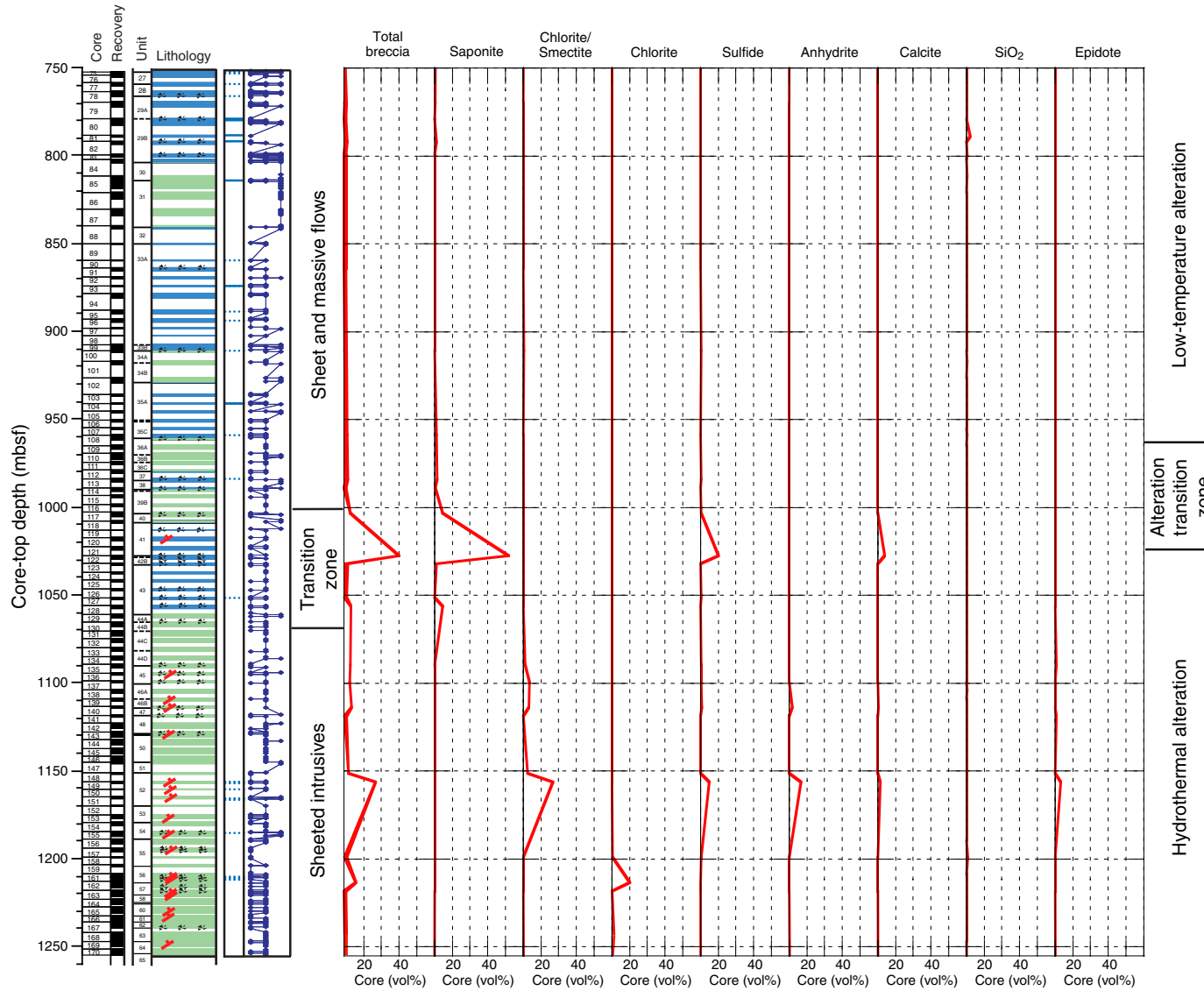
Figure F38. Abundance of secondary mineral veins with depth in Hole 1256D for the section drilled during Expedition 309. Numbers of veins are normalized to amount of recovered material per core (veins per meter) and plotted versus depth to top of core.
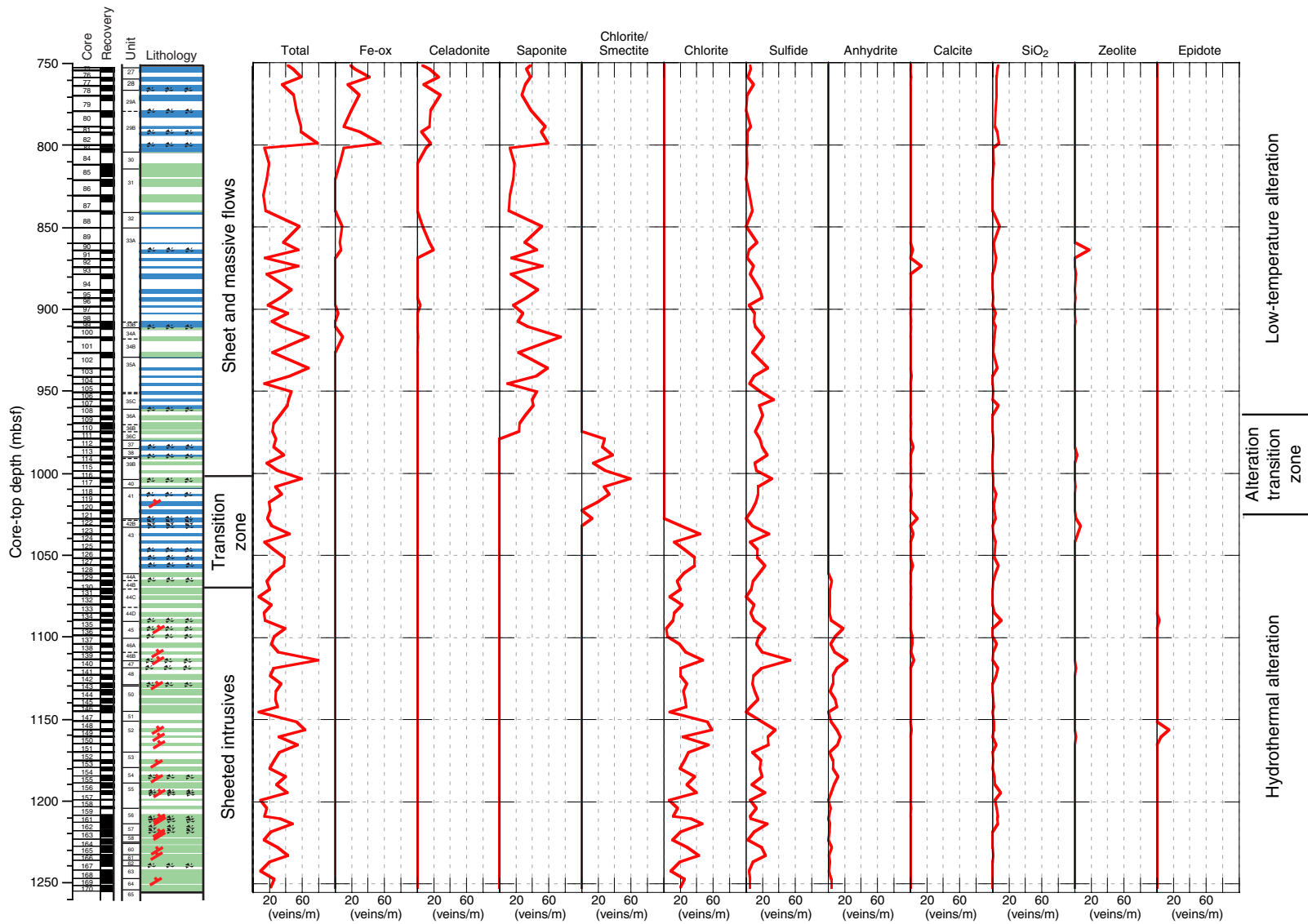
Figure F39. Mineral plot versus depth, including results from hand specimen and microscopic observation and X-ray diffraction analysis.
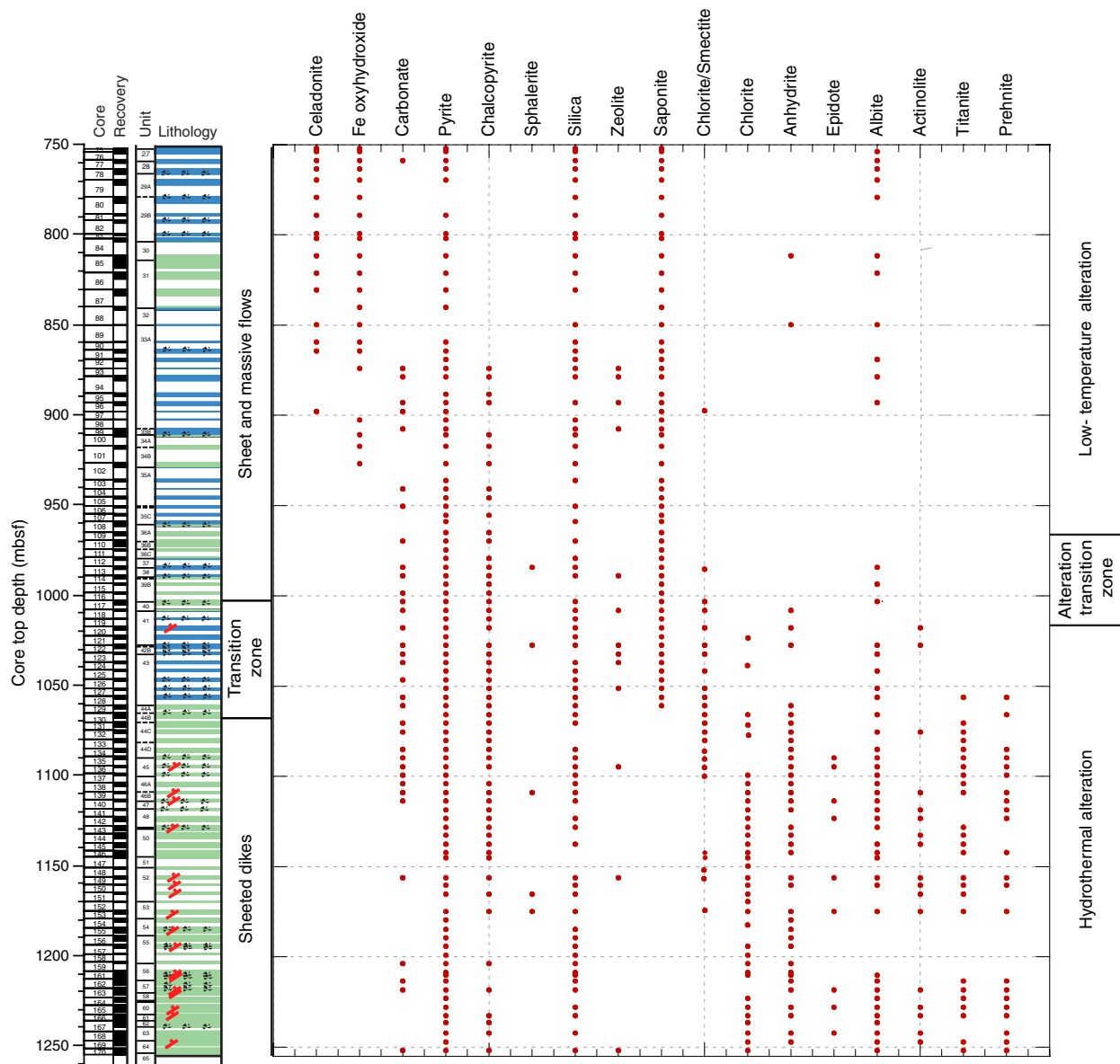
Figure F40. A. Downhole distribution of structural features. **B.** Downhole variation of the intensity of fracturing.
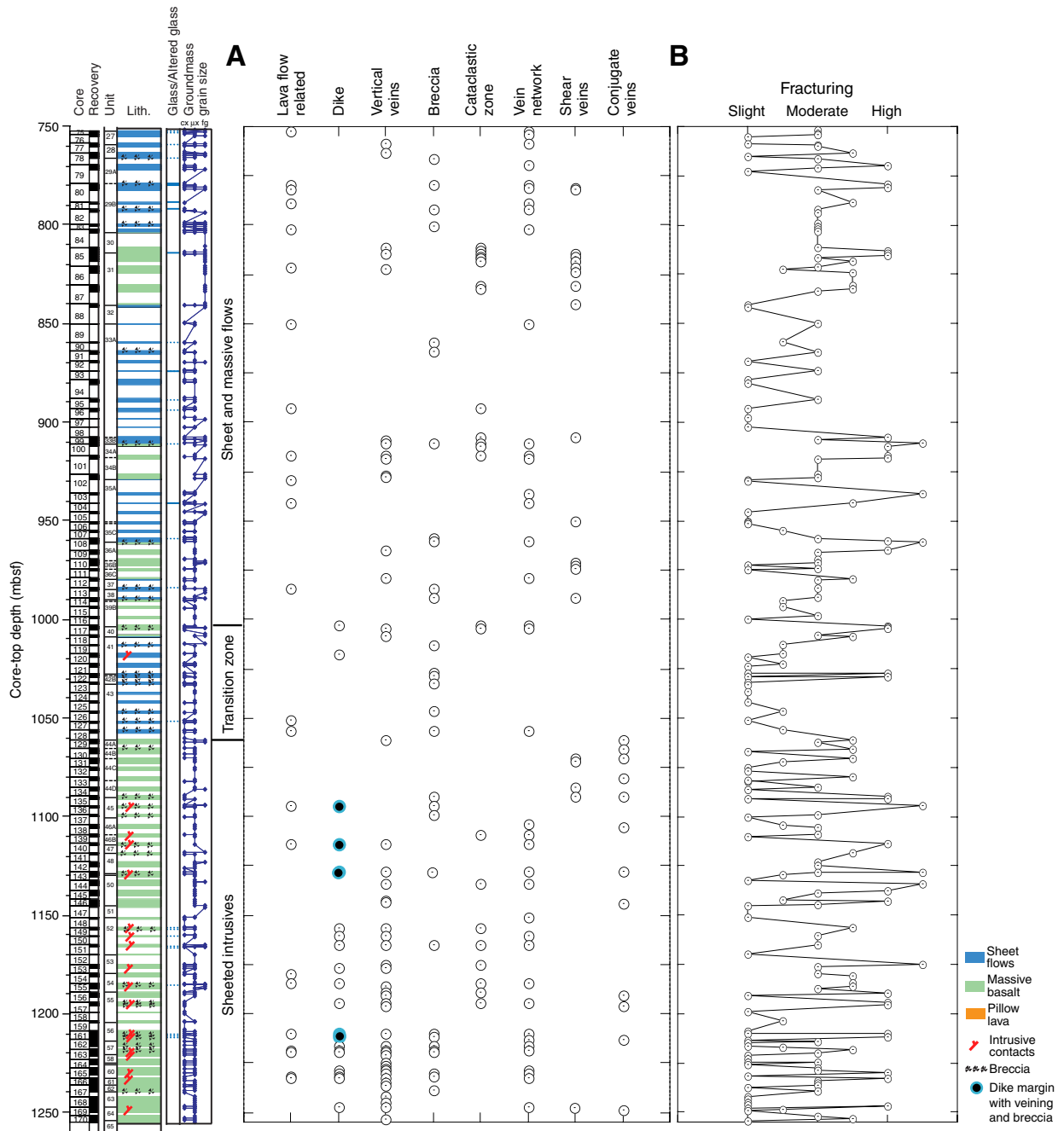
Figure F41. Cataclastic zone at contact with clast of chilled basalt (cataclastic massive unit) (Sample 309-1256D-117R-1 [Piece 12, 122–125 cm]). **A.** Core piece and thin section. **B.** Detail of thin section. Inset shows the crosscutting relationships between different events of veining (1 is the oldest); protocataclasite (protoc) and cataclasite are cut by ultracataclasite (ultracat) and gouge veins (plane-polarized light, blue filter; field of view = 10 mm; thin section 67).
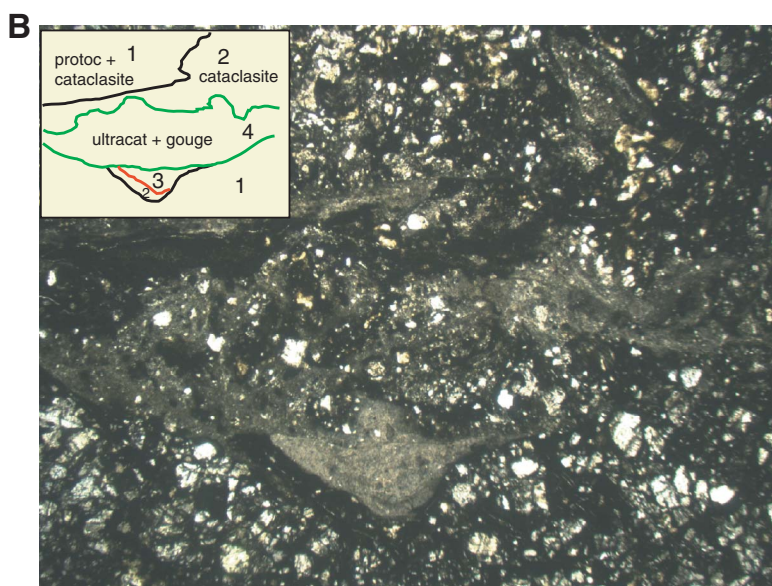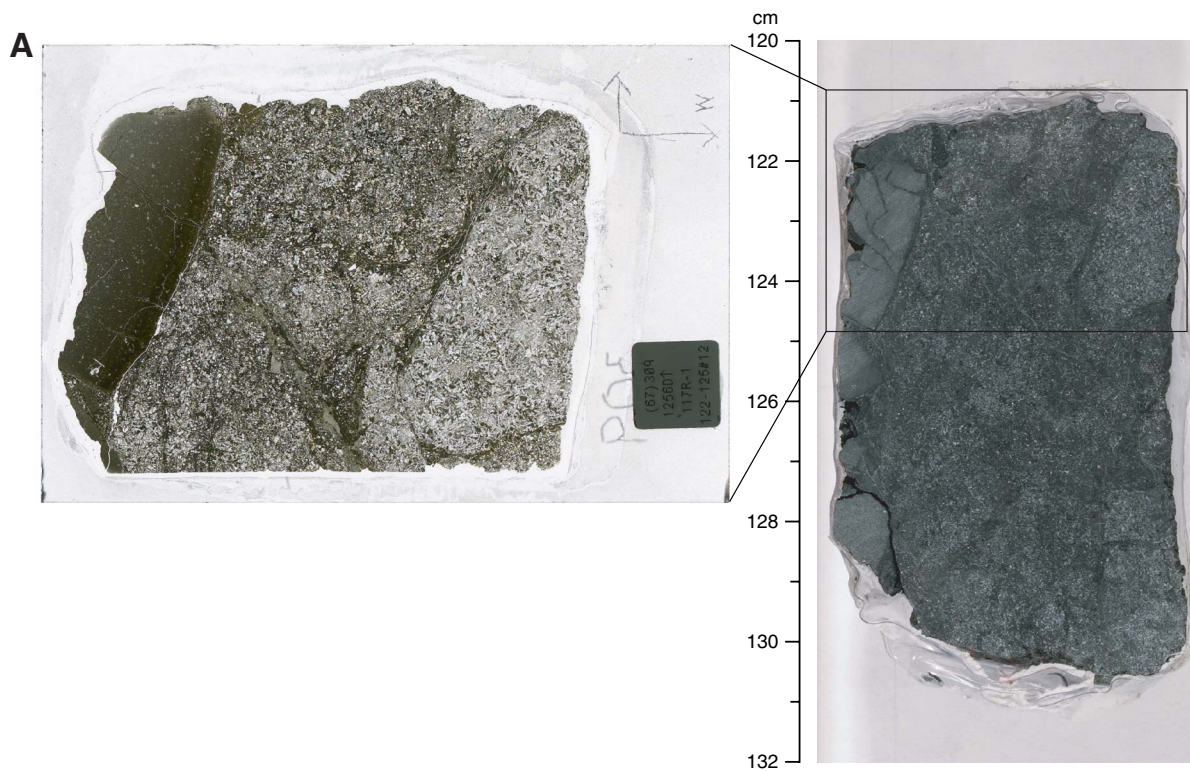
Figure F42. Subtype of hyaloclastite consisting of basalt clasts and altered glassy clasts and glassy shards cemented by quartz, carbonate, and sulfide (mineralized volcanic breccia). **A.** Thin section (Sample 309-1256D-122R-1 [Piece 19, 140–142 cm]) (thin section 80). **B.** Spherulitic texture in cryptocrystalline basalt clasts of the hyaloclastite (Sample 309-1256D-122R-1 [Piece 16, 119–124 cm] (plane-polarized light, blue filter; field of view = 5 mm; thin section 78). Light spots are sulfides.
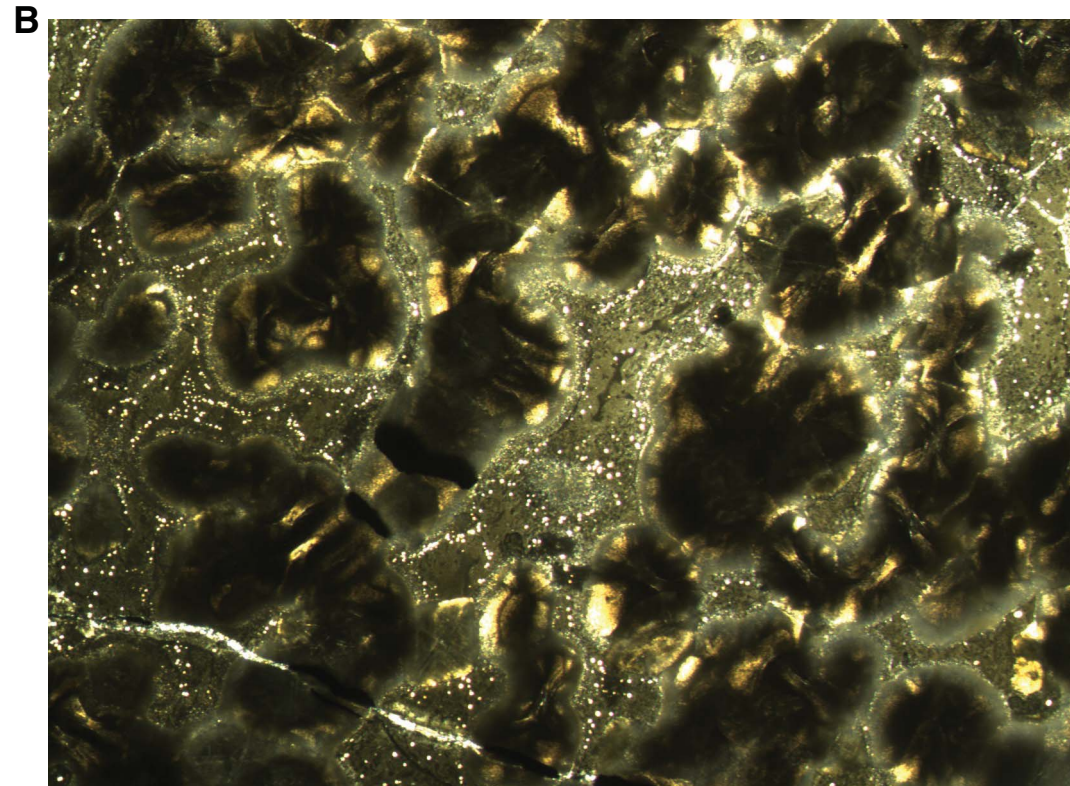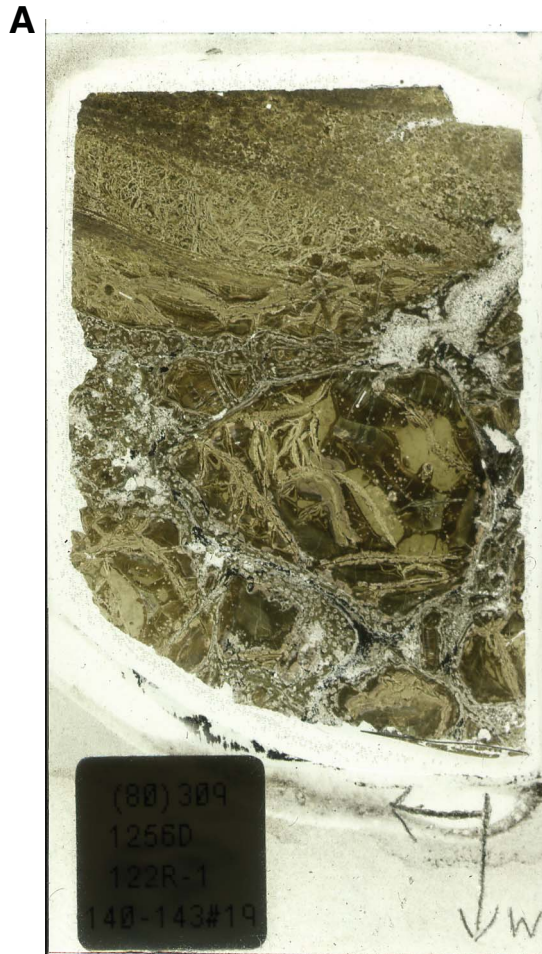
Figure F43. Hyaloclastic breccias characterized by different colors linked to alteration of clasts and matrix from the same core. **A.** Green bluish breccia (interval 309-1256D-122R-1, 29–51 cm). **B.** Light green breccia (interval 309-1256D-122R-1, 105–125 cm).
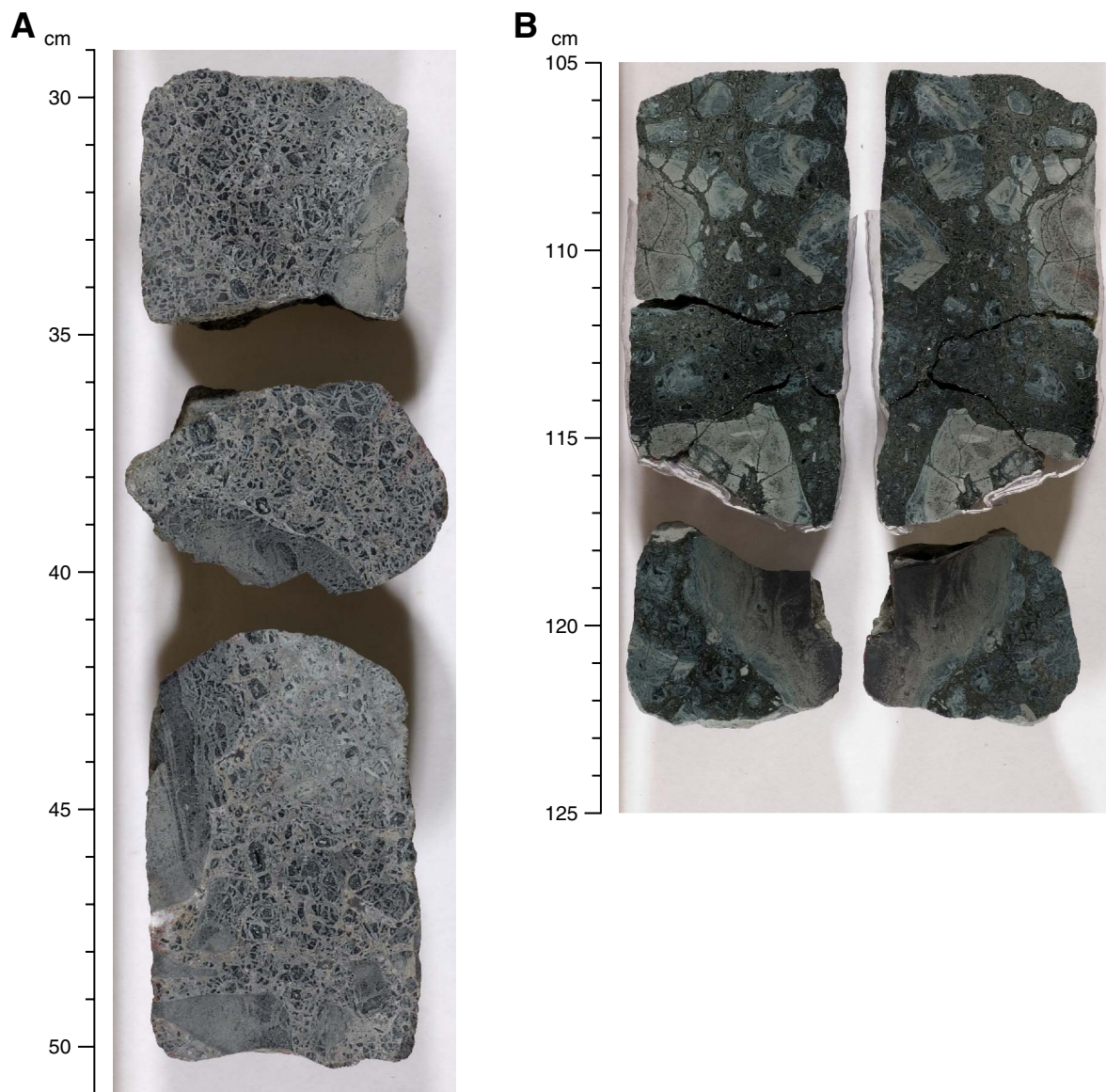
Figure F44. Cataclastic zone at dike contact characterized by flow structures and multiple veining. Veins have dilational features and different mineral fillings; clear crosscutting relationships are visible. **A.** Close-up of core (interval 309-1256D-140R-1, 42–58 cm). **B.** Close-up of thin section (Sample 309-1256D-140R-1, 41–59 cm) (thin section 117).
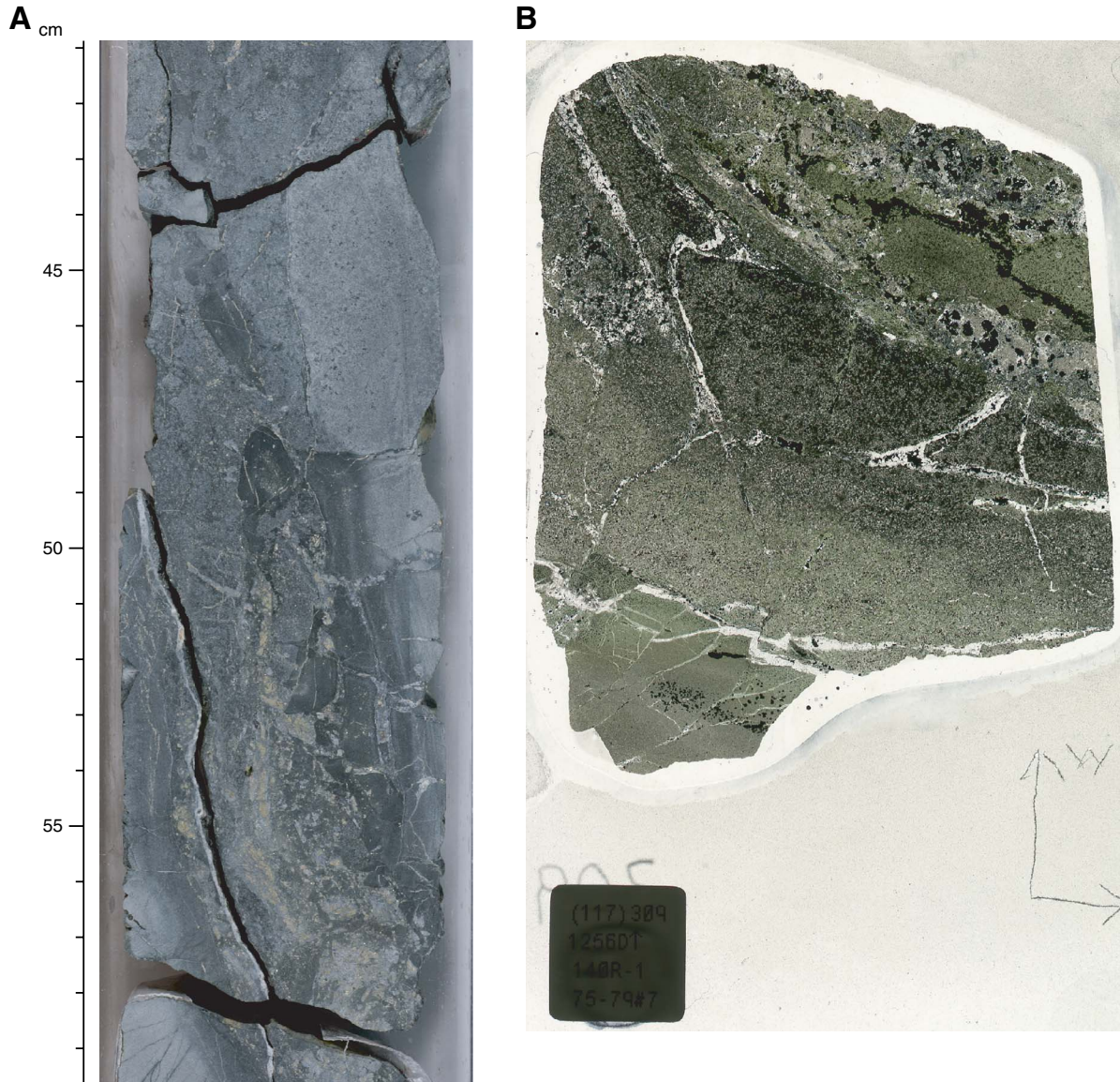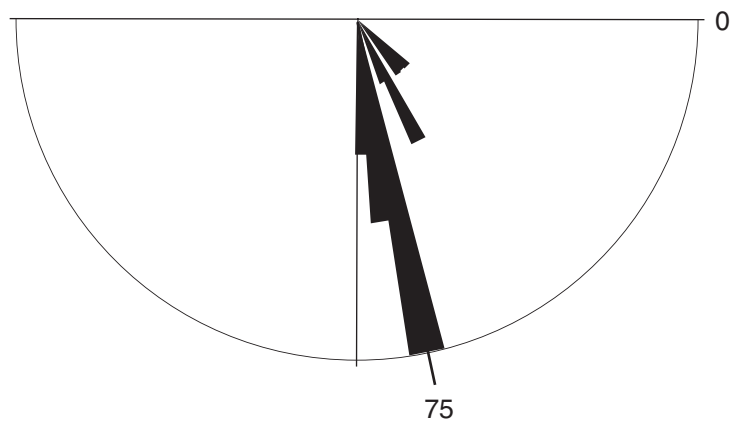
Figure F45. Rose diagram of true dips of the dike contacts.

N = 16

Circle = 31%

Size of the largest petal = 31.3%

Equal area

Figure F46. AF demagnetization behavior of one of the most stable samples studied (discrete Sample 309-1256D-161R-2, 21–23 cm). Normalized intensity versus demagnetization level is at upper left; component diagrams and direction plots are on the right. Dots on the data table and double squares on the intensity plot = values used for principal component analysis (PCA), with results listed at top left. High demagnetization (Demag) fields are required to reduce the intensity, and inclination (Inc) changes at progressive demagnetization steps are smaller than for other samples. MAD = maximum angular deviation, Dec = declination.
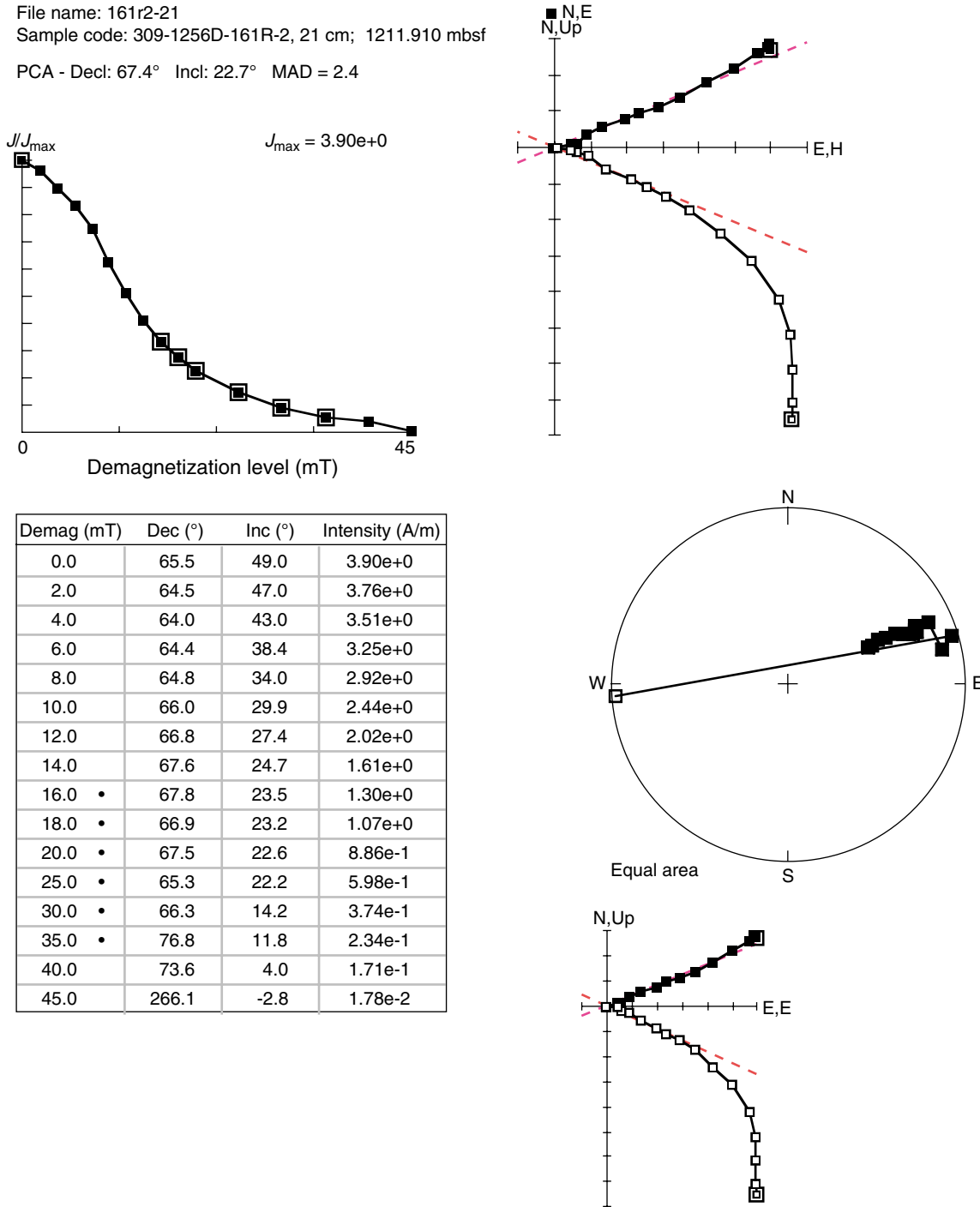
File name: 161r2-21
Sample code: 309-1256D-161R-2, 21 cm; 1211.910 mbsf

PCA - Decl: 67.4°   Incl: 22.7°   MAD = 2.4

J/J_{max} J_{max} = 3.90e+0

Demag (mT)		Dec (°)	Inc (°)	Intensity (A/m)
0.0		65.5	49.0	3.90e+0
2.0		64.5	47.0	3.76e+0
4.0		64.0	43.0	3.51e+0
6.0		64.4	38.4	3.25e+0
8.0		64.8	34.0	2.92e+0
10.0		66.0	29.9	2.44e+0
12.0		66.8	27.4	2.02e+0
14.0		67.6	24.7	1.61e+0
16.0	•	67.8	23.5	1.30e+0
18.0	•	66.9	23.2	1.07e+0
20.0	•	67.5	22.6	8.86e-1
25.0	•	65.3	22.2	5.98e-1
30.0	•	66.3	14.2	3.74e-1
35.0	•	76.8	11.8	2.34e-1
40.0		73.6	4.0	1.71e-1
45.0		266.1	-2.8	1.78e-2

Figure F47. A. Examples of intensity variation in demagnetized archive-half samples that correlate with petrographic igneous units; from left to right: single behavior, multiple behavior, and irregular behavior. **B.** Histogram showing frequency of thickness (m) of concave shapes.
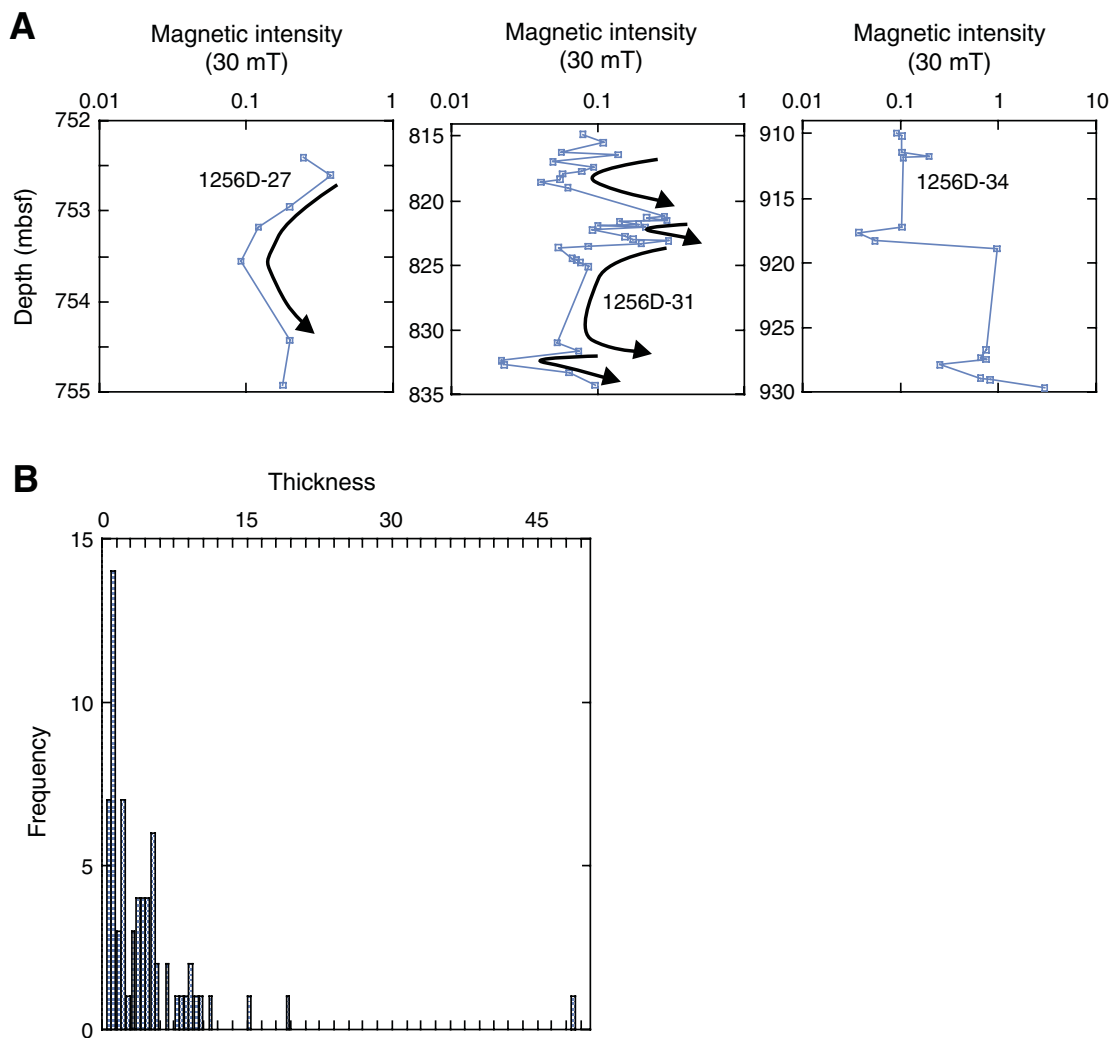
Figure F48. Discrete sample results (bulk density, V_P, and thermal conductivity [TC] data) with lithologic summary. V_P measurements were made on discrete samples, and bulk density results were calculated using measured mass and volume of each discrete sample. TC was measured on half-round cores.
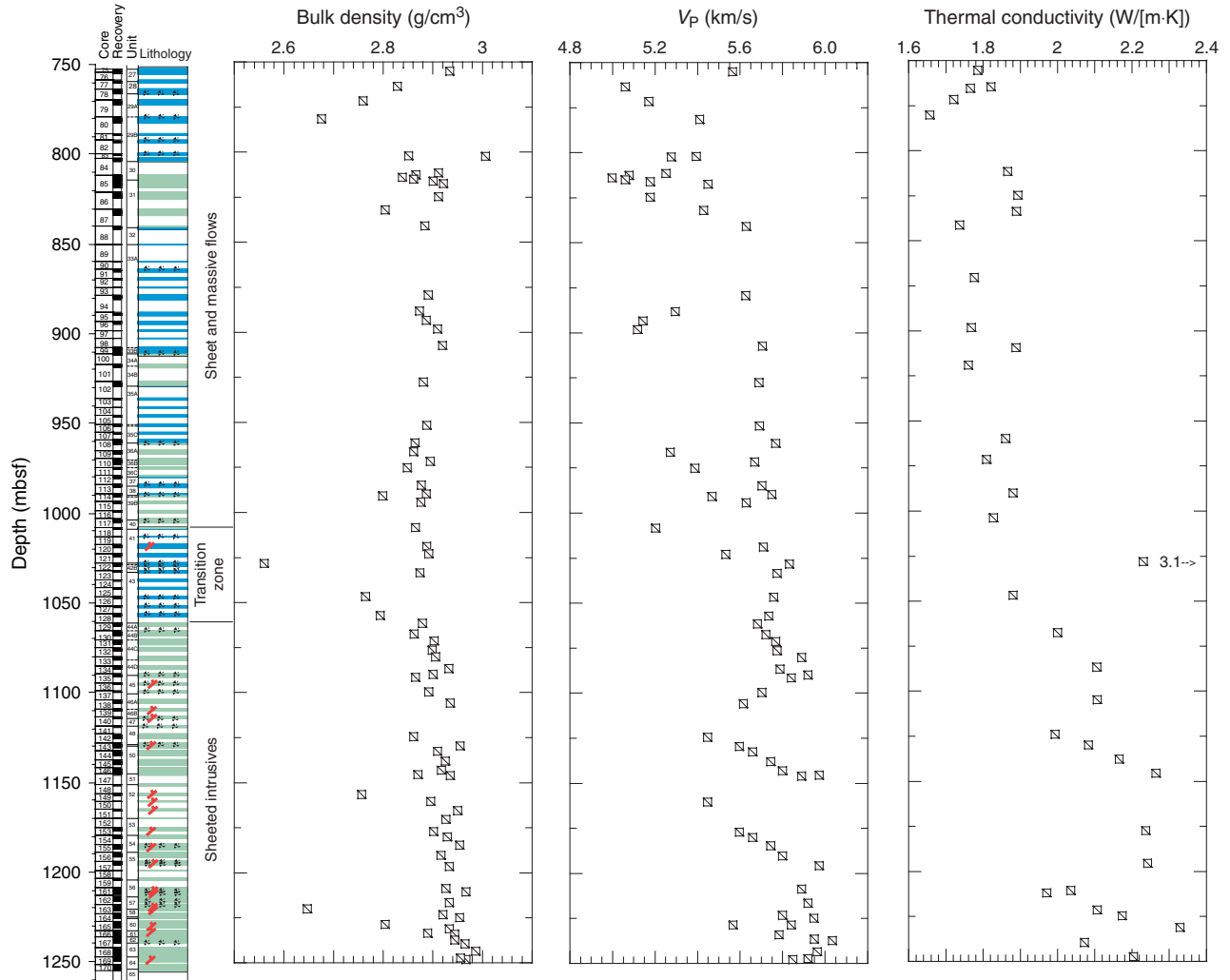
Figure F49. Variation in porosity with depth through Hole 1256D.
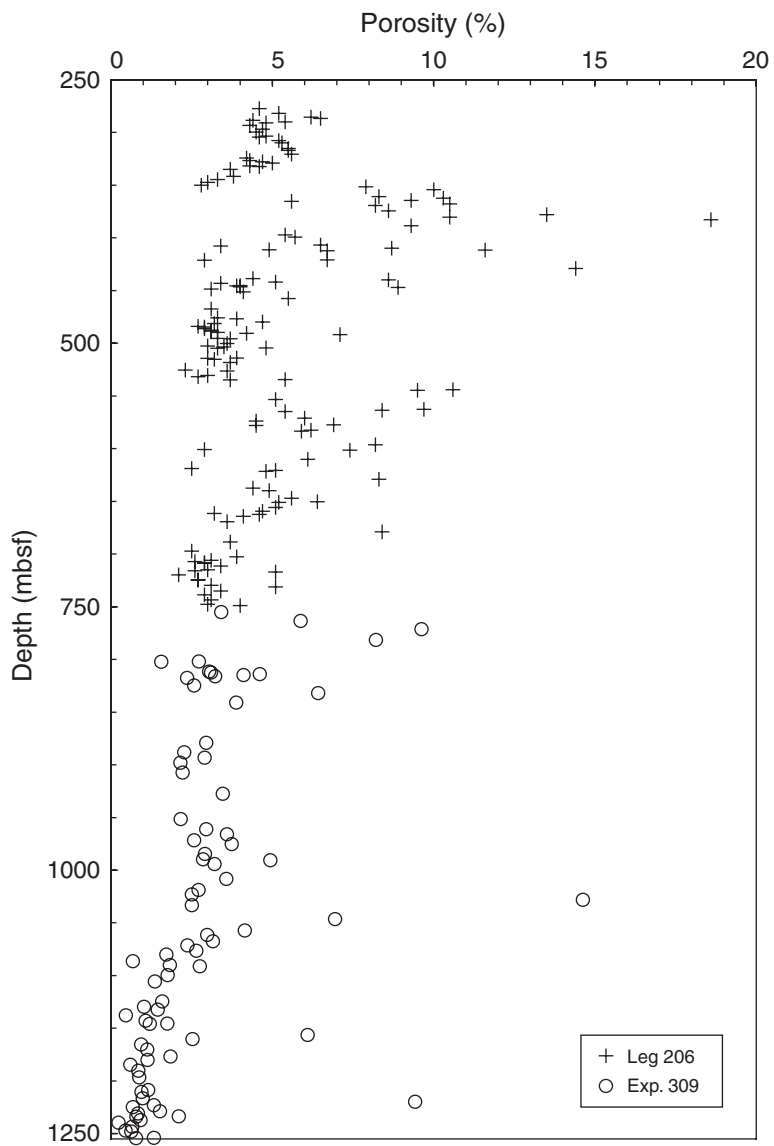
Figure F50. Average thermal conductivity (with error bar standard deviations) for Leg 206 and Expedition 309 by (**A**) rock type and (**B**) upper crustal subdivision.
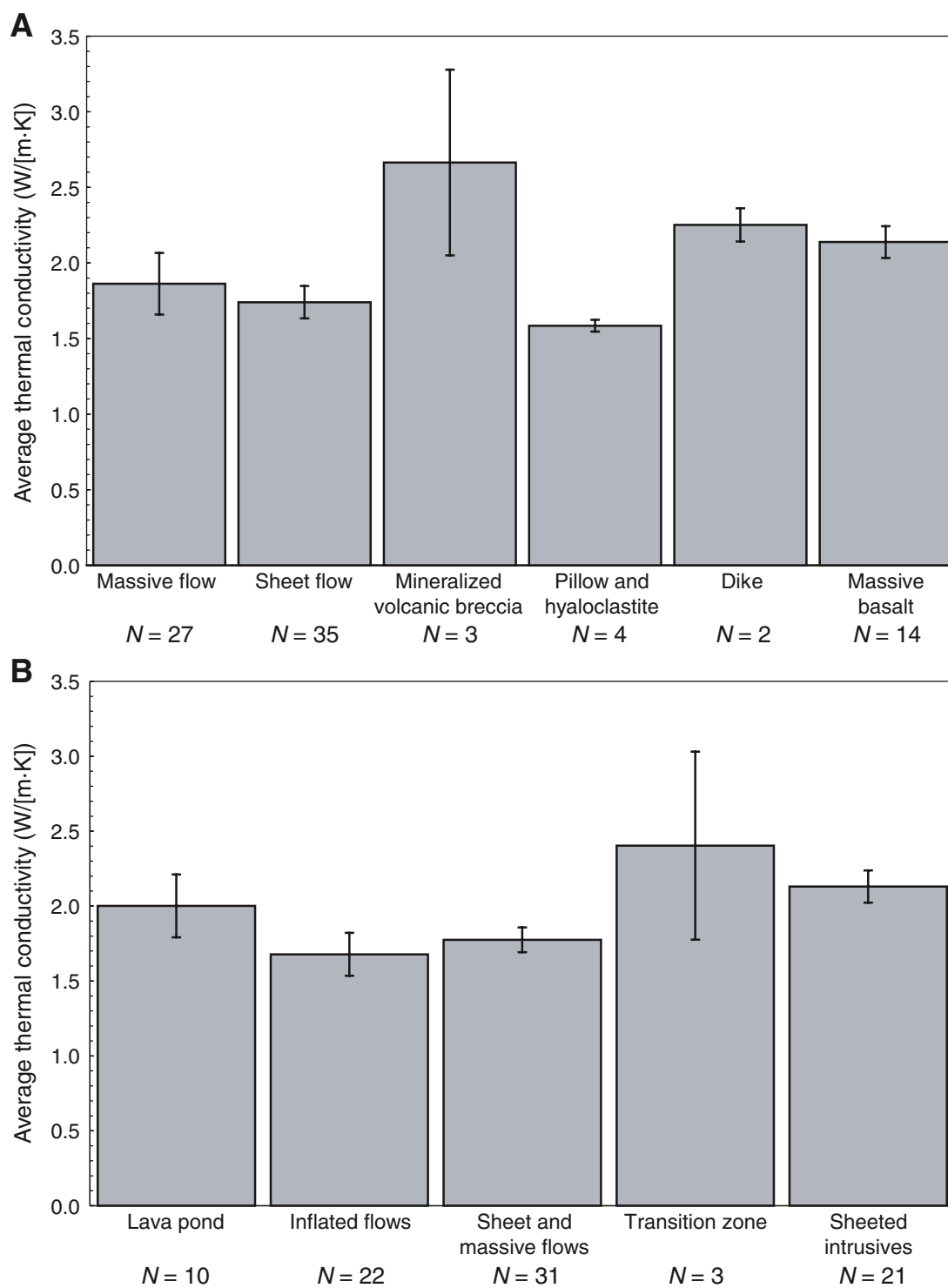
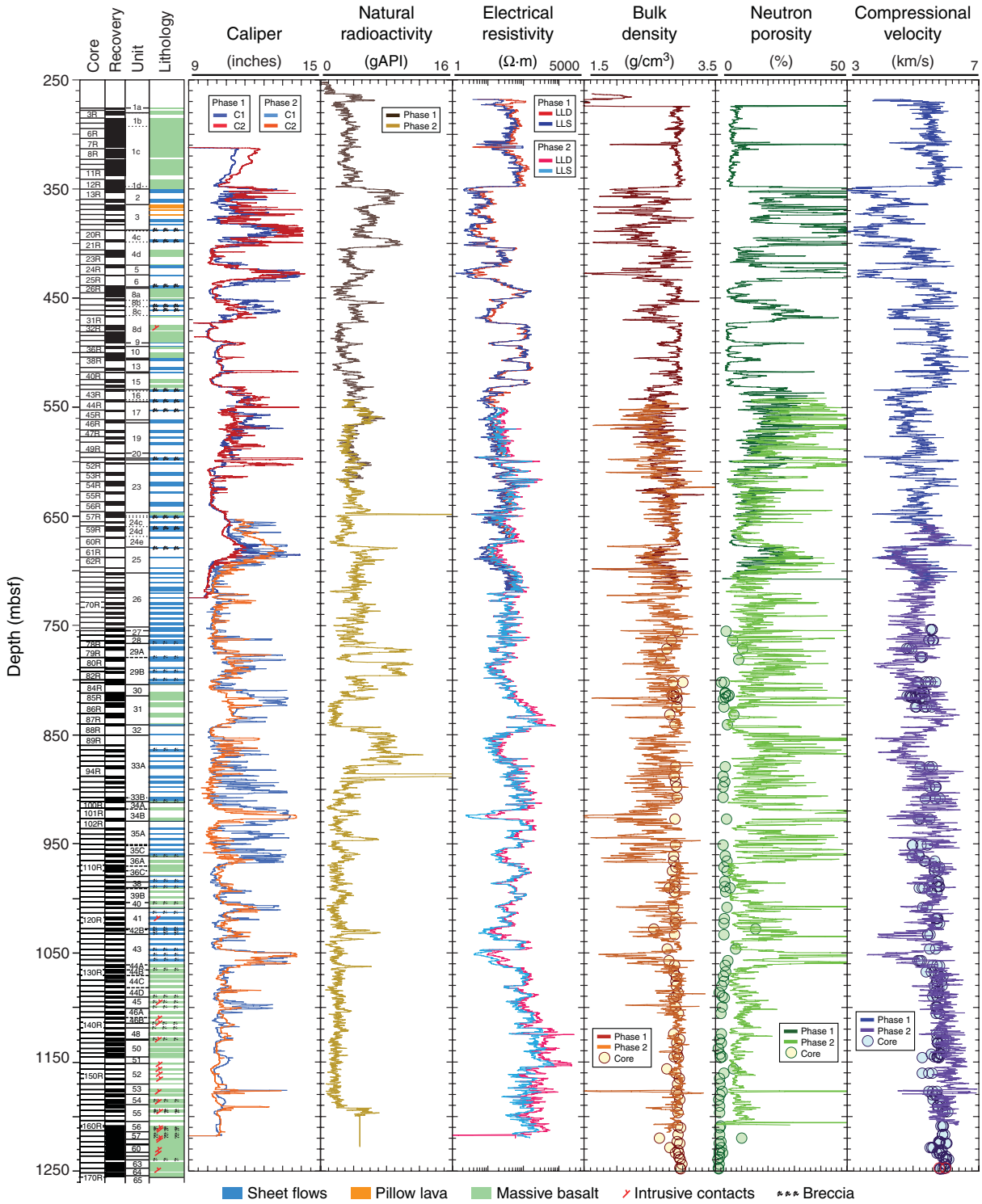**Figure F51.** Selected preliminary logging measurements from Hole 1256D.

Figure F52. A. Temperature profiles of Hole 1256D measured with the TAP tool before the commencement of drilling operations (black curve) and after completion of drilling (red curve) and electrical resistivity measured with the Dual Laterolog. **B.** FMS data illustrating the correspondence of temperature anomalies with portions of the borehole with low resistivities (black interval).
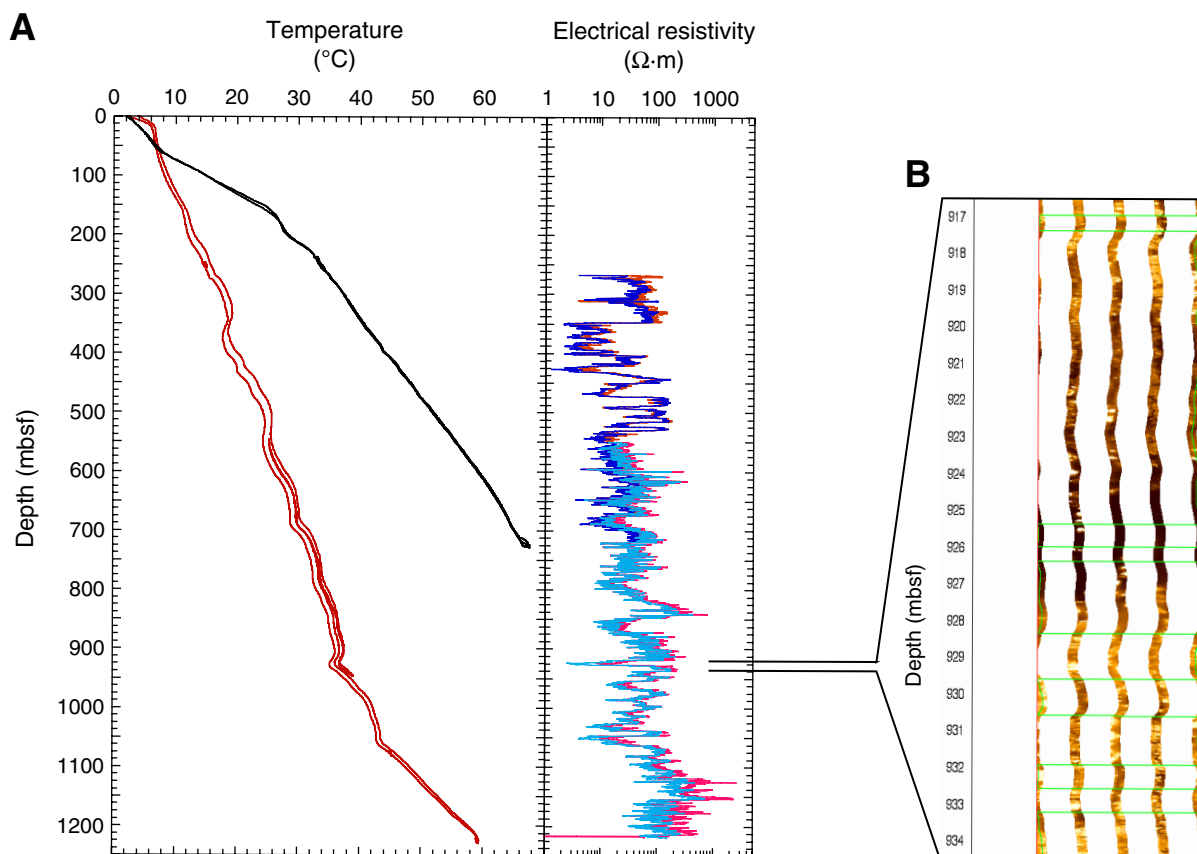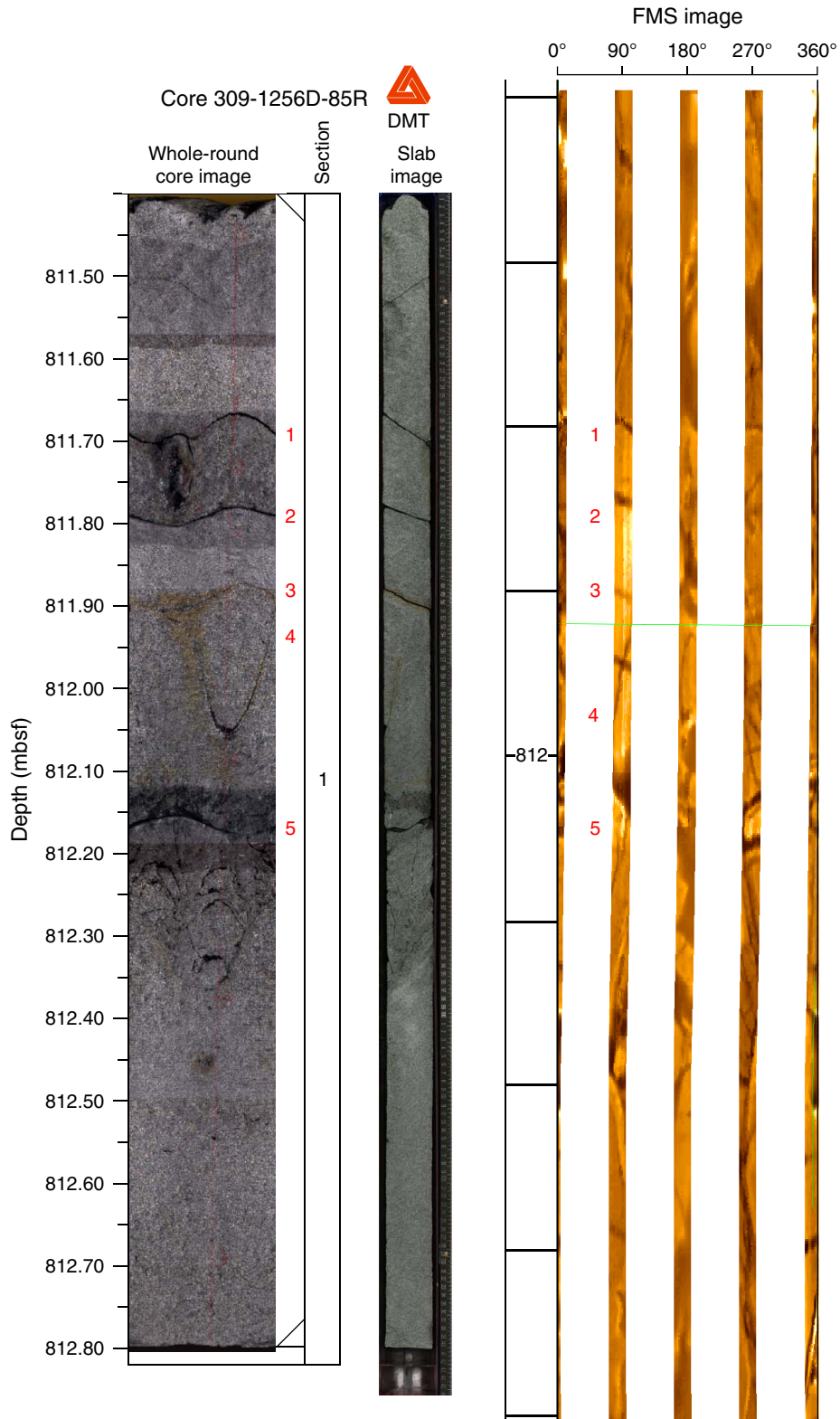
Figure F53. An example of a whole-round image (left) and matching slab image. Fractures appear as sinusoids in the whole-round image and lines in the slab image. Preliminary FMS image (right) has been depth-shifted <10 cm to align fractures with the core images. Red numbers adjacent to the whole-round image and within the FMS image identify matching fractures.

Movie M1. Video from the VIT camera showing the first reentry of Hole 1256D during Expedition 309.

Movie M2. Video from the VIT camera showing vigorous jet of drilling mud exiting the 5 inch pipe from a crack.

Movie M3. Video from the VIT camera showing the tenth reentry (ninth RCB coring bit) of Hole 1256D during Expedition 309.